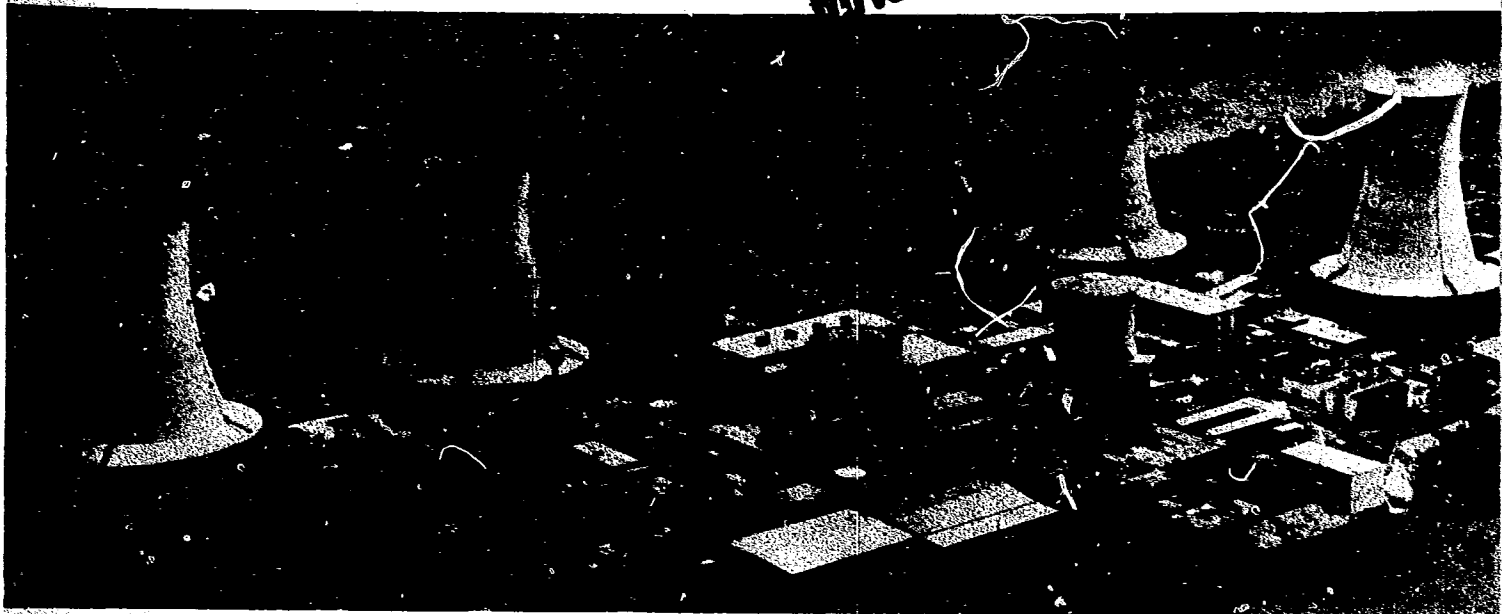B8309

GEND

General Public Utilities • Electric Power Research Institute • U.S. Nuclear Regulatory Commission • U.S. Department of Energy

Nondestructive Techniques for Assaying Fuel Debris in Piping at Three Mile Island Unit 2

Krishna Vinjamuri
Charles V. McIsaac
Laurence S. Beller

Louis Isaacson
John W. Mandler
Richard R. Hobbins, Jr.

November 1981

NONDESTRUCTIVE TECHNIQUES FOR ASSAYING FUEL DEBRIS IN PIPING AT THREE MILE ISLAND UNIT 2

Krishna Vinjamuri
Charles V. McIsaac
Laurence S. Beller
Louis Isaacson
John W. Mandler
Richard R. Hobbins, Jr.

Published November 1981

EG&G Idaho, Inc.
Idaho Falls, Idaho 83415

ABSTRACT

Four major categories of nondestructive techniques--ultrasonics, passive gamma ray, infrared detection, and remote video examination--have been determined to be feasible for assaying fuel debris in the primary coolant system of the Three Mile Island Unit 2 (TMI-2) Reactor. Passive gamma ray detection is the most suitable technique for the TMI-2 piping; however, further development of this technique is needed for specific application to TMI-2.

SUMMARY

As a result of the March 1979 accident at the Three Mile Island Unit 2 (TMI-2) Nuclear Plant, fuel debris is expected to be distributed in the reactor's primary piping system. This report investigates the feasibility of using nondestructive fuel-debris assay techniques in the TMI-2 piping. The categories of nondestructive techniques investigated are ultrasonics, nuclear radiation detection, infrared detection, optical techniques (which include fiber optics and remote video examination), and the pulsed eddy current (PEC) technique.

A preliminary investigation of the feasibility of using these fuel-debris assay techniques suggests that a passive gamma ray technique is most feasible for locating and characterizing fuel debris within the TMI-2 primary coolant system, with or without insulation. The ultrasonic technique is feasible only for assaying pipes without insulation. The passive gamma-ray and ultrasonic techniques are complementary, and together could be used to determine the fuel and non-fuel fraction, and the thickness and extent of the debris in pipes without insulation. The detection limit of the passive gamma ray technique is 47 mg of fuel per meter of insulated primary coolant pipe. The minimum thickness of debris that can be detected by ultrasonic techniques in an uninsulated pipe is about 0.13 mm. The minimum detectable length, which is dependent on band width of ultrasound, is about 0.25 mm. The infrared technique is feasible for detecting fuel debris; however, the minimum detection limit is relatively high. The fiber optics technique is not feasible, due to radiation damage to the fiber optics system, difficulty in obtaining a water-tight seal, and the need for fiber bundles longer than available with the current state-of-the art. Closed-circuit video examination is feasible provided the head of the reactor core is removed. The pulsed eddy current technique is not feasible, because of magnetic effects of the carbon steel piping, and large dimensions of the piping.

Assay of the fuel debris will enable accumulation of data on the post-accident condition of the primary system and contribute to the cleanup operation. But further experimentation, using mock-up pipes and fuel standards, is necessary for the application of the passive gamma ray technique.

ACKNOWLEDGMENTS

CONTENTS

FIGURES

TABLES

NONDESTRUCTIVE TECHNIQUES FOR ASSAYING FUEL DEBRIS IN PIPING
AT THREE MILE ISLAND UNIT 2

1. INTRODUCTION

The accident that occurred on March 28, 1979, at TMI-2 constitutes one
of the most severe tests of nuclear power plant safety systems ever, and the
post-accident conditions of the pressurized water reactor offers a unique
opportunity to measure the performance of and damage to instrumentation and
electrical and mechanical equipment resulting from high radiation exposure,
to assess core damage in terms of the metallurgical and physical behavior
of uranium dioxide fuel, zircaloy cladding, control material, and other core
components during and after the accident, and to assess new technological
developments for decontamination and the disposal of radioactive waste.
This experience will expand knowledge of light water reactor behavior fol-
lowing an accident involving severe core damage. The knowledge could lead
to further improvements in nuclear power plant safety, reliability, regula-
tion, operation, and public safety. The object of this report is to evalu-
ate the feasibility of nondestructive techniques for assaying fuel debris
within the primary coolant and connecting piping of the TMI-2 reactor, sel-
ect the best technique, and identify development needs.

Due to severe core damage and subsequent core flooding during the acci-
dent, fuel debris is expected to be dispersed in the reactor's primary cool-
ant system and its connecting piping. A nondestructive technique for
locating fuel debris is expected to (1) contribute to the TMI-2 cleanup
operation, and (2) provide data on accumulation of fuel debris in a primary
coolant system following a severe fuel damage accident. The categories of
techniques discussed are (a) acoustic, (b) nuclear radiation, (c) thermal
radiation, (d) optical, which includes fiber optics and remote video exami-
nation, and (e) pulsed eddy-current. These nondestructive assay techniques
have been investigated by EG&G Idaho Inc., a prime contractor to the Depart-
ment of Energy, and Geo-Centers Inc., a consultant to EG&G Idaho.

In Section 2 we briefly describe the location of fuel debris in the primary coolant system, and present the accident sequence at TMI-2. In Sections 3 and 4, the essential elements of the nondestructive assay techniques and discussion are summarized. In Section 5 we present our conclusions and recommendations. Detailed information on each technique is presented in Appendices A through F.

2. THE LOCATIONS OF FUEL DEBRIS IN THE TMI-2 PIPING

This section describes the TMI-2 primary coolant system and aspects of the accident that may have influenced the location of debris in the piping. Likely debris locations are identified.

The TMI-2 reactor is a pressurized water reactor (PWR) designed by Babcock & Wilcox Co. The system is a two-loop design that employs one once-through steam generator and two reactor coolant pumps in each loop. Thus, the system as a whole is characterized as having two hot legs (A and B) and four cold legs (1A, 2A, 1B, 2B). These six legs connect to the reactor vessel as shown in Figures 1 and 2. The pressurizer surge line connects to hot leg A. From the reactor vessel outlet nozzles, the hot leg piping extends horizontally about 9 ft and rises vertically about 41 ft where it turns 180° and enters the top of the once-through steam generator (OTSG), as shown in Figures 1 and 3. From each steam generator outlet nozzle, cold leg piping extends horizontally about 6.5 ft and rises vertically 36 ft and joins the reactor coolant pump. From the coolant pump outlet nozzle, the cold leg piping extends about 26 ft, and decends 4.5 ft before reaching the inlet nozzle of the reactor pressure vessel. The inner diameters of the hot leg and cold leg are, respectively, 36 in. and 28 in., and the wall thick-nesses are, respectively, 2.875 and 2.250 in. The pressurizer is connected by a 10-in. ID surge line (1 in. thickness) to hot leg A, and by a 2.5-in. ID spray line to cold leg 2A. The primary coolant letdown is removed from the system via a 2.5-in. ID pipe that connects to cold leg 1A upstream of reactor coolant pump 1A. The decay heat removal system is fed by a 12-in. ID line connected to hot leg B. The core flood and decay heat removal sys-tem is fed by 14 in. ID piping as shown in Figure 2.

The TMI-2 reactor accident was initiated by a loss of feedwater to the steam generators, resulting in a turbine trip. The pressurizer relief valve opened several seconds after the turbine trip and remained open.[1] The block valve (RC-V2) was closed for 2 hours 20 minutes into the accident. At 15 minutes after the turbine trip, the reactor coolant drain tank rupture disk burst causing flooding of the reactor building sump. At 1 hour

3
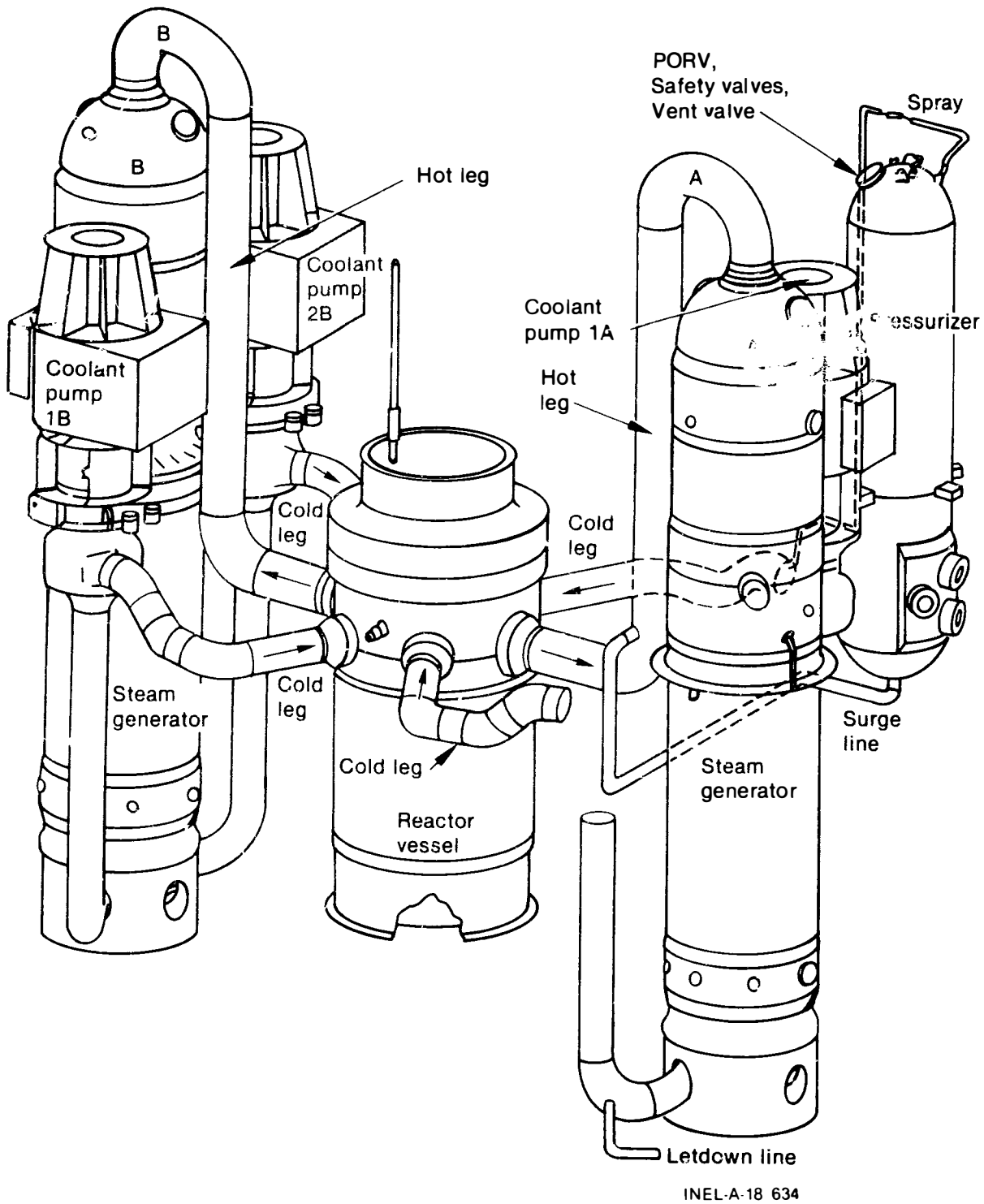
Figure 1. Isometric drawing of the TMI-2 reactor primary coolant system.
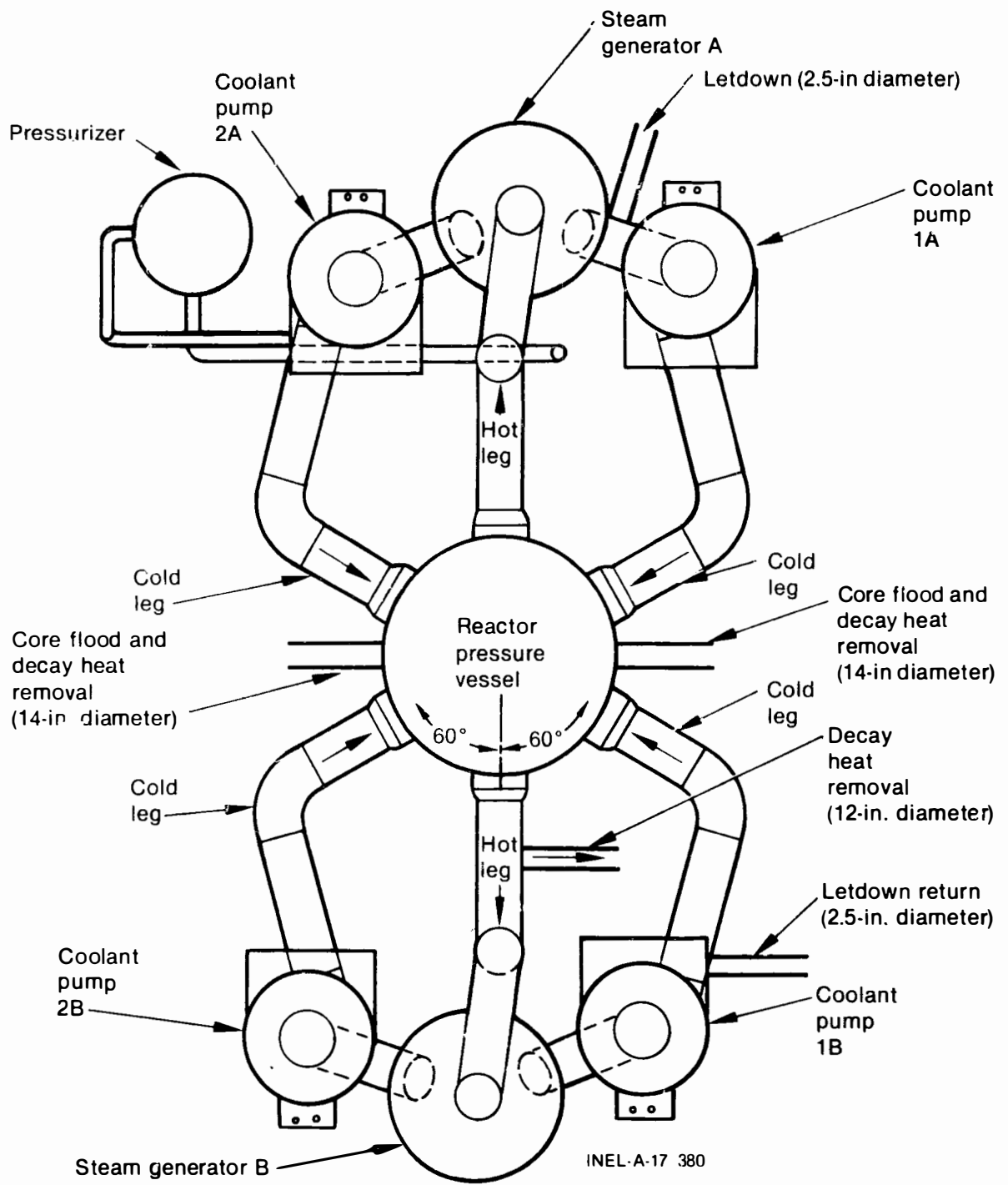
Figure 2. Schematic drawing of the TMI-2 reactor primary coolant system.

5

Reactor Coolant (T_H)
Inlet

Upper plenum

Tube sheet

Emergency
feedwater inlet
(auxiliary feed
nozzles)

Tubes

Baffle

Steam outlet

Bypass steam
for feedwater
heating

Feedwater
inlet

Downcomer
section

Shell

Tube sheet

Lower plenum

Reactor coolant
outlets (T_C)

INEL-A-18 636
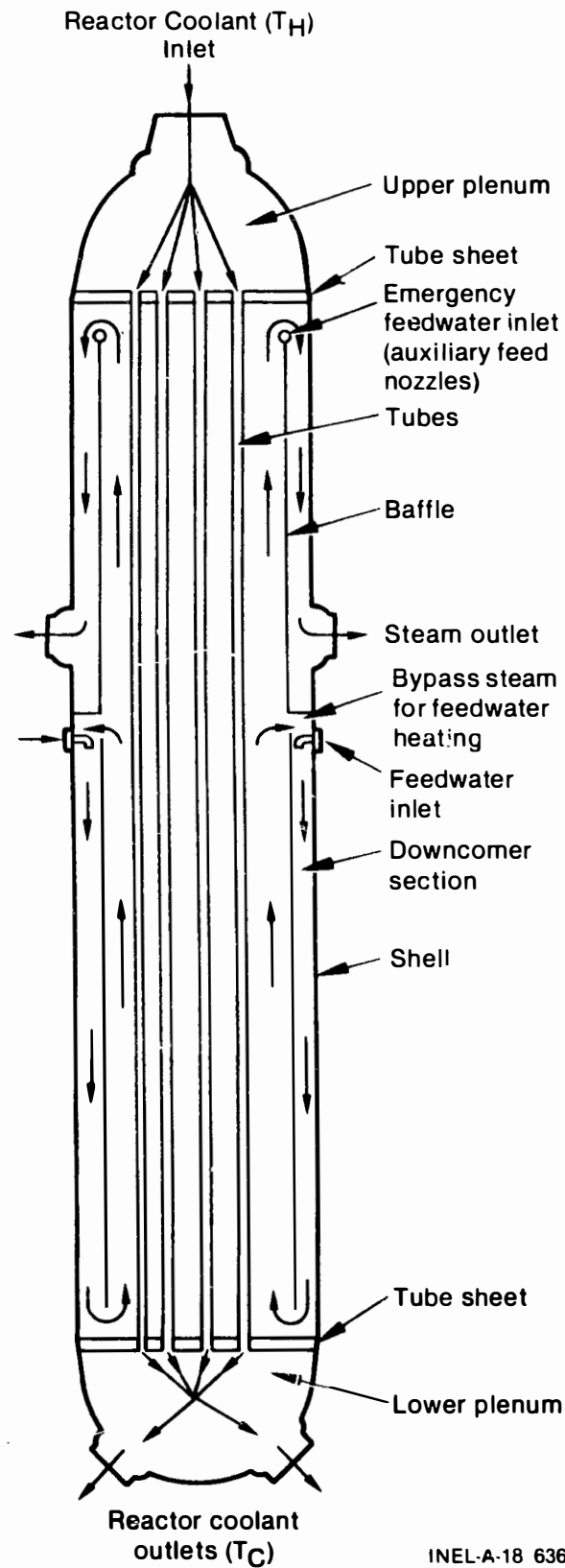
Figure 3. Once-through steam generator.

13 minutes, the reactor coolant pumps in loop B were stopped. At 1 hour 41 minutes, both remaining reactor coolant pumps in loop A were stopped because of increasing vibration and erratic coolant flow. Reactor coolant was purposely channeled to the letdown line for RCS volume control and purification. This resulted in the contamination of the demineralizers, flow lines, coolers, volume control tank, bleed tanks, and charging pumps of the makeup and purification system. Coolant loss caused the upper region of the reactor core to become uncovered, which eventually resulted in fuel rod heat-up in the uncovered region. This condition persisted long enough to cause significant core damage and release of fission products from the fuel rods. When the core was quenched, extensive fuel rod fragmentation may have occurred because the cladding was severely embrittled. A detailed description of the probable status of the core is contained in Reference 2.

The most likely locations within the primary coolant system for concentrations of fuel debris are (a) the hot leg elbows, (b) the horizontal portions of the cold and hot legs, (c) the cold leg elbows beneath the reactor coolant pumps, (d) the upper and lower plenums of the once-through steam generators (OTSGs), (e) the bottom of the pressurizer, and (f) the rough and irregular inner surfaces of vertical pipes. Hot leg fuel debris is limited in size to particles whose diameters are less than the diameter of the holes in the perforated guard plate of the outlet nozzle. The size of fuel debris in the cold leg and the lower plenum of the OTSG is limited by the 1.4-cm ID of the steam generator tubes. Fuel debris larger than 1.4-cm ID of the OTSG tubes is expected to be lodged on the upper plenum sheet of the OTSG, shown in Figure 3. Access to the upper and lower plenums of the OTSGs is practical through the 16-in. man ways and 5-in. inspection openings. All debris is expected to consist primarily of UO_x (oxidized) fuel pellets, fragments, fine particles, and nonfuel debris from cladding and structural materials.

The boron level has been maintained at >3500 ppm since the accident. Criticality calculations[3] suggest that subcriticality can easily be maintained at 3 000 ppm boron, assuming the fuel to be in a reflected sphere at the optimum fuel-to-water-volume ratio (63% fuel in borated water) and taking no account for any structural, cladding, or neutron absorbers.

7

3. NONDESTRUCTIVE FUEL DEBRIS ASSAY TECHNIQUES

The nondestructive fuel debris assay techniques investigated are divided into five broad categories primarily based on acoustics, nuclear radiation detection, thermal radiation detection, optical techniques (which include fiber optics and remote video examination), and the pulsed eddy current technique. Acoustic techniques include the pulse-echo and reflected sound intensity methods; the former is based on the time required for an echo to return, and the latter on the reflected sound spectrum. Degradation of the acoustic signal by the insulation around the coolant pipe is a major problem with the ultrasonic techniques. The insulation would need to be removed in order to use this technique effectively. The radiation detection techniques include gamma spectral scanning and neutron counting of radiation emitted by isotopes that have been retained by the fuel. The thermal radiation detection technique measures infrared (IR) emission from the thermally warm debris; the heat being used as a signature to differentiate debris from its cooler surroundings. The fiber-optics technique is not feasible because of low radiation (10^3R cummulative dose) tolerance, difficulty in obtaining a water tight seal around the lens, problems associated with bending the fiber bundle, and difficulty in obtaining adequate bundle length for the TMI-2 application. Remote video examination has field proven technology, but it is feasible only after the reactor core head is removed. The pulsed eddy current technique is not feasible for assaying fuel debris because of the magnetic effects of carbon steel piping, nonmagnetic properties of ceramics (uranium dioxide and zirconium oxide), and the difficulty in obtaining large coils suitable for the dimensions of TMI-2 piping. A brief description of techniques, detection systems, and detection limits are presented in Sections 3.1 through 3.5. A brief summary of detection limits, advantages, and disadvantages is presented in Section 4. Detailed investigations of these techniques are presented in Appendices A through F.

3.1 Acoustic Techniques

Acoustics, the science of sound, describes the phenomenon of mechanical vibrations and their propagation in solids, liquids, and gases. Sound below approximately 10 Hz and above 15 to 20 KHz is inaudible to the human ear.

8

Sound waves above 20 kHz are arbitrarily referred to as ultrasonic. The ultrasonic frequencies appropriate for penetration and measurement of materials and geometries in TMI-2 piping range from 0.5 to 5.0 MHz. These frequencies correspond to wave lengths of 1.2 to 12.0 mm, and are easy to generate and detect with commercially available equipment. An ultrasonic transducer operated in the pulse-echo mode can be used to examine the inside surface of a pipe.

When ultrasound is incident normal to a boundary, part of the sound pressure is reflected and part is transmitted. The reflected (R) and transmitted (T) sound pressures are respectively given by

$$R = \frac{W_2 - W_1}{W_2 + W_1} \tag{1}$$

and

$$T = \frac{2 W_1}{W_2 + W_1} \tag{2}$$

where

$$W_1 = \rho_1 V_1$$

and

$$W_2 = \rho_2 V_2$$

are the acoustic impedences of materials 1 and 2, respectively, and ρ_i and V_i ($i = 1,2$) are densities and velocities of sound in the respective media.

Ultrasonic sound waves show interference effects when incident on boundaries such as pipe insulation/pipe wall, or pipe wall/water, or water/debris. Each of these media, pipe insulation, pipe wall, water, and

fuel debris has a distinct acoustic impedence (W_i), and a portion of the
energy is reflected and transmitted at each boundary. For example, the hot
leg piping wall is carbon steel and is 3 inches thick. The pipe is clad on
its inner surface with 0.313-in.-thick type 304 stainless steel, and is
shrouded by a 3.5-in. shell of "metallic mirror" insulation. The inner and
outer insulation shell walls are 0.037- and 0.019-in.-thick stainless steel,
respectively. Between the insulation shell walls are 13 evenly spaced con-
centric cylindrical sheets of stainless steel, each 0.004 in. thick. Since
each boundary degrades the reflected and transmitted sound energy, acoustic
methods are impractical for piping surrounded by metallic mirror insulation.
Debris in the lower and upper plenums of the OTSGs can be assayed with the
ultrasonic technique through the inspection access, radiation level
permitting.

3.1.1 Ultrasonic Detection Methods

Debris within a pipe can be detected by introducing a beam of ultra-
sound at the top outside surface of the pipe without insulation. The sound
beam passes through the pipe wall, through the water in the pipe, and is
reflected from the surface to be examined. The pipe is scanned in a raster
pattern to examine the inner surface of the pipe for the presence of debris.
The geometry for ultrasonic detection and characterization of debris in the
piping without insulation is presented in Figure 4.

Two extreme cases of debris configuration, large pieces and thin layers
of fine powder, are expected to be present in the primary piping system.
Large pieces of UO_x fuel, zircaloy cladding, and structural materials can
be detected from range and amplitude measurements. The time required for
the ultrasound echo to return to the transducer (detector) is proportional
to the distance (range) from the transducer to the surface of interest.
From the reflected ultrasound, a small computer constructs either a contour
map or perspective display of distance to the target. The contour map and
perspective display are images of the surface and any debris on it. The
contour map is an exact analogy to a topographic map of a valley (pipe sur-
face) and hills (debris). From the same reflected pulse, a map of reflected
sound amplitude of the surface can also be constructed. The amplitude map

10

Scanning

Transducer

Sound beam

Debris

INEL-A-17 376
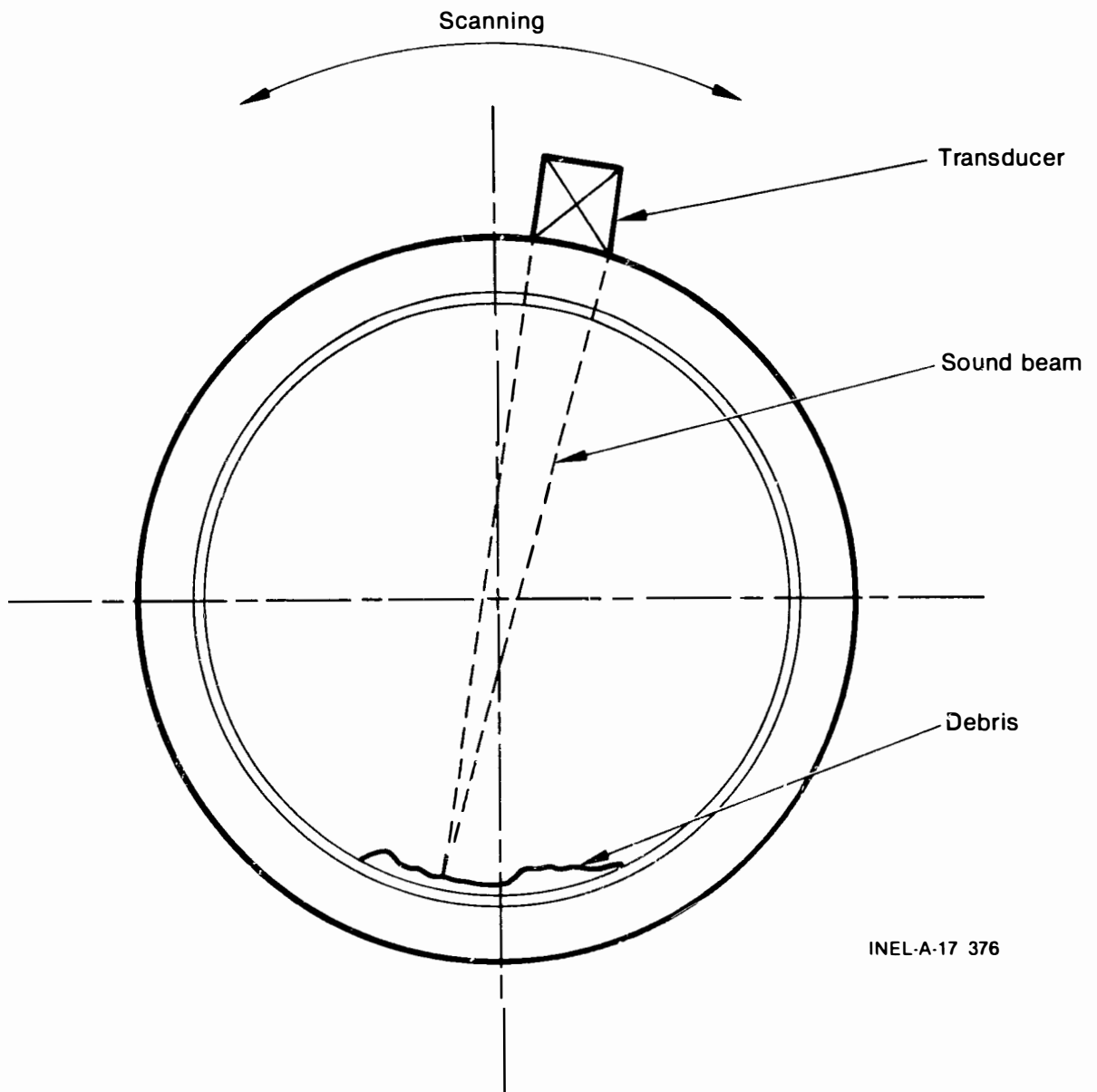
Figure 4.   Geometry for ultrasonic detection and characterization of debris
in TMI-2 piping without insulation.

represents an image of surface reflectivity. An amplitude map prepared by the Idaho National Engineering Laboratory (INEL) Automated Ultrasonic Testing System (AUT) is presented in Figure 5. This map is the image of a weld root and a pipe counterbore. Figure 5(a) is a contour map, and 5(b) is a perspective display of the same data. The irregular indication running from top to bottom at left-center of Figures 5(a) and 5(b) is the weld root. The more regular, isolated indication at right-center is the pipe counterbore. To the extreme left, are small and scattered indications of weld splatter. The contour maps will certainly reveal the presence of large fuel pieces, whole pellets and large pieces of nonfuel debris, and can be applied for assaying debris in other systems such as lower and upper plenums of OTSGs, through manways and inspection openings. However, problems in pattern recognition can be encountered in the mapping of small particles and layers of fine powder.

The presence of small particles and layers of fine powder can be detected from the reflected sound spectrum. The same reflected signal that is used to construct topographic maps is used to obtain the reflected sound spectrum. The signal is subjected to a fast fourier transform from which the computer calculates the reflected sound intensity per unit frequency and unit incident energy. Experiments conducted with sand and water at INEL show that there are signatures in the reflected spectra that are characteristic of the geometry of fine particles that have settled out of water. The signatures result from the coherent scattering from particles much smaller than the sound wavelength, and from interference effects within the sand layer and the underlying surface. Since the ultrasonic method depends on media densities, a mass measurement would be feasible. However, mass measurement depends on certain conditions, namely, configuration volume, porosity fraction, and effective density of fuel debris.

3.1.2 Ultrasonic Detection System

The ultrasonic detection system consists of electronic (computer) and mechanical hardware. The type of system that can be used for ultrasonic measurements at TMI-2 is shown in Figure 6. The system is field

12
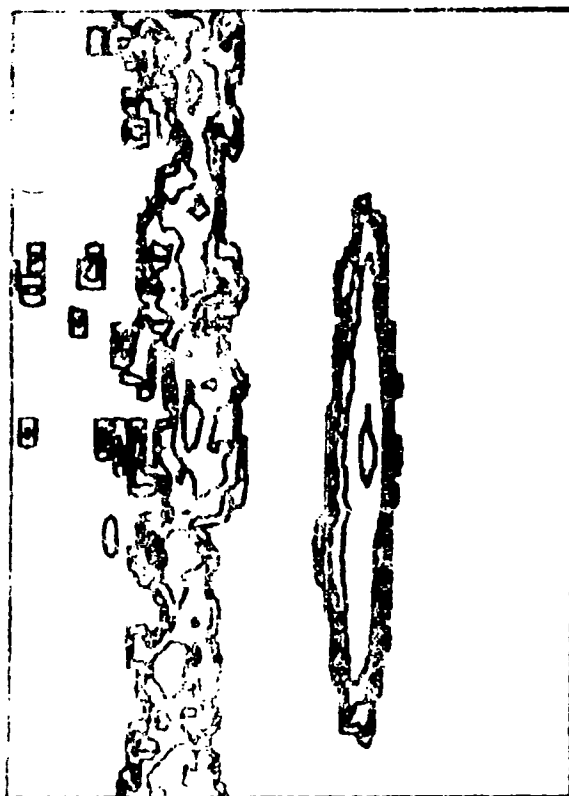
5(a)   A contour map.
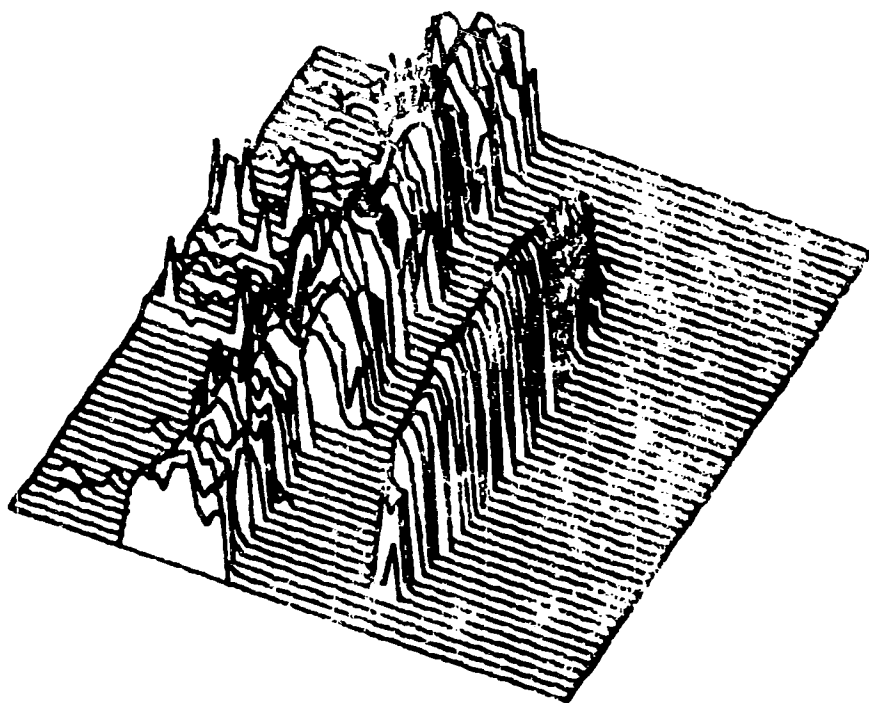
5(b)   Perspective display of same data.

Figure 5.   Signal amplitude map of a surface inside a pipe.
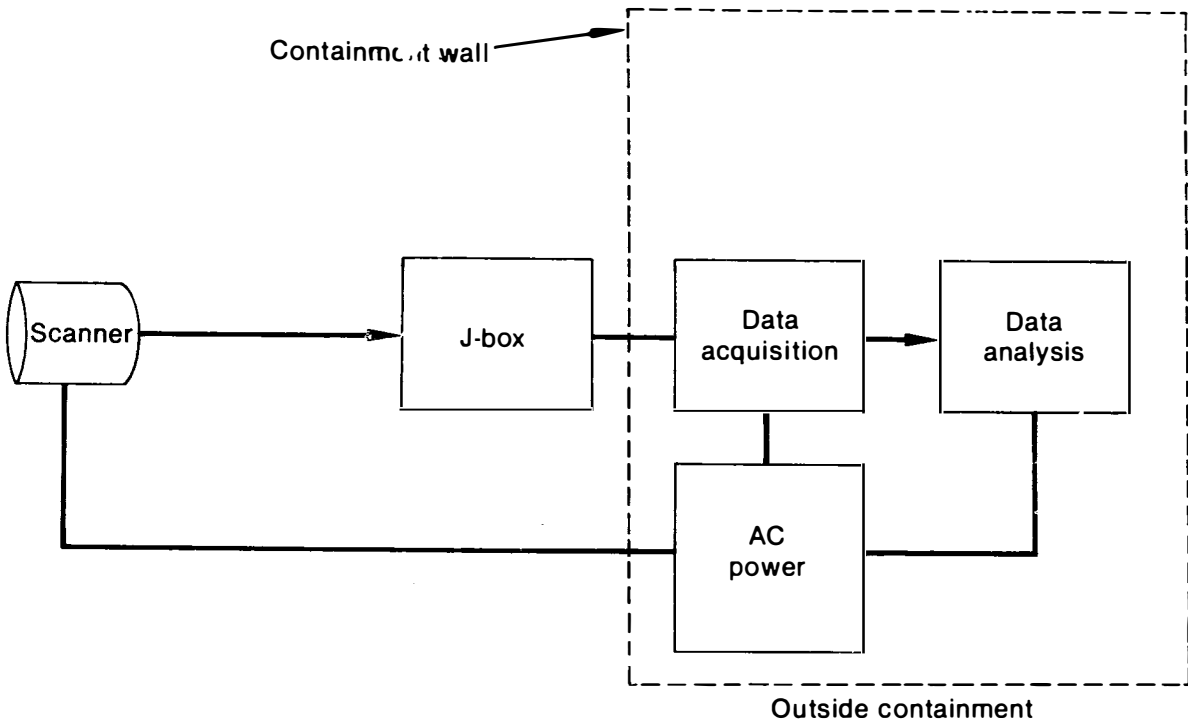
13

Figure 6.   Automated ultrasonic testing system.

INEL-A-18 633

transportable, and is being used at the Loss-of-Fluid Test (LOFT) Facility at INEL. It was designed for examining relatively narrow strips at and near welds in piping; however, it could be modified for TMI-2 measurements. The basic computer software for mechanical control, data acquisition, data processing, and display exists at EG&G Idaho's Nondestructive Evaluation Engineering Laboratory. The automated ultrasonic testing (AUT) system shown in Figure 6 consists of a scanner, a J-box, and a data acquisition and analysis system. The J-box serves as a junction box between the data acquisition and analysis system that is outside the containment, and the scanner inside the containment. The scanner can be located up to 500 feet from the J-box. Details of the data acquisition and analysis system, including AC power requirements, are presented in Appendix A. The AUT system is housed in an air-conditioned semi-trailer for easy transport.

3.1.3 Ultrasonic Detection Limits

Experiments performed at INEL suggest that an ultrasonic transducer operated in a pulse-echo mode is capable of detecting and locating (by range and amplitude maps) the full range of potential fuel debris configurations, from complete fuel pellets through broken pellets and pieces of nonfuel debris. The longitudinal resolution for this measurement is about 0.25 mm. On the other hand, spectral experiments using fine powders of sand (silicon dioxide) under water suggest that, under field conditions, it is possible to detect and map the location of powder deposits with thicknesses as little as 0.13 mm. Under ideal conditions in the laboratory, it is possible to detect the presence of even finer grains scattered independently on a smooth surface. From the same ultrasound echo, the ultrasonic detection system is capable of obtaining range and amplitude maps of large pieces, and spectral maps of fine powders. Since mass measurement depends on effective density of debris, the minimum detectable mass ranges from 4.5 to 8.4 mg of U per m of pipe length. These limits are based on effective densities ranging from 50 to 93% of theoretical density.

3.2 Nuclear Radiation Detection Techniques

Two kinds of nuclear radiation detection techniques are considered: passive and active. Passive techniques involve the detection of gamma rays and neutrons emitted by the irradiated fuel; active techniques involve the detection of nuclear radiation induced by interrogation of the fuel debris with a neutron source. Passive techniques, namely gamma spectral scanning and counting of neutrons that are emitted due to (α, n) reactions and spontaneous fission events are presented in Sections 3.2.1 through 3.2.3.

The active neutron interrogation techniques considered employ either isotopic neutron sources (e.g., ^{88}YBe, ^{252}Cf) or a Cockroft-Walton neutron generator. The requirement that the isotopic sources be substantially shielded, and the potential hazard they present to personnel, are disadvantages that make them less attractive than the neutron generator. The detection limits achievable with neutron techniques are found to be substantially larger than those achievable using a passive, gamma-ray assay technique. In light of the disadvantages of the activation techniques, only the passive techniques are presented here. The active techniques are presented in Appendix B.

3.2.1 Gamma-Ray Detection and Analysis

The gamma rays associated with the decay of fission products can be measured using a high-resolution gamma-ray spectrometer. This technique relies on the detection of signature gamma rays of ^{144}Ce, ^{154}Eu, or other radioactive isotopes that have been retained by the fuel. The amount of fuel in a primary coolant system pipe can be determined using these measurement data, if the fuel isotopic composition is known. The Oak Ridge National Laboratory isotopic generation and depletion code ORIGEN was used to estimate fission product activity concentration for the TMI-2 fuel; the results are presented in Table 1. The fission products ^{134}Cs, and ^{137}Cs are known to migrate toward the cooler radial and axial regions of the fuel and are water soluble, and are therefore expected to be leached when the fuel is exposed to the coolant. The fission product ^{106}Ru is volatile and tends to concentrate around the centerline of a fuel pellet.

16

TABLE 1.   ISOTOPIC ACTIVITY CONCENTRATIONS PER GRAM URANIUM
(As of June 1982)

Nuclide	dps/g U	Nuclide	dps/g U
93 Zr	1.24 E + 04	Cs 137	3.72 E + 08
95 Zr	1.28 E + 05	Ce 144	6.14 E + 08
95 Nb	2.76 E + 05	Eu 154	3.06 E + 06
106 Ru	1.49 E + 08	Eu 155	4.10 E + 06
125 Sb	1.13 E + 07	U 235	2.41 E + 03
134 Cs	4.68 E + 07	U 238	1.20 E + 04

High gamma-ray flux per gram of uranium deposited on the lower inside surface of a pipe can be measured at Detector Position 5, as illustrated in Figure 7. Calculated uncollided fluxes (S_j) at Detection Position 5 are listed in Table 2. From the source term and the detector geometry, S_j is calculated using the computer code QAD. The calculation includes the pipe insulation. The count rate of a detector subjected to this flux can be calculated, if the intrinsic photopeak efficiency and surface area of the detector are defined. The isotopes ^{144}Ce and ^{154}Eu are selected as the most suitable for gamma ray detection because of their chemical inertness, low volitility, long half-lives, and associated high-energy gamma-rays. Cesium and ruthenium isotopes are not considered because of their migration and leaching characteristics.

The conceptual design of a gamma-ray detection and analysis system is presented in Figure 8. The system consists of a hyperpure germanium detector housed in a collimator shield and fixed on the end of a telescopic boom having three degrees of freedom. The electronics includes a preamplifier, analog-to-digital converter, analog pulse shaping modules, and a pulser. A multichannel, pulse-height analyzer (MCA) is mounted within a mobile rack which houses the electronics system. For remote data acquisition, the MCA is interfaced to a central processing unit (CPU) located outside the reactor building.

A portable gamma spectrometer system was developed by EG&G Idaho for use in the TMI-2 reactor and auxiliary buildings, and spectra were taken at locations within these buildings during May 1981. A Princeton Gamma Tech.,
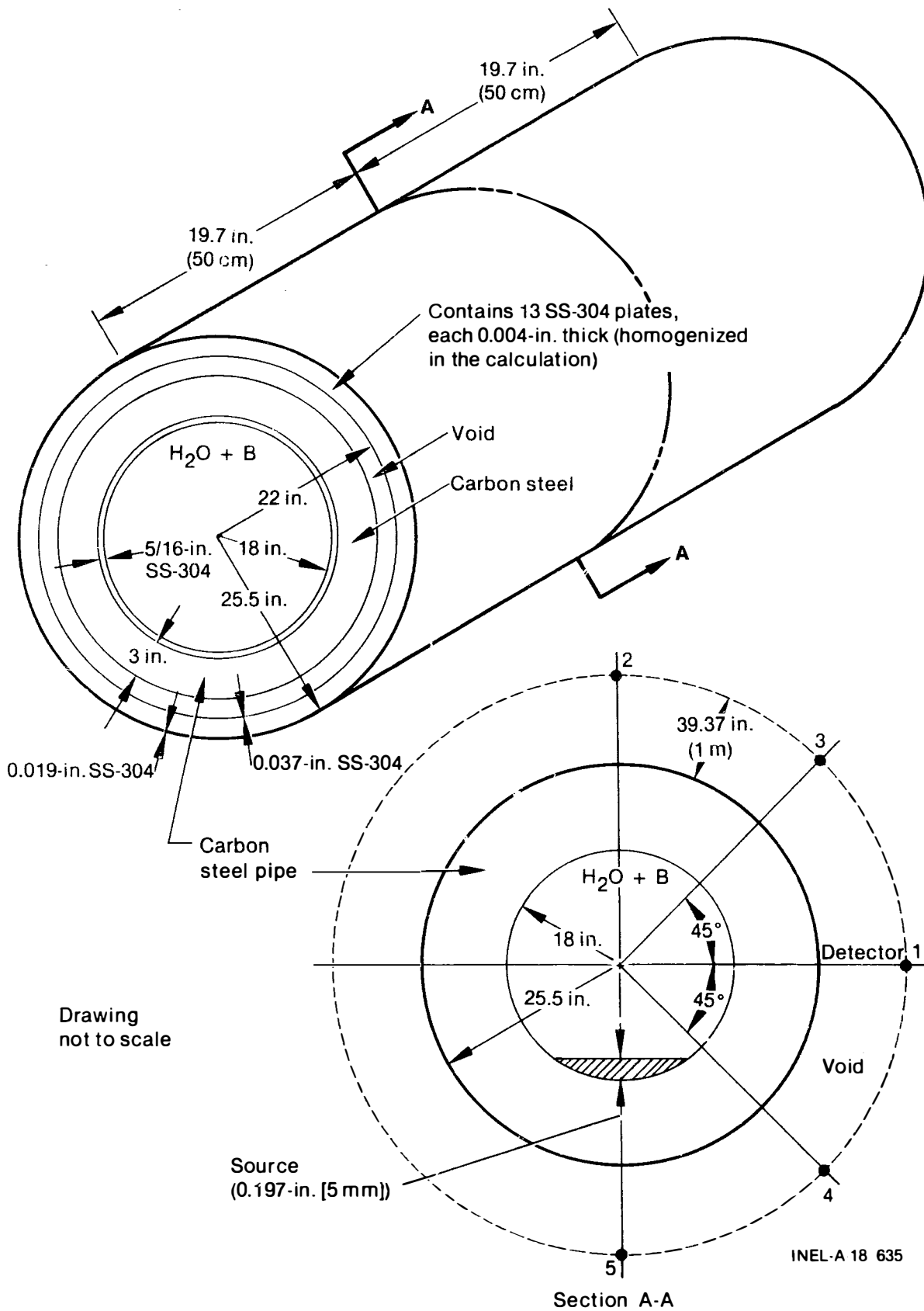
Figure 7. Cross-section of TMI-2 hot leg piping and insulation.

18

TABLE 2. UNCOLLIDED GAMMA RAY FLUX PER GRAM URANIUM AT DETECTOR POSITION 5
(As of June 1982)

Nuclide	Half-Life	Energy (keV)	Branching Intensity (%)	Uncollided Flux γ/cm^2-s/g U
137 Cs	30.174 Y	661.645	8.50 E + 01	1.03 E + 01
134 Cs	2.062 Y	795.845	8.54 E + 01	1.97 E + 00
144 Ce	284.4 D	2 185.700	6.94 E - 01	1.26 E + 00
134 Cs	2.062 Y	604.699	9.76 E + 01	1.17 E + 00
106 RuD	368.2 D	621.800	9.81 E + 00	4.05 E - 01
144 CeD	284.4 D	696.480	1.34 E + 00	3.04 E - 01
144 CeD	284.4 D	1 489.150	2.78 E - 01	2.94 E - 01
134 Cs	2.062 Y	1 365.150	3.04 E + 00	2.12 E - 01
134 Cs	2.062 Y	801.932	8.73 E + 00	2.04 E - 01
106 RuD	368.2 D	1 050.100	1.46 E + 00	1.96 E - 01
134 Cs	2.062 Y	569.315	1.54 E + 01	1.60 E - 01
154 Eu	8.5 Y	1 274.450	3.55 E + 01	1.44 E - 01
134 Cs	2.062 Y	1 167.940	1.80 E + 00	9.45 E - 02
134 Cs	2.062 Y	563.227	8.38 E + 00	8.47 E - 02
125 Sb	2.71 Y	600.770	1.79 E + 01	5.08 E - 02
154 Eu	8.5 Y	1 004.760	1.74 E + 01	4.34 E - 02
134 Cs	2.062 Y	1 038.570	1.00 E + 00	4.11 E - 02
125 Sb	2.71 Y	636.150	1.15 E + 01	3.83 E - 02
125 Sb	2.71 Y	427.950	3.00 E + 01	3.52 E - 02
154 Eu	8.5 Y	996.320	1.03 E + 01	2.52 E - 02
154 Eu	8.5 Y	723.300	1.97 E + 01	2.42 E - 02
125 Sb	2.71 Y	463.510	1.05 E + 01	1.55 E - 02
125 Sb	2.71 Y	606.820	4.92 E + 00	1.44 E - 02
95 Nb	35.1 Y	765.781	9.98 E + 01	1.25 E - 02
154 Eu	8.5 Y	1 596.480	1.67 E + 00	9.84 E - 03
238 U	4.47 E + 09 Y	1 001.100	8.28 E + 01	8.08 E - 06
238 U	4.47 E + 09 Y	766.390	3.13 E - 01	1.73 E - 06
235 U	7.04 E + 08 Y	185.720	5.400 E + 01	3.19 E - 07

Figure 8. Gamma-ray acquisition and analysis system.

INEL-A-18 632

20

Inc., intrinsic germanium detector was mounted on a cart and shielded with approximately 500 lbs of lead brick. The shield was constructed so as to allow collimation in both horizontal and vertical directions. A detailed description of the system and a presentation of the results of the measurements are reported in an internal technical report of the EG&G Idaho physics division.

3.2.2 Gamma-Ray Detection Limits

The minimum detectable levels of fuel in the primary piping with insulation are presented below, for a germanium spectrometer with a front face surface area of 15 cm^2 located at detecter position 5. Intrinsic photopeak efficiencies were estimated, using the measured absolute efficiency of a Ge (Li) spectrometer for a point source at a distance of 30 cm. A live time of 1 000 s and background count rates equal to 10% of the source full-energy peak count rates were assumed. The detection limits presented in the following table range from 47 to 110 mg U per meter of insulated pipe.

Nuclide	(keV)	Detectable Level (mg U) per meter of insulated pipe
^{144}CeD	2 186	47
^{144}CeD	1 489	84
^{154}Eu	1 274	110
^{144}CeD	697	54

If the source distribution is discrete, then the detection limits are smaller than the values given above.

3.2.3 Neutron Counting and Detection Limits

The spontaneous fissioning of transuranic isotopes (eg., ^{238}Pu, ^{240}Pu, ^{242}Cm, and ^{244}Cm) produces neutrons, but they may also decay by the emission of alpha particles, which interact with light elements such as oxygen and produce singly emitted neutrons [e.g., ^{16}O (α,n) ^{19}Ne].

21

The neutron source strength per gram of UO_x due to spontaneous fissioning of even mass transuranics and (α,n) reactions has been calculated for the TMI-2 fuel inventory, and is presented graphically as a function of time through 1983 in Figure 9. The source strength remains essentially constant at a value of 0.34 n/s·gUO_x beyond January 1, 1980.

The source strength can be determined from the neutron flux (n/cm^2·s) at a detector location external to a pipe containing a source and the detector geometry. Neutron detectors, which consist of four helium-filled proportional counters embedded in a polyethylene moderator, have intrinsic efficiencies of about 10%; an efficiency of 5% was assumed for the detectors. The surface area of the detector considered in this investigation is about 1×10^3 cm^2.

Given a UO_x linear concentration of 1 g/cm in a pipe (with insulation), the passive neutron count rate would be 5.5×10^{-2} cps. The minimum detectable fuel concentration for a 1 000 s count is 4.7×10^5 mg U per meter of pipe.

3.3 Thermal Radiation Detection

Infrared (IR) radiation is thermal radiation of wavelengths longer than 0.75 µm, ranging to about 1000 µm. IR radiation detectors are sensitive to ambient thermal radiation and changes in temperature of the surroundings. An increase in the wall temperature of TMI-2 primary piping would occur due to decay heat if fuel were deposited in the piping. Thus, the measurements of the localized temperature increases along the surface of the primary pipe wall should indicate the location and quantity of fuel deposited in the primary system.

In Appendix D, the outside pipe wall temperature T_{sw} due to a finite thickness of fuel deposited in the pipe is calculated from heat conduction in a plane wall with convective cooling of walls and with a heat source. Since the radius and length of the pipe are sufficiently large compared to

22
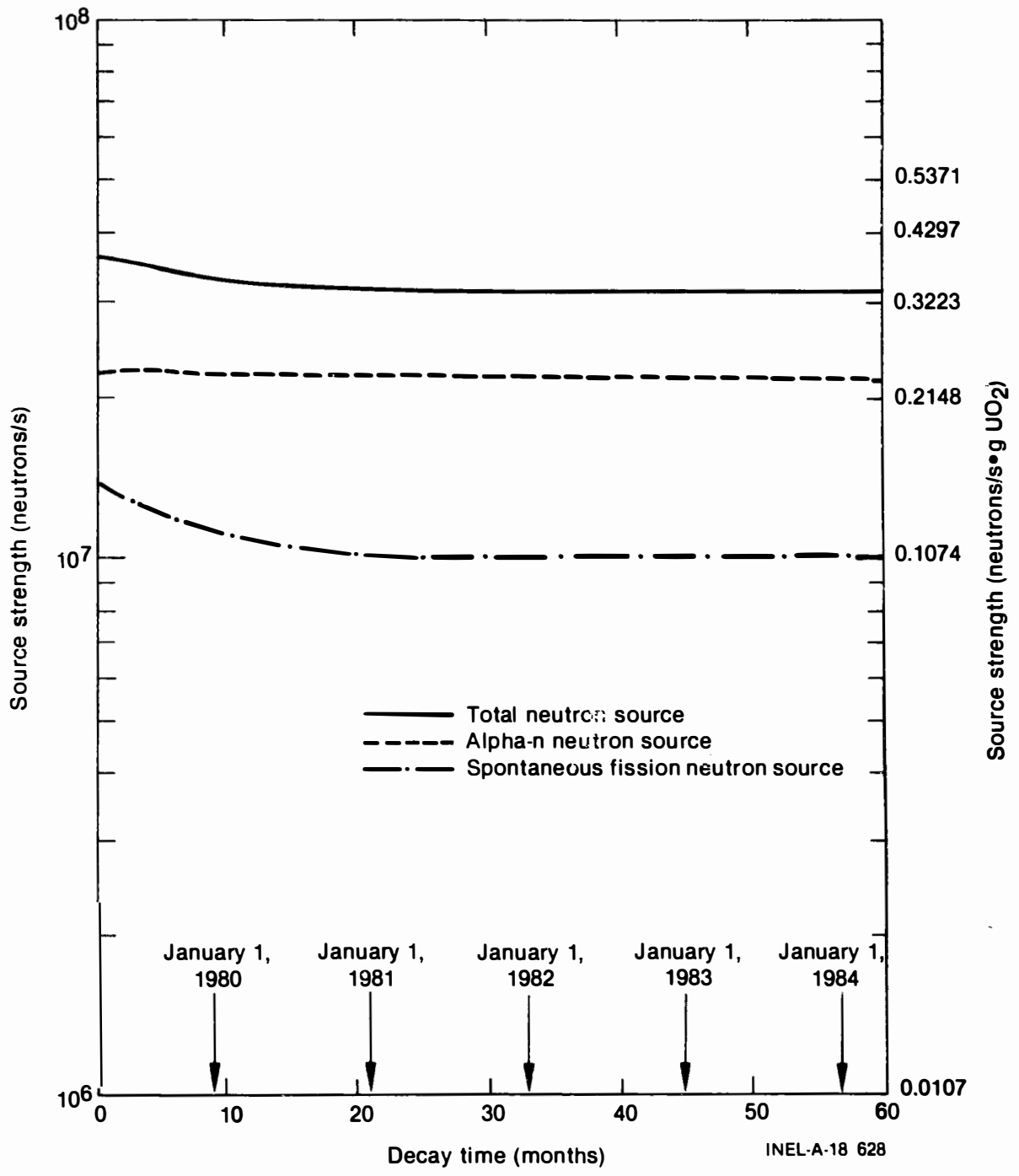
Figure 9.   Neutron source strength in TMI-2 full core inventory.

wall thickness, only one-dimensional slab geometry was assumed. Circumferential heat losses in the pipe have been neglected. Consequently, the temperature (T_{sw}) at the surface of the insulated pipe will be somewhat less than that calculated with this assumption. It is also assumed that the system is in a steady state condition. The increase in wall temperature is $\Delta T = T_{sw} - T'_{sw}$ where T'_{sw} is the ambient temperature of the outside, insulated pipe wall, in the absence of fuel deposition. A plot of fuel layer thickness in an insulated pipe and ΔT is shown in Figure 10. Details of the infrared technique are presented in Appendix C.

A number of infrared thermographic systems are available, the characteristics of which are summarized in Table C-3. A thermographic probe with a Hg-Cd-Te-detector would be suitable for assaying debris in the TMI-2 piping. The Hg-Cd-Te-detector system is portable, and the output can be displayed on a television monitor or a video tape recorder.

3.3.1 Limit of Infrared Radiation Detection

The minimum detectable temperature difference of the Hg-Cd-Te detector is 0.36°F (0.2 K), and the temperature range is -4 to 2732 °F (253 to 1773 K). The infrared technique can be used to detect fuel deposition in the insulated primary coolant pipe provided $\Delta T > 0.36°F$ (0.2 K). From Figure 10, the minimum thickness of fuel layers that can be detected with an infrared probe is about 9 mm. The detection limit is relatively high for assaying debris.

3.4 Optical Techniques

The optical techniques investigated for this report include fiber optics and remote video examination.

The use of fiber optics has been investigated for the inspection of the reactor vessel used in the loss of fluid test (LOFT) at the Idaho National Engineering Laboratory. The investigation suggests that the fiber optics technique is currently limited. The technique is not suitable for assaying
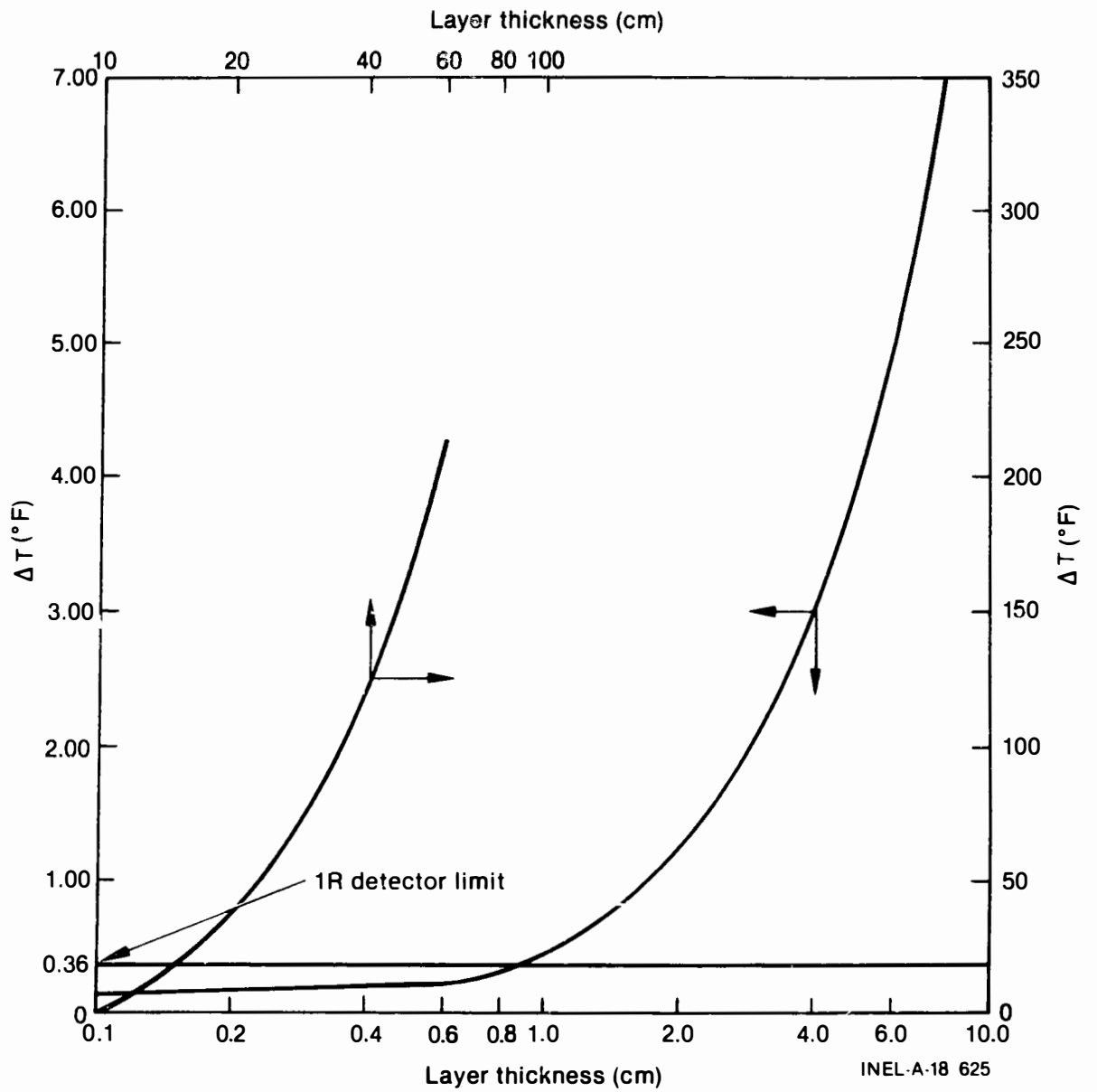
24

Figure 10. Plot of ΔT versus debris layer thickness.

25

fuel debris in the primary coolant system at TMI-2 because of low radiation tolerance (10^3 R cumulative dose), difficulty in obtaining a watertight seal around the fiber bundle lens, difficulties associated with bending the insertion into fiber bundle, and difficulty in obtaining bundles with sufficient length for TMI-2 piping.

Remote video examination is feasible for assaying debris. The system is field proven and is designed for rugged and demanding environments: operating temperatures from -13 to +140 F (248-333 K), an underwater depth of 900 ft (272 m), and a gamma radiation total absorbed dose of 10^8 R. Video examination systems are being used in a number of nuclear utilities for monitoring critical areas.

The disadvantage of using this technique in TMI-2 piping is that the reactor core head must be removed to gain access to the piping. Also, the hot leg guard plate may cause problems for inserting the camera's viewing head.

3.5 The Pulsed Eddy-Current Technique

The pulsed eddy-current technique has been successfully used in detecting cladding surface defects and in measuring cladding wall thickness of light water reactor type fuel rods.[4]

The system uses a series of current pulses to induce eddy currents in the specimen under investigation. The eddy currents are influenced by the permeability, conductivity, and wall thickness of the material under investigation, and the distance between the probe and the sample. The eddy currents produce a pulsed magnetic field that induces a voltage field in the primary coil.

The pulsed eddy-current technique is not suitable for TMI-2 piping, because of large dimensions (36-in. diameter and 3-in. wall thickness), which cause distortion in eddy currents, interference caused by the magnetic effects of carbon steel, and inaccessibility to the piping. Also, nonmagnetic materials such as urania and zirconia cannot be detected.

26

4. DISCUSSION

The major, practical problems associated with the nondestructive assay techniques and with the physical configuration of the TMI-2 piping system are discussed. A suitable technique is selected, based on detection limits and advantages.

Three major problems are expected to be encountered in locating and assaying fuel deposited in the primary piping system of the TMI-2 reactor: (a) accessibility to the primary coolant piping, (b) high radiation fields, and (c) coolant pipe insulation.

Access to the pipes to be interrogated is the primary problem. Floor and platform elevations (in feet) are presented in Figure 11. Cold leg elbows are close to the floor at elevation 282.5 and can be assayed without difficulty. The cold and hot leg horizontal piping have centerlines at elevation 315.5 and can be reached from the floor at the elevation 305. However, about 8 ft of hot leg and 16 ft of cold leg horizontal piping are embedded in the 4-ft-thick primary shield wall. Access to the remaining horizontal piping may be practical from the top of the primary shield wall at elevation 322.5. A detector probe may be extended to the piping by a cable. Access to upper and lower OTSG plenums is possible from floors 347.5 and 282.5, respectively.

High radiation in the containment building may pose a problem. During August 1980, radiation measurements were taken at elevations 305 and 347.5. Gamma radiation ranged between 2 to 45 Rem/hr and 0.05 to 2.5 Rem/hr, respectively. At the time of debris deposition measurements, the radiation field is expected to be substantially reduced, and sensitivities of the detectors used for locating debris are not expected to be affected by radiation. However, the exposure time of the personnel conducting the fuel debris assay should be minimized.

The walls of the piping are about 3 in. thick. The inner surface is clad with 0.3125-in.-thick 304 stainless steel, and the outer surface is shrouded by a 3.5-in.-thick shell of "metallic mirror" insulation. Evenly

27
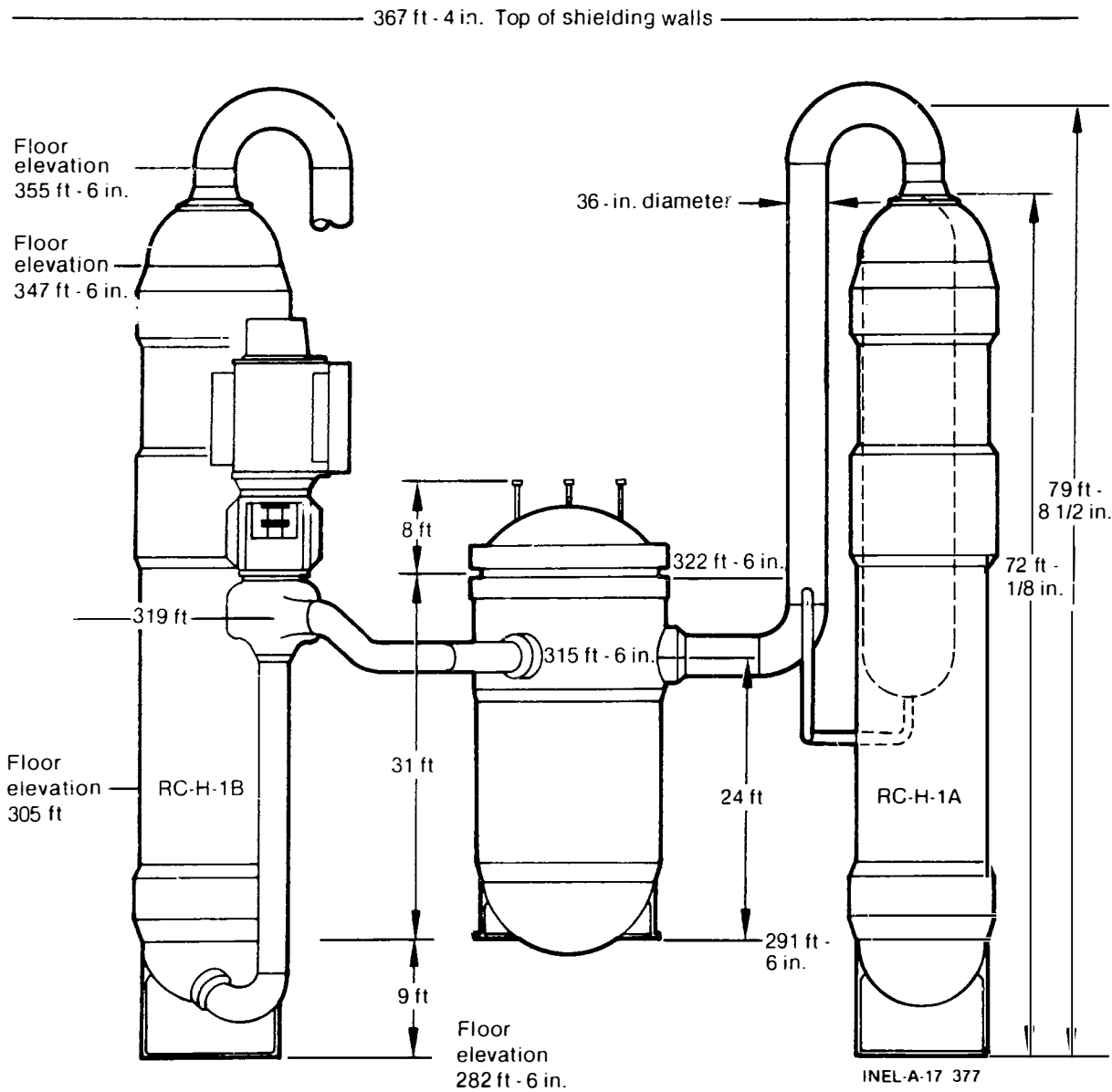
Figure 11. Physical arrangement of TMI-2 coolant system and floor levels.

spaced between the insulation shell walls are 13 concentric cylindrical
sheaths, each 0.004 inch thick. The cross section of an insulated hot leg
pipe is shown in Figure 7. The shell walls of the insulation degrade the
acoustic signal, so acoustic techniques are only feasible if the insulation
can be removed. Removal of the insulation before fuel assaying may not be
possible due to high radiation fields.

Preliminary analysis and experimentation suggest that gamma-ray, neu-
tron counting, and infrared techniques are suitable for assaying pipes with
or without insulation, and ultrasonic techniques are feasible for fuel and
nonfuel debris deposition measurements in pipes without insulation. These
techniques are field-proven, and current technology exists. Fiber optics
and pulsed eddy-current techniques are not suitable for assaying debris.
The remote video technique is feasible provided the reactor core head is
removed to gain accessibility to the piping. Also, the size of holes in the
hot leg guard plate may cause problems for inserting the camera's viewing
head. A brief summary of detection limits, and advantages and disadvantages
is presented in Table 3.

Based on the detection limits and the advantages and disadvantages, the
passive gamma-ray assay technique appears to be the most suitable technique
for fuel debris assay at TMI-2. However, the ultrasonic technique would
also be suitable, if the radiation level will permit removal of the
insulation.

Assaying the fuel debris in the primary coolant system has been the
subject of this report, but passive gamma ray, and possibly ultrasonic
techniques, may be considered also for assaying debris in the following
areas:

1.   reactor buildup sump

2.   auxiliary building sump

3.   pit beneath the reactor vessel

29

TABLE 3. DETECTION LIMITS, AND ADVANTAGES AND DISADVANTAGES OF NONDESTRUCTIVE TECHNIQUES INVESTIGATED

Assay Technique	Detection Limits Without Insulation	Detection Limits With Insulation	Advantages	Disadvantages
1. Ultrasonics	4.5 to 8.4 mg/m of pipe			
a. Amplitude Maps	Complete pellets through broken fuel pellets, and nonfuel debris. Longitudinal resolution ~ 0.25 mm	Not applicable	1. Suitable for detecting fuel and nonfuel debris 2. Not affected by radiation	1. Cannot distinguish from fuel and nonfuel debris 2. Not suitable for pipes with insulation
b. Spectral	Fine powders of ~ 0.13 mm thickness	Not applicable	3. Detection limits excellent 4. Represents proven current technology	
2. Nuclear Radiation (Passive)				
a. Gamma-ray detection	Same or better than with insulation	47-110 mgU per meter of pipe	1. Suitable for detecting fuel debris	1. Not suitable for detecting nonfuel debris
b. Neutron counting	2.8×10^5 mgU per meter of pipe	4.7×10^5 mg U per meter of pipe	2. Suitable for pipes with or without insulation 3. Function in high ambient radiation fields 4. Gamma-ray detection limits very good 5. Represents proven, current technology	2. Neutron detection limits relatively poor
3. Infrared	7.0 mm-thick layer	9.0-mm thick layer	1. Suitable for detecting fuel debris 2. Suitable for pipes with or without insulation 3. Not affected by radiation 4. Represents proven technology	1. Not suitable for detecting nonfuel debris 2. Dependent on ambient containment and primary coolant temperatures and coolant flow rate 3. Minimum detection limits relatively poor

TABLE 3. (continued)

Assay Technique	Detection Limits Without Insulation	Detection Limits With Insulation	Advantages	Disadvantages
4. Optics				
a. Fiber Optics				1. Low-radiation tolerance
				2. Bundle length limitation
				3. Difficulty in obtaining water tight seal around the lens
				4. Bent radii restrictions
				5. Not suitable
				6. State-of-art limitation
b. Remote Video Examination			1. High-radiation tolerance	1. Core head must be removed prior to video examination to gain access
			2. Large transmission distance	2. Holes in the hot-leg guard plate may prevent inserting the camera's viewing head
			3. Can be operated remotely at temperatures ranging from -25 to 50°C	
			4. Water immersible	
			5. Field-proven technology	
5. Pulsed Eddy Current				1. Interference due to magnetic effects of carbon steel piping
				2. Does not detect non-magnetic materials such as UO_2 or ZrO_2
				3. Requires large coils and very low eddy-current frquencies
				4. Not suitable for assaying IMI-2 piping

4.   RCS drain tank

5.   demineralizer

6.   makeup tank and makeup circuit

7.   submerged demineralized system

8.   associated piping.

High radiation levels and accessibility are two major problems to be encoun-
tered. The applicabilities of each technique can be assessed for each
individual system, but this task is beyond the scope of this report.

5. CONCLUSIONS AND RECOMMENDATIONS

From the investigation and analysis of nondestructive techniques appli-
cable to assay of fuel debris, the following conclusions are reached:
ultrasonic, passive gamma-ray and neutron counting, infrared techniques, and
remote video examination are all capable of detecting fuel debris. The
passive gamma-ray counting technique, however, is suitable for detection and
assaying of TMI-2 piping with or without insulation, whereas the ultrasonic
technique is suitable only for pipes without insulation. The passive gamma-
ray and ultrasonic techniques, if both can be used, are complementary.
Together they can locate fuel and non-fuel debris, determine the fuel and
non-fuel fractions, and measure the amount, thickness, and physical distri-
bution of the fuel and non-fuel debris in pipes without insulation. The
passive gamma-ray technique is fuel specific and has an expected detection
limit of 47-mg fuel per meter of insulated pipe. The ultrasonic technique
can detect debris particles that range in size from large pieces to fine
powders. It does not distinguish between fuel and non-fuel debris. By
remote video examination, the primary coolant piping can be surveyed prior
to the use of gamma ray or ultrasonic techniques. However, the reactor core
head must be removed to gain accessibility to the piping for video
examination.

Both the ultrasonic and passive gamma-ray techniques represent proven,
current technology. In order to effectively apply the techniques to the
specific TMI-2 application, however, some further development is necessary.
Such development needs to include determination of the reflective properties
of the water-uranium dioxide interface as a function of ultrasonic frequency,
and ultrasonic and passive gamma-ray experiments using mock-up pipes and
fuel standards. A complete evaluation of practical problems such as removal
of insulation may eliminate further development of ultrasonic techniques.
Further development of the passive gamma technique is needed to optimize the
detection and assay of fuel at TMI-2.

6. REFERENCES

1. M. Rogovin and G. T. Frampton, Jr., Volume II part 2, Three Mile Island, a Report to the Commission and to the Public, NUREG/CR-1250, Vol. II. Part 2.

2. D. W. Croucher, Three Mile Islant Unit-2 Core Status Summary: A Basis for Tool Development for Reactor Disassembling and Defueling, GEND-007, May 1981.

3. F. M. Alcorn and M. R. Gudorf, "Criticality Safety Considerations for TMI-2," American Nuclear Society Transactions, Vol. 35, November 1980.

4. M. E. Yancey et al., "Inspection System for Zircaloy Clad Fuel Rods," TID-4500, October 1975.

APPENDIX A
INVESTIGATION OF ACOUSTIC METHODS FOR DETECTING TMI-2 FUEL DEBRIS

1. INTRODUCTION

As a result of the March 1979 accident at the Three Mile Island-2 (TMI-2) nuclear plant, debris is expected to be distributed throughout those portions of the primary piping system in which water was circulating during the accident. The debris is expected to consist primarily of UO_2 fuel ranging in physical size from fine, flour-like powder to broken pieces and whole pellets, but may include some non-fuel debris coming from cladding and structural materials. It may be assumed that the debris rests on or near the bottom of horizontal pipe runs, with concentrations of debris at the foot of vertical runs.

This appendix details investigations into acoustic (ultrasonic) methods for detecting and characterizing such debris. The basis for the methods is described, and details of confirming experiments are given. Equipment and techniques that might be employed for this service are described in concept; the system is based on field-proven hardware and software. Finally, recommendations on further effort are given.

1.1 Applicable Ultrasonic Considerations

The following is a short discussion of ultrasonic principles and considerations that are directly applicable to the present problem.

Sound is a wave phenomenon. As such, it obeys many of the same equations and shows the same behavior as does light. In fact, many of the results of physical and geometric optics apply directly, at least as analogies.

37

Sound may be refracted at a boundary. Refraction follows Snell's law:

$$\frac{\sin \phi_1}{v_1} = \frac{\sin \phi_2}{v_2}$$

(1)

where ϕ_1 is the angle of incidence on the boundary from a medium having a speed of sound v_1, and ϕ_2 is the angle of refraction in the medium having speed of sound v_2.

Because of refraction, ray paths are deviated when crossing a boundary between media having different v_i. Sound beams may thus be focussed, much as light is, by a lens. Use will be made of this property to distribute the sound on the entry surface of the pipe over a relatively large diameter to average out small irregularities in materials and their properties, then focus the energy on a spot of small diameter for precise measurements on the surface of concern.

We shall be interested in sound in the ultrasonic frequency range from roughly 0.5 MHz to perhaps 5.0 MHz. These frequencies are appropriate for penetration and measurement in materials and geometries of the TMI-2 piping, and are easy to generate and detect with commercially available equipment.

These frequencies correspond to wavelengths of 1.2-mm to 12.0-mm, depending on the medium and mode of propagation. Since ultrasonic transducers are typically 12 mm to 50 mm in diameter, the ratio of lens or aperture diameter to wavelength for ultrasound is typically much lower than for corresponding optical systems. Diffractive effects, both at apertures and for "images," are therefore relatively much more important. Because of this, analogies to geometric optics are only approximate at best; an optical system corresponding to an ultrasonic transducer and lens would be only a few microns in diameter.

Methods for precise calculation and modelling of ultrasonic systems are the subject of much current research and development effort.[1-3]

38

The speed of sound is a function of the elastic constants of the medium through which the sound is propagating. For longitudinal (compressional) waves in an isotropic medium, the speed of sound is given[4] by

$$v_1 = \frac{E}{\rho} \frac{1 - \sigma}{(1 + \sigma)(1 - 2\sigma)} \tag{2}$$

where E is the modulus of elasticity, ρ is the density and σ is Poisson's ratio. The speed of shear (transverse) waves is given by

$$v_s = \frac{E}{\rho} \frac{1}{2(1 + \sigma)} . \tag{3}$$

In metals the speed of sound thus depends on composition of the alloy and on its state of stress, which in turn depends on cold work, annealling, and welding and fabrication stresses. (This property, in fact, has been used to infer such stresses.)

Speeds of sound for some typical materials are given in Table A-1. Variations of a few percent between different heats of the same alloy in the same stress state are common. Variations of as much as 10% caused by differing fabrication methods and stress history are not uncommon.

Of particular interest to the present problem are local microscopic variations in the effective speed of sound within a given part, caused for example by inhomogeneities or local stress concentrations. It will be shown that these will determine the ultimate longitudinal resolution by which the radial dimension on a debris deposit can be measured.

When ultrasound is incident normally on a boundary, part of its energy is reflected and part is transmitted. The sound pressure in the reflected wave relative to that incident on the boundary is given[4] by

$$R = \frac{W_2 - W_1}{W_1 + W_2} \tag{4}$$

39

TABLE A-1.   REPRESENTATIVE SPEEDS OF SOUND AT 20°C

	Speed	$(mm/\mu s)$
Material	Shear Mode	Longitudinal Mode
Type 316 SS:		
18 in. NPS, LOFT	333[a]	--*
14 in. NPS, LOFT	326[a]	--*
Type 304 SS	312[a]	--*
Carbon Steel	323[b]	585[b]
Aluminum	308[c]	632[c]
Inconels	302[b]	572[b]
UO_2	271[d]	516[d]
SiO_2	352[c] •	557[b]
Water	--	149[a]
Oil, Rotary Compressor	--	141[a]

*   Not measured.

a.   Unreported measurements by the author in connection with Loss-of-Fluid Test (LOFT) requalification and AUT system development.

b.   See Reference 10; this is a general compilation of useful cases in extensive field use.

c.   See Reference 4, Table A1, page 476.

d.   H. B. Patel, "Ultrasonic Testing of Irradiated Fuel Sheathing," Materials Evaluation XXXIII (49), March 1975.

where W = ρv and ρ is the density, and the subscripts 1 and 2 refer to the media before and after the boundary, respectively. The relative sound pressure in the transmitted wave is given by

$$T = \frac{2W_1}{W_2 + W_1} .$$ (5)

Using Equation (4) and the typical values for constants shown in Table A-1, we find that the reflection coefficient (R_z) is 0.88 for a steel-water interface and 0.90 for a steel-UO_2 interface. Although solid UO_2 has a high density, this is combined with a relatively low speed of sound in such a way that surface reflectivity should not be significantly different from that of steel.

Much of the debris we are to detect, however, may be in the form of sand- or flour-sized particles deposited from water. Little information on the ultrasonic properties of such mixtures is available in the literature. There are at least two extreme possibilities for treating the situation:

1. Assume that because the particles are very much smaller than the wavelength the mixture of water and particles has an intermediate acoustic impedance. Calculations[5] based on this assumption showed that (a) results are sensitive to the assumed water fraction in the mixture, and that (b) the reflection and transmission properties were dominated by UO_2, and were not dramatically different from those of steel.

2. Assume that the mixture behaves as a point-scattering "cloud" illuminated with coherent waves. (Such calculations are beyond the scope of the present study.[6]) Qualitatively, one might expect strong frequency-dependent effects arising ultimately from the coherent nature of the illuminating sound.

An experiment was designed to distinguish between these two cases. It will be shown that possibility (b) was indeed the case in these experiments, and that many of the properties of such mixtures were determined.

41

Since it is a wave motion, ultrasound also shows interference effects. Consider a broadband ultrasonic wave normally incident from water on a thin film of water-UO_2 particle mixture resting on a steel surface. Each of these three media has a distinct acoustic impedance, and Equations (4) and (5) predict that a portion of the energy will be reflected and part transmitted at each boundary. Given the finite speed of sound and finite ultrasonic pulse length, there will be interference between reflections from the water-mixture and mixture-steel boundaries. This interference forms the basis for one form of thickness gauge in which a continuous-wave ultrasonic signal is tuned to a resonance at the film thickness, whose dimension is then determined from the standard wavelength-frequency relation. More recent practice uses broadband pulsed excitation followed by frequency analysis of the returned echo; peaks in the spectrum correspond to resonance thicknesses.

Interference may also arise whenever energy is returned from more than one target in the field of view. It should be noted that interference requires spatial and temporal coherence across the field of view. This is indeed the case. Figure A-1 shows the calculated phase relationships for a typical ultrasonic transducer, whose amplitude distribution is given in Figure A-2[8] (see "CW3 Program," Reference 2).

1.2 Ultrasonic Measurements

The function of an ultrasonic transducer is the interconversion of electrical and mechanical energy. The active element is usually a piezoelectric ceramic of lead zirconate titanate or similar crystal structure. The mechanical resonance of the ceramic, its mounting, and backing material, determine its properties in the frequency domain. A small additional damping can be obtained electrically. The resonance of a typical transducer has a Q of two or three.

For most purposes, the most useful mode is pulse-echo, in which the transducer serves as both transmitter and receiver, in a manner similar to active sonar or to radar. The transducer is shock-excited by a narrow, high-voltage electrical pulse. It then generates sound waves mechanically

42
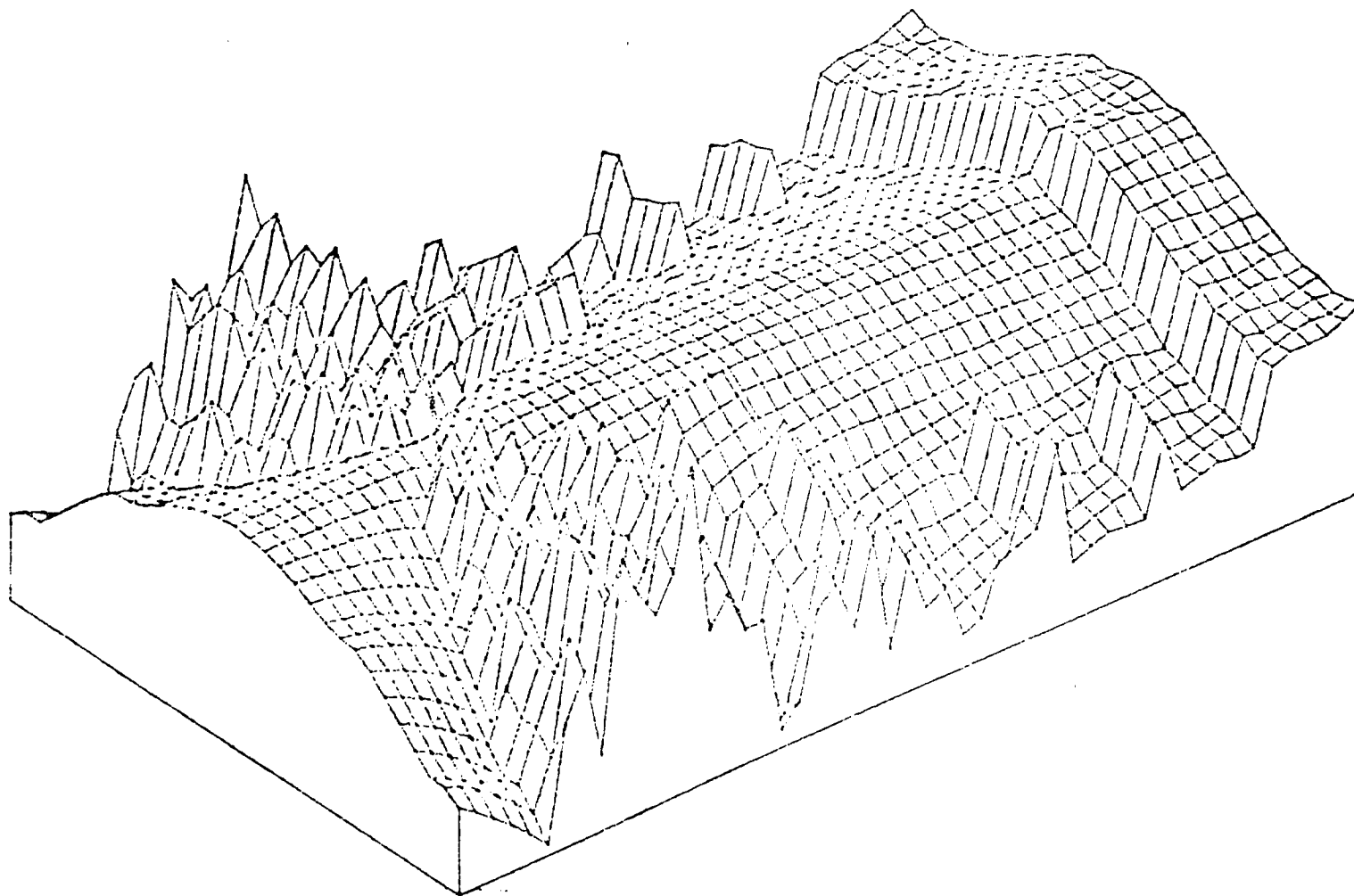
Figure A-1. Calculated phase distribution for transducer of Figure 2.
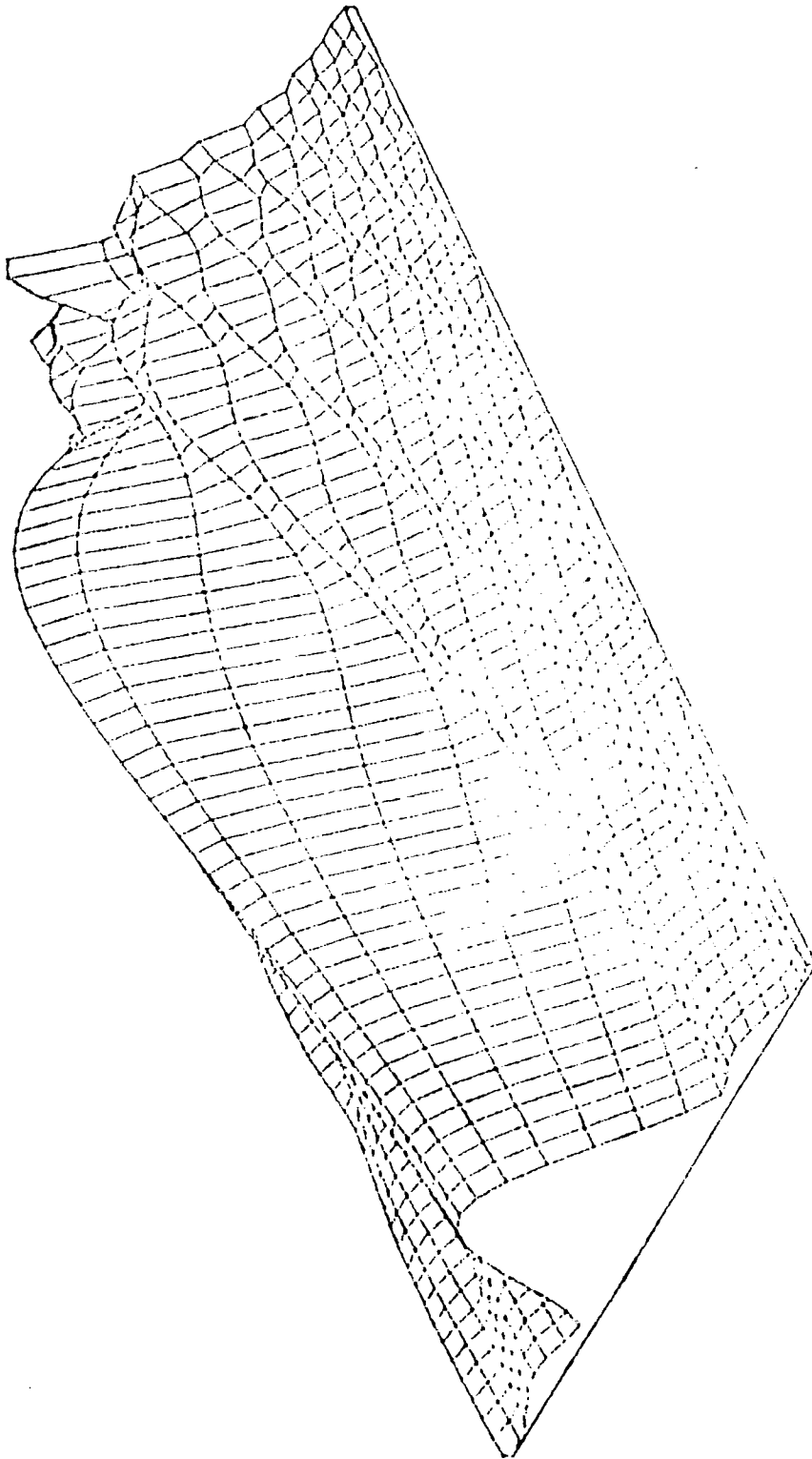
Figure A-2. Calculated amplitude distribution for typical transducer.

as its resonance decays, creating a relatively short pulse of ultrasound (see Figures 3 and 4). Returning echos from a target excite the transducer mechanically, producing a small electrical signal that is amplified for further processing.

The low radio frequencies of these signals, one to five megahertz, are easily accessible to both analog and digital processing techniques. Digital processing starts with analog-to-digital conversion, in which the selected portion of the signal is converted to precise digital values at 50-ns intervals and placed in a computer memory. Figure A-3 was prepared by a computer using such a process.

Once in memory, sophisticated processing techniques are available. The data of Figure A-3 were subjected to a fast Fourier transform to obtain the power spectrum shown in Figure A-4. Power spectra can be manipulated readily by digital filtering, windowing, normalization, and other techniques to extract the required information, limited only by noise.

Digital techniques are significant aid in reducing the effects of noise. Consider a data set, such as that illustrated in Figure A-3, which consists of signal plus time-random noise. Over a sufficiently long time, the average of the noise component will be zero. If one averages M independent samples of each point, it can be shown that the signal-to-noise ratio (S/N) improves as

$$S/N \ a \ \left(\frac{1}{M}\right)^{-1}. \tag{6}$$

Therefore, if one is willing to wait a sufficiently long time and average many samples of the data, he can obtain an essentially arbitrary S/N. Improvements of 20 to 30 dB are readily obtained. This technique was used in the experimental study to be discussed below to extract precise timing, spectral, and signal amplitude information over a very broad range.
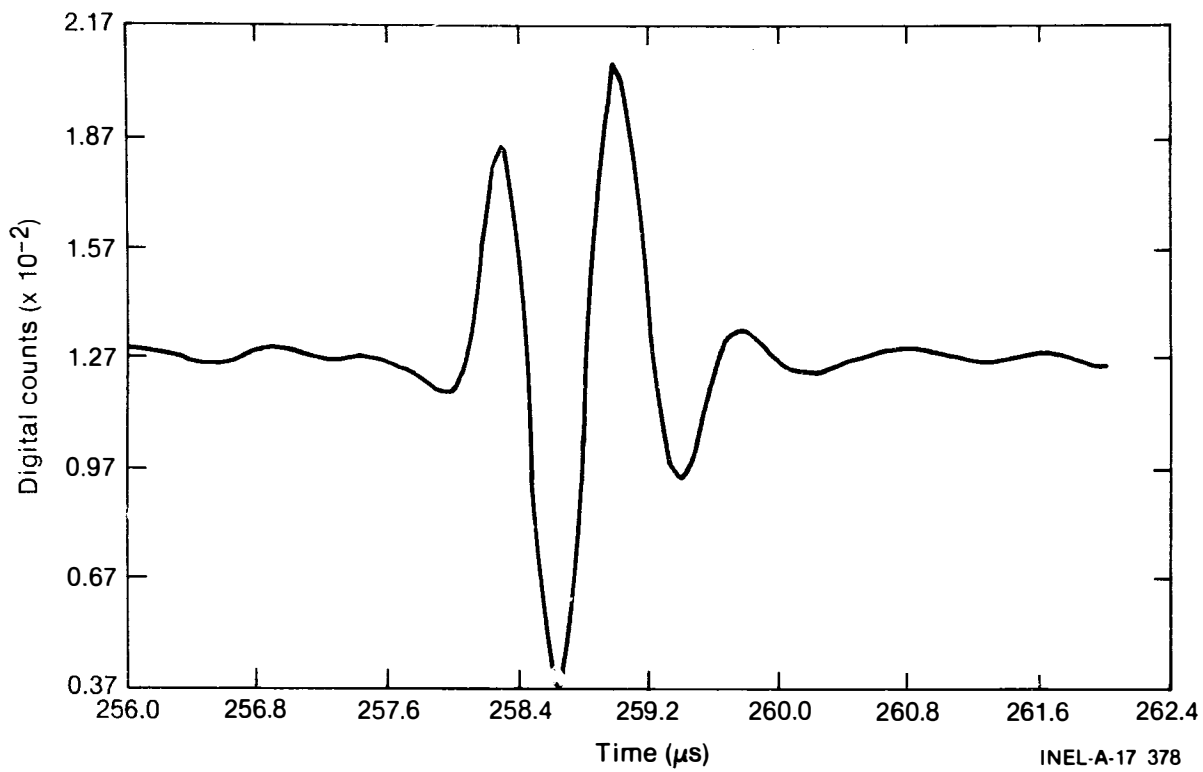
Figure A-3. Typical flat-target response for transducer used in the experiments.
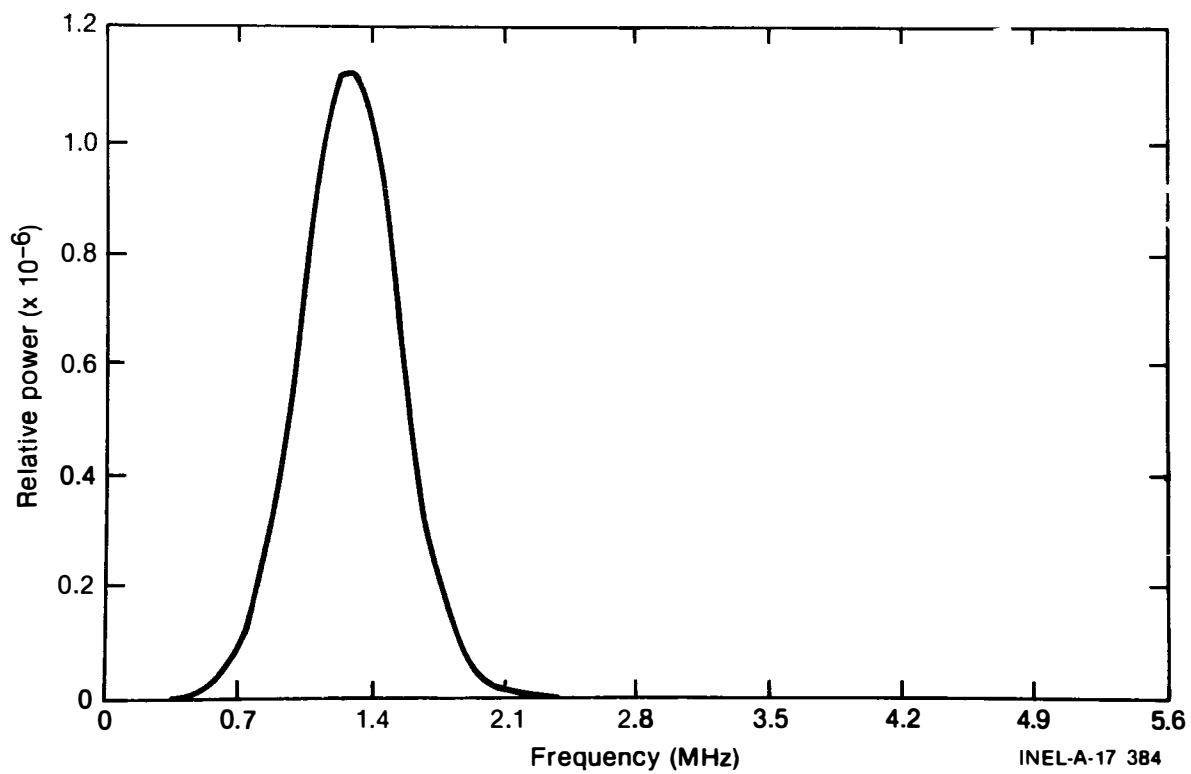
Figure A-4. Power spectrum of the pulse represented in Figure A-3.

The radio frequency signal, as shown in Figure A-3, can be regarded as a carrier whose modulation envelope carries signal amplitude and time-of-occurrence information. (The radio frequency signal itself is not directly useful in measuring time and amplitude because the phase relations within the envelope are not fixed.) The envelope is usually recovered by detection circuitry in the analog domain. The modulation envelope may also be obtained more precisely by manipulations in the digital processing domain.

The most precise time-of-occurrence or range information is obtained at the half-amplitude point on the leading edge of the signal envelope. This is the point of largest dS/dt (where S is the envelope signal), corresponding to the rate of change of the signal at a zero-crossing of the radio frequency carrier. Timing errors caused by noise or by variations in envelope shape are minimized at this point.

The measurement is most precisely done in the digital processing domain. After having found the maximum signal amplitude and accounted for baseline depression, a special algorithm interpolates between 50-ns digital samples to find the required amplitude point. Precision and reproducibility for measurements reported below were a few nanoseconds, corresponding to a distance of a few micrometers in water. The overall accuracy of the measurement is usually set by small temperature fluctuations, since the speed of sound is a function of temperature.

The width of the envelope depends primarily on the Q of the transducer, but may also be a function of target orientation relative to sound beam direction; not all portions of the advancing wavefront need arrive at the target simultaneously. Because of this finite and sometimes varying width of the signal envelope, the longitudinal resolution of the system, that is, the ability to distinguish successive targets in the direction of the beam, is relatively poor, and the resolution can amount to a centimeter or more. Digital processing methods for improving the longitudinal resolution of an ultrasonic system by deconvolution of the target signal from the delta-function response of the transducer are being investigated,[8] but are not yet at a stage where they can be used routinely.

The limited longitudinal resolution for successive targets forces a measurement geometry such that range to target is always measured from a direction in which there are no competing targets for several centimeters before the target of interest. This is discussed in the next section.

1.3 Potential Methods for Implementation of Debris Detection and Characterization

Ultrasonic technique, as outlined above, is a sensitive tool for measuring the geometry and orientation of surfaces. While ultrasonic measurements are not directly sensitive to mass of debris in the same way that measurements of nuclear properties would be, one may take advantage of a combination of the properties of ultrasound and ultrasonic systems to detect and characterize essentially the full range of debris configurations and determine the mass of debris deposited. A potential system for doing so is outlined in this section. Its characteristics, some of which needed to be determined by experiment, will then be examined, as described in the following section.

Let a pulse-echo sound beam enter the top outside surface of the pipe and be focused to a small spot on the diametrically opposite inside surface, which is to be examined for the presence of debris. The geometry is sketched schematically in Figure A-5.

The two extreme cases for debris configuration are thin layers of fine powder or large pieces. Both rest on the inner clad surface, but the large pieces may be in contact only at a few points. Sound entry from the top surface of the pipe allows us to take advantage of leading-edge timing to determine the precise distance from transducer to the first target; no solid echos occur as the wave crosses the diameter of the pipe. (Such would not be the case for sound entry from the bottom of the pipe, where the echo from the clad surface would not be distinguishable by time measurements from debris just after it because of the poor longitudinal resolution.)

48

Scanning

Transducer

Sound beam

Debris

INEL-A-17 376
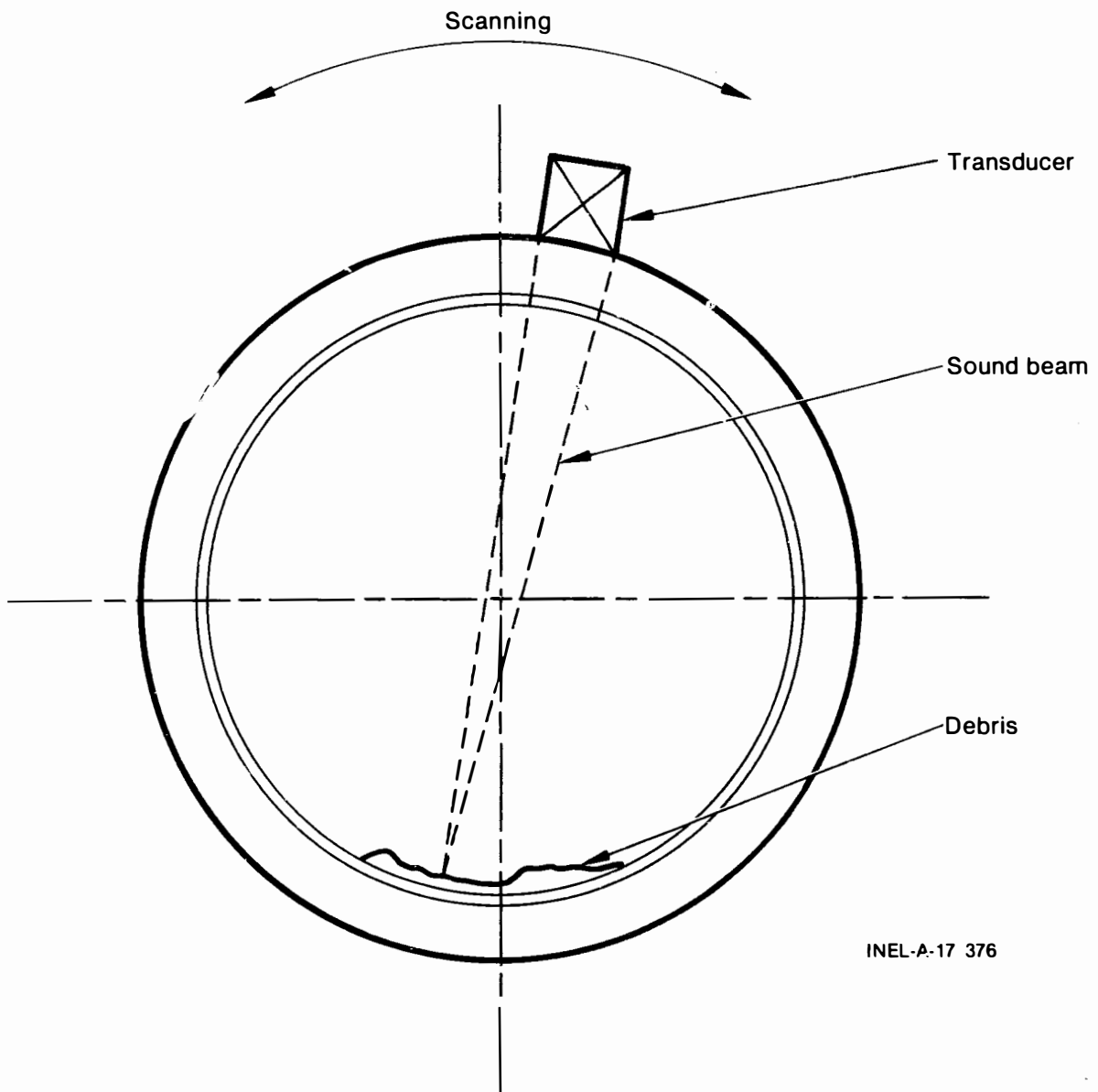
Figure A-5. Geometry for ultrasonic detection and characterization of of debris in TMI-2 piping.

49

If we now scan the transducer in a raster pattern normal to the top surface of the pipe, we can "view" any desired portion of the inside surface and examine it for the presence of debris. At each grid point on the raster, the system measures the range to the first echo in the vicinity of the expected location of the clad surface. From this information a small computer constructs a contour map of distance to target, where the contours can be expressed in fractions of a millimeter.

The contour map is an image of the surface, including any debris on it, in exact analogy to a topographic map of a valley floor from which some hills (the debris) arise. At the same time, a second map, which contains somewhat different information, can be constructed. This map would be prepared from signal amplitude information instead of range, and would represent an image of surface reflectivity. Figure A-6 is such a map. The figure was prepared by the INEL Advanced Ultrasonic Testing (AUT) system in
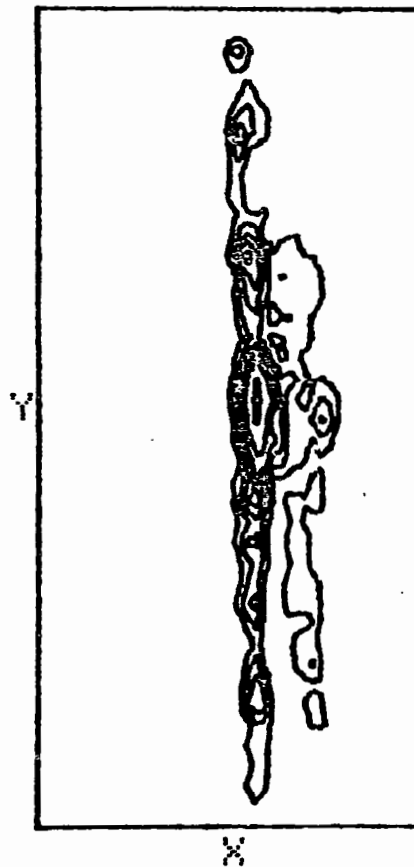
Figure A-6. Contour image of an IGSCC.

50

near-real time using hardware and computer software that have been in routine field use for several years. The image is of an intergranular stress corrosion crack in a sample. Target reflectivity is influenced by target size and shape, orientation, material, and surface conditions, and is useful in characterizing debris, if not in precise measurement of its dimensions. Maps of the surface topography and reflectivity as outlined here will certainly reveal the presence of fuel pieces, whole pellets, and the larger pieces of non-fuel debris.

The detectability of small particles and layers of powder by mapping becomes a problem in pattern recognition. In the topographic map analogy above, the smoother the valley floor, the smaller the hills and mounds one will be able to detect on the map. In our case, the "valley floor" is the surface of the cladding; its smoothness depends on the method by which the cladding was applied. We have not yet been able to determine this method. If the cladding was applied from a sheet form, for example by explosive bonding, roll bonding, or similar process, the surface will be relatively smooth. Very thin layers of debris will be discernible, primarily by their shape and departure from the underlying surface. It is more likely that the cladding was applied as a weld deposit. Each of several methods in common use for doing this leaves its own distinctive pattern on the surface. All leave a repeating pattern of ridges, against which deposits of particulate debris would be recognizable by the manner in which they fill, obscure, or otherwise modify the underlying pattern on the surface of the cladding. In either case, we may expect debris deposited from flowing water will have formed distinctive "dunes" or "drifts," perhaps graded by size as fluvial deposits are in geological settings, enhancing detectability.

For more reliable detection of aggregates of fine particulate matter, the system would make use of the wave properties of ultrasound. One can expect thin-layer interference effects in almost any particulate deposit. Further, diffractive scattering and other forms of wave-particle interaction can be expected to modify the incident ultrasonic spectrum in such a way as to be readily detectable. These hypotheses were tested successfully by experiments described below.

51

In summary, the debris detection and characterization system will use an ultrasonic transducer in a repeating raster pattern to view the surface to be examined for the presence of debris. At each point of the raster grid, measurements are made of the range to the target (inside diameter of the pipe and any debris lying on it), of the gross reflectivity, and of the reflectivity as a function of frequency. The first two measurements will be used to detect, image, and characterize at least the larger debris, while spectral measurements will be used to detect, map the extent of, and measure the thickness of aggregates of fine debris powders. These functions have been shown to be within the power of minicomputers operated in real or near-real time.[9]

Scanners of the requisite speed and precision, control circuitry and software, the ability to acquire data of each of the three types, and the ability to process, display, and interpret the data have all been demonstrated under field conditions. The primary question to be addressed here is the quantitative one of defining expected system performance in terms of resolution limits for detectability.

2. EXPERIMENTAL MEASUREMENTS

Two series of experiments addressed factors that determine minimum detectability in the type of system discussed above. The first series addressed factors that set limits to range resolution (measurement of time-of-echo), while the second series was an investigation of the ultrasonic properties of mixtures of powders or fine particles resting on a metallic surface under water. The results of these measurements allow us to predict in a general way the behavior of the system under study. They also point to additional work needed to characterize the system response in complete quantitative detail.

2.1 Range Resolution Measurements

With a homogeneous medium, such as water, between the transducer and target, the measurement methods outlined in Section 1.2 above are easily capable of reproducible range resolution of micrometers at constant temperature and at the frequencies of interest. That resolution would still be obtainable in layered media if each material were individually homogeneous and the interfaces flat and perpendicular to the beam.

Our sound beam must traverse three media: ferritic steel pipe wall, stainless steel or Inconel cladding, and water. Small-scale inhomogeneities in the speed of sound in bulk metal or irregularities in any of the inter-faces will degrade the timing resolution of the system by the amount of the inhomogeneities and irregularities. The dimensional scale of concern is roughly that between a few wavelengths and perhaps twice that of the largest aggregate of debris to be detected. (Larger scale inhomogeneities caused by, for example, eccentricity, varying wall or cladding thickness, or out-of-round pipe, are not of concern since they would represent a slowly vary-ing elevation against which local changes in elevation will signal the presence of debris.) Further, large fractional variations in the speed of sound in bulk cladding will still represent only a small fraction of the total metal path length, and are not therefore of much concern.

53

The largest contribution to range resolution degradation comes from surface irregularities on the cladding and from local inhomogeneities in the ferritic pipe wall. Of next concern is the interface between ferritic wall and cladding. The effects of the latter two were measured. The cladding-surface effects can be determined only when the cladding-surface configuration becomes known.

The measurement geometry is shown in Figure A-7. The target was a 60 x 60-mm aluminum extrusion about 400 mm high, resting on the bottom of an immersion tank. The (near) target surface of the block was in approximate alignment with the vertical drive of the transducer assembly. The material being studied was placed between the transducer and the target surface.

The measurement procedure was to scan vertically, measuring nominal time to target-surface echo at 10-mm intervals. These data were then fitted by least-squares regression to a straight line.
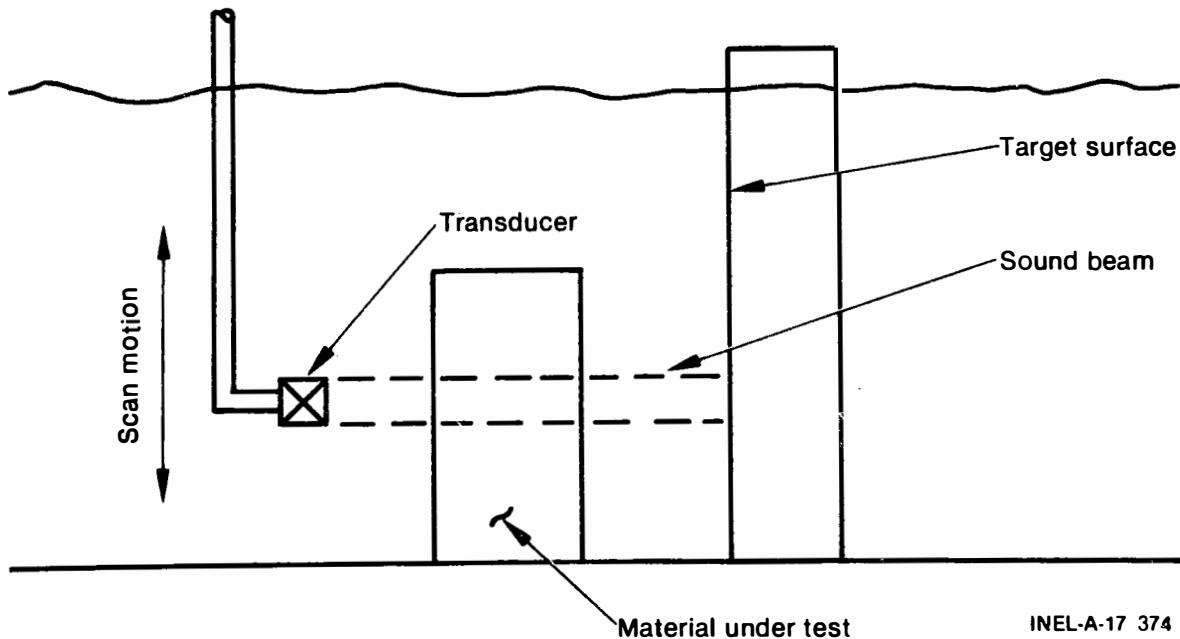
Figure A-7. Geometry for measurement of range resolution.

54

Consider the first case, without test material between the transducer and target surface. If the surface is accurately flat, the standard deviation of the observed points about the regression line represents the standard deviation of the measurement. (It is actually composed of two statistically independent components; measurement error and lack of flatness of the surface. The latter was not statistically evident in any of the measurements.) The slope of the straight line is a measure of the lack of alignment between the target surface and vertical axis of the transducer.

Let the line be

$$x = a_0 + a_1 y \qquad\qquad (7)$$

and δx be the standard deviation of the measurement of x.

If the material under study, in the form of a slab, is placed between the transducer and target surface, and the parameters of the target-surface line are redetermined, any change in

- a_0 is a measure of the mean speed of sound in the intervening medium, relative to water

- a_1 is a measure of either taper in the intervening medium or of large-scale variation in its speed of sound

- δx is a measure of the local variations in the speed of sound in the intervening medium.

Note that δx is composed of components that are statistically independent; the individual components add in root mean square (RMS) fashion.

The material under test, the "intervening medium," was an ultrasonic calibration block cut from the nozzle dropout of the loss-of-fluid-test (LOFT) reactor vessel. It was a rectangular solid, approximately 76 x 102 x 250 mm, machined to about RMS 125 finish. One surface had been clad with

55

a Type 308 stainless steel by weld deposit; approximately half of the thickness of the cladding had been removed during machining, leaving a smooth surface. The base metal of the block was ASTM type A508B. This block was chosen as probably representative of typical pressure vessel materials and fabrication techniques, to give an estimate of possible variations in the speed of sound. The cladding was deposited by a single-torch process; the cladding/base-metal interface, therefore, probably represents a worst case for any variations in the speed of sound from this source.

The transducer was 37 mm in diameter and unfocussed. Its gross spectrum is shown in Figure A-4. The center frequency was 1.4 MHz, but there was useful energy (which does not show on this linear plot) to at least 4 MHz.

First, the target surface was measured without the test block, as outlined above. Next, the 76-mm-thick face (without cladding) of the test block was inserted into the beam, and finally the 102-mm face of the test block (with cladding). The results are shown in Table A-2.

It was assumed that the test block was isotropic, but not necessarily homogeneous. Then,

$$\delta\nu = \left(\frac{\delta x_{102}^2 - \delta x_1^2}{102}\right)^{1/2} \tag{8}$$

is the local statistical variation of the speed of sound per unit path length in the block, and

$$\delta I = \left[\delta x_{76}^2 - \delta x_1^2 - \frac{9}{16}\left(\delta x_{102}^2 - \delta_1^2\right)\right]^{1/2} \tag{9}$$

is the statistical variation caused by the cladding/base-metal interface, where δx_1 is the measurement error (bare target surface), and δx_{76} and δx_{102} are the measured standard deviations from the fitted straight line when the beam passed through the 76-mm and 102-mm faces, respectively.

TABLE A-2. SUMMARY OF RESULTS OF RANGE RESOLUTION MEASUREMENTS

---

1. Sound path through water only--defines error of these measurements

$$\delta x_1^{(1)} \qquad\qquad 4.93 \times 10^{-2} \text{ mm} \qquad\qquad\qquad \text{(Equation 7)}$$

$$S^{(2)} \qquad\qquad 1.3 \times 10^{-3} \text{ mm}$$

2. Sound path through water plus steel (102-mm thickness)--measures RMS sum of measurement error and microscopic-scale variations in speed sound

$$\delta x_{102} \qquad\qquad 1.13 \times 10^{-1} \text{ mm}$$

$$S_{103}(c) \qquad\qquad 1.4 \times 10^{-2} \text{ mm}$$

$$\delta v \qquad\qquad 1.33 \times 10^{-3} \text{ mm/mm} \qquad\qquad \text{(Equation 8)}$$

3. Sound path through water plus steel plus clad interface (76-mm metal thickness) - measures RMS sum of both of above, plus effect of clad/base-metal interface

$$\delta x_{76} \qquad\qquad 1.09 \times 10^{-1} \text{ mm}$$

$$S_{76} \qquad\qquad 3.6 \times 10^{10-2} \text{ mm}$$

4. Effect of clad/base metal interface

$$\delta I \qquad\qquad 6.09 \times 10^{-2} \text{ mm} \qquad\qquad\qquad \text{(Equation 9)}$$

$$\sigma, \text{ uncertainty} \qquad 4.1 \times 10^{-2} \text{ mm}$$

---

a. δx_i is statistical uncertainty in range under each of the measurement conditions.

b. S is the standard deviation of replicated measurements of δx_1.

c. Si is as in (2), averaged over traverses on different portions of the block.

57

The local variations in the speed of sound in this sample were approximately 0.1 percent. To this must be added, in RMS fashion, the effect due to the clad/base-metal interface (0.008-mm thickness) and any effect due to surface irregularities on the cladding to obtain an estimate of minimum range resolution. The clad-surface irregularities will probably dominate for weld-deposited cladding.

The geometry described in Section 1.4 above was chosen in part to give a large area over which to average the local variations near the sound entry surface, and thus minimize these variations. Using such an average and reasonable values for clad-surface ripple, one can estimate a minimum resolution ranging from 0.12 to perhaps 0.25 mm (0.005 in. to 0.010 in.) for direct measurements of radial dimensions in the geometry considered.

2.2 Ultrasonic Properties of Aggregates of Fine Particles in Water

The ultrasonic properties of aggregates of fine particles in water formed a second set of investigations. The results of these investigations showed that it is feasible to detect and measure the dimensions of layers of fine particles that are significantly thinner than can be detected by direct ranging, in a manner that is, at least to a first order, independent of the geometry and materials of fabrication.

The experimental geometry is shown in Figure A-8. The test materials were graded silica powders. The target surface was the same aluminum extrusion used previously, with sloping frame. The silica powders were deposited within the side rail area, then scraped off flat with a straight edge to form a flat-surfaced deposit varying from zero thickness at the "toe" of the frame to 7 mm over a length of 200 mm. The bare portion of the target block was carefully brushed free of powder with a camelhair brush. Sound incidence was normal to the surface of the extrusion.

The effective speed of sound and acoustic impedance of the powder-water aggregate were measured as follows. Range-to-target was measured along the centerline of the block at 10-mm intervals. A typical curve is shown in

58
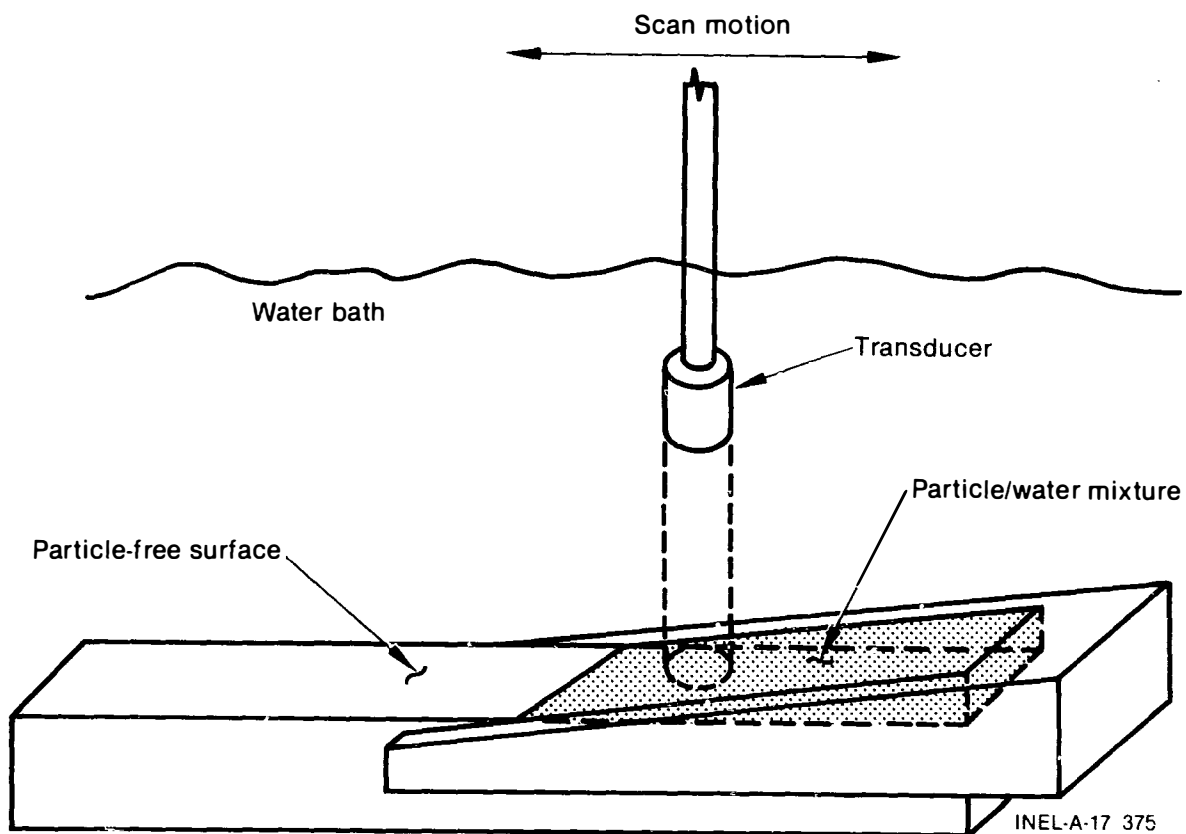
Figure A-8. Geometry for measurement of ultrasonic properties of mixtures of fine particles in water.

Figure A-9. The points on the bare end of the target block were fitted by least-squares regression to a straight line that was extrapolated under the wedge of powder to define the range to that point. (The block had been previously ultrasonically determined to be flat, and this procedure minimized any errors due to changes in apparent range caused by variations in temperature of the water in the immersion tank.) The difference in time-to-first-echo from the surface of the powder and the extrapolated time-to-block-surface at each point, multiplied by the speed of sound in water at the temperature of the tank, gave the thickness of powder at each point. The larger thicknesses of powder were enough to allow clear separation in time between the echoes from powder surface and underlying block surface at that point. The measured aggregate thickness divided by the difference in time between these two echoes gives the effective speed of sound in the mixture.

Given the known acoustic impedance of water and aluminum and the measured ratios of reflectivity at the water-mixture surface to the mixture-aluminum surface immediately under it, the acoustic impedance of the mixture was

59
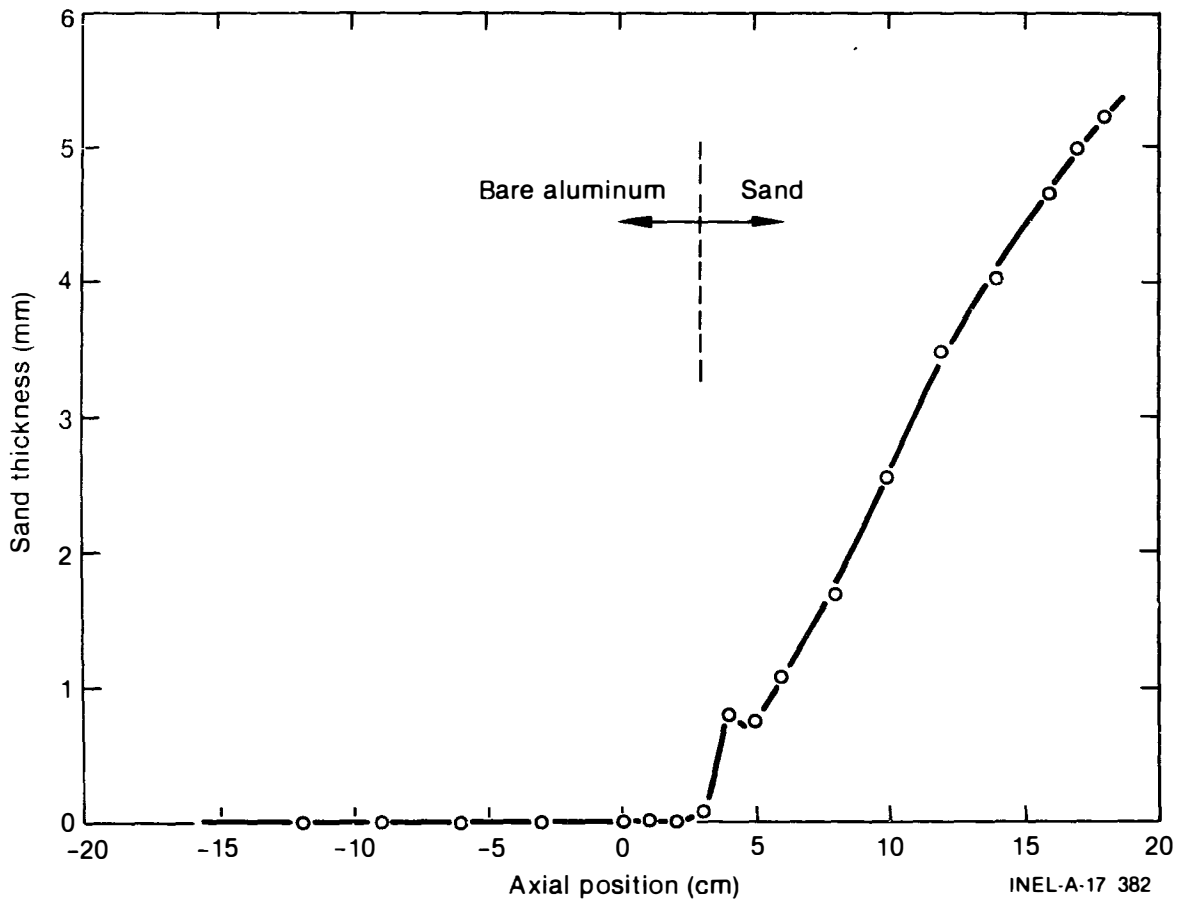
Figure A-9. Course sand thickness vs axial position.

calculated by simultaneous solution of Equations (4) and (5) at the water-mixture, mixture-aluminum and mixture-water interfaces that the pulse-echo signal traversed. The measured acoustic impedance was 3.48×10^3 kg/m^{2}s.

The measured speed of sound in the mixture was (1.570 ± 0.005) $\times 10$ m/s, which is about 5% higher than the speed of sound in water, independent of particle size over the range tested. The measured speed of sound and the effective acoustic impedance inferred from the reflectivity measurements imply that the mixture acts as a medium with essentially the speed of sound of water and the density, in this case, of bulk SiO_2.

Both results are somewhat surprising, but can be understood on the following basis. Equation (2) predicts that the speed of sound is a function of the elastic constants of the medium. The fine powder and water

aggregate is a two-phase mixture in which the relevant elastic constants are those of the interstitial phase, the water. Ultrasonic reflectivity, on the other hand, is also a function of the inertia per unit volume, i.e., the density, immediately adjacent to the interface. For fine powders, the packing fraction is high; the inertia seen by the wavefront is dominated by the SiO_2.

The small difference between speed of sound in water and that in the mixture is presumably due to adhesion or friction between particles or to inertial effects.

The reflective properties of the water-mixture interface were studied as a function of ultrasonic frequency and of incident angle. The technique was pulse-echo in all cases, the reflected signal being backscattered toward the transducer. Spectra were obtained by fast Fourier transformation of the quantized signal.

Sound was incident at angles of 0° (normal to the surface), and at 10 and 15° tilted in the plane normal to that of Figure A-8. The fully and partially resolved peaks in the backscattered spectrum, shown in Figure A-10, follow two different patterns of behavior as a function of incident angle. The peaks below one megahertz decrease in frequency as the angle of incidence is changed from normal incidence. Higher-frequency peaks remain constant in frequency. The high-frequency peaks are interpreted as scattering from the surface itself, while the low-frequency peaks have the behavior to be expected from Bragg scattering within the volume of the mixture. In both cases, the scatterers are presumed to be "clumps" of grains in a somewhat irregular settling pattern, since the dimensions implied by the measured speed of sound and frequency correspond to many times the size of the individual grains in the "140 grit and finer" used for this test.

The last series of tests was an investigation of thin-film interference effects coming from interference between the echos from the mixture surface and from the block surface immediately beneath it. The experiments used the same powder configuration shown in Figure A-8.

61
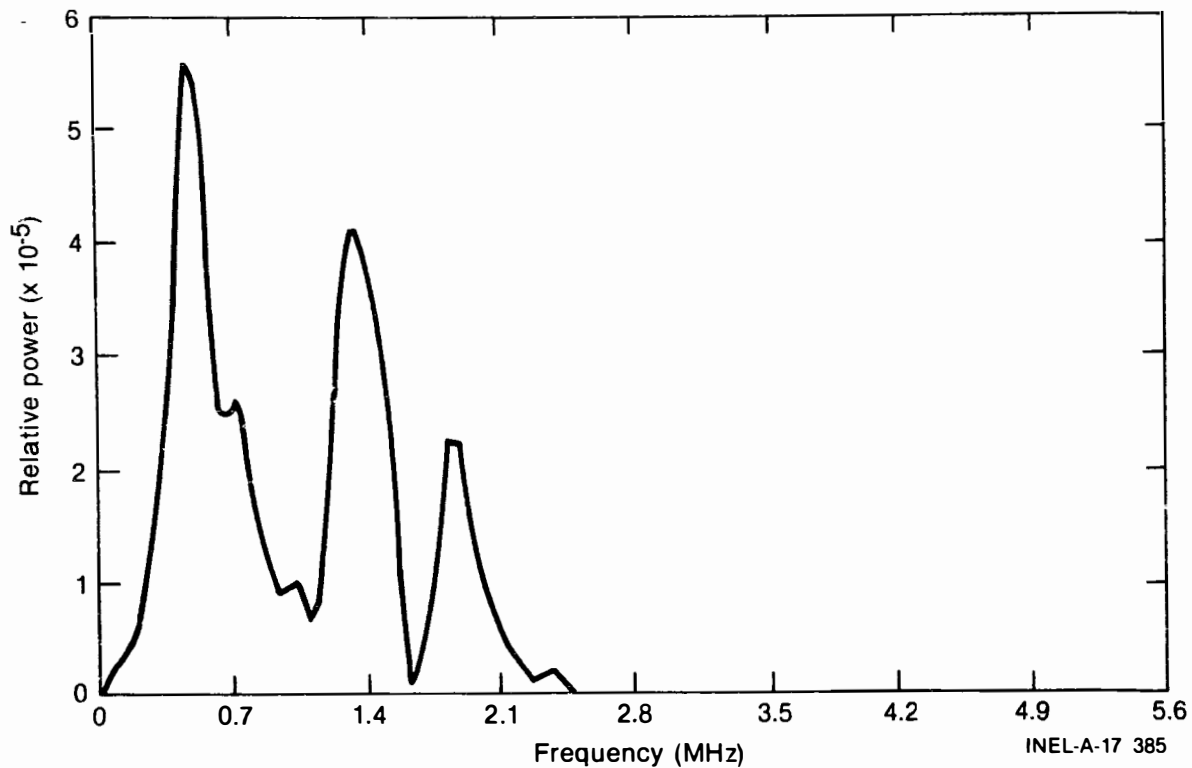
Figure A-10. Backscattered spectrum from surface of thick layer of sand, at 15° tilt, showing typical response.

Conclusive demonstration of interference requires a broad band of wave-lengths in order to discern harmonic relationships, and is easiest to inter-pret if the system response is flat as a function of frequency. This was obtained by normalizing the spectral measurements to a spectrum obtained from the bare target surface of the aluminum block. This normalized spectrum represents the unmodified energy per unit frequency of the transducer. The transducer spectrum contains small, but significant, amounts of energy up to at least 4 MHz, which does not show on the linear plot of Figure A-4. With sufficient signal integration, M of several thousand, the signal-noise ratio at high frequencies was adequate. Figure A-11 is a typical test for signal-noise ratio; it represents the ratio of two successive spectra from the bare block. The curve should be identically unity; departures from this are caused by noise, and represent the precision of the measurement.

Two grades of SiO_2 powder were used. The coarse sand is estimated at 50-120 grit, while a finer sand was "140 grit and finer." This latter grade included significant fractions of very fine powder that required several days to settle from suspension in water.

62
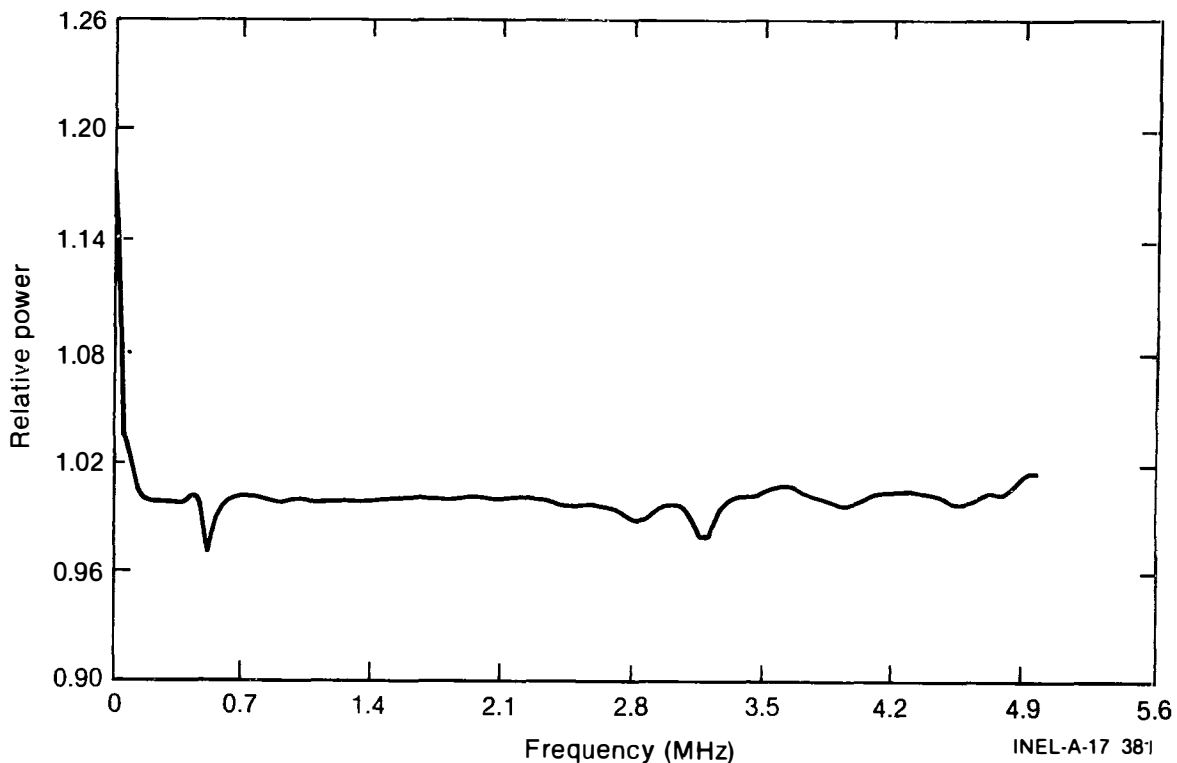
Figure A-11. Test for S/N of spectral normalization measurements.

The key measurements were performed at the thin end of the sample wedge, where thicknesses ran from zero to about 0.5 mm. Longitudinal resolution was not sufficient to distinguish between echoes from the mixture surface and underlying block. The signal subjected to fast Fourier transform was the distorted composite of both.

Typical normalized results are shown in Figure A-12. These spectra contain peaks and valleys arising from at least three different effects. The first are the surface-scattering peaks noted previously. A second group are apparently due to the Bragg scattering effects also noted previously, but have lower amplitude and modified frequency. The final features to be noted here are nulls at wavelengths corresponding to odd quarter-wavelength multiples of the thickness of the mixture at that point, thus demonstrating interference. The peaks arising from the surface and volume scattering were found to be characteristic of the grade of sand used, and varied from place to place on the sample. The effects characteristic of interference depended only on the thickness of the layer, and not on the grade of sand.

63
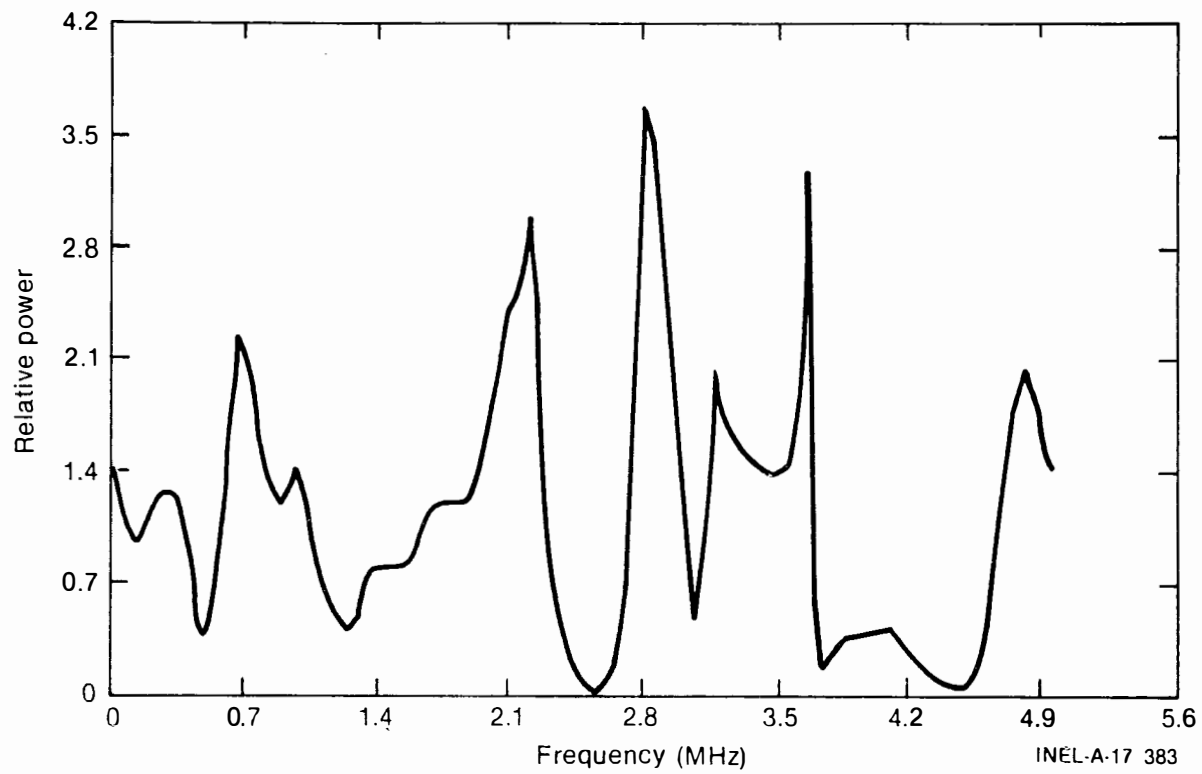
Figure A-12. Typical backscattered spectrum from thin layer of fine sand, normalized to response from flat, sand-free surface.

3. CONCLUSIONS

For detecting and characterizing thin layers of flour-like (and larger) particles that have settled out of water on a metallic surface, the key experiments were measurements of the ultrasonic properties of such mixtures. The measurements showed that there are a number of different, distinctive effects that are understood at least semi-quantitatively, and that can be used to detect such mixtures unambiguously.

All effects, thin-film interference and surface and volume scattering, lead to normalized spectra that have distinct peaks and valleys. Either of two very simple algorithms would have detected the presence of powder-water mixtures in any thickness in these experiments. The first is simply a threshold: if spectral peaks are greater (or valleys lower) than a speci-fied multiple of the reproducibility of the measurement of the unmodified transducer spectrum, the mixture is present. The second algorithm is more sensitive and more easily adaptable to field measurements: compute the standard deviation of the normalized spectrum about its average value; if this is greater than a specified multiple of the standard deviation of a "blank" spectrum representing the surface of the pipe cladding (taken, for example from the sidewall), the mixture is present.

The experiments easily detected monolayers of the sand used, and there is evidence that they also detected scattered individual grains on the smooth target surface. The sensitivity of the method would be ultimately limited by the roughness of the clad surface of the pipe. There are methods for minimizing this effect by the manner in which the data are taken.

Measurements relating to the spectrum of sound reflected and scattered from the surface of the sand and cladding would thus be the primary method for detecting and characterizing powdered debris. They should be capable of detecting debris layers a few tenths of a millimeter in thickness or less. To a first order, the methods are independent of materials and geo-metry. To a second order, the detectability limit would be set by surface roughness and transmissibility as a function of frequency of the walls of

65

the pipe. It is feasible to measure debris mass by ultransonic techniques. Depending on the effective density of the debris, the mass detection limits range from 4.5 to 8.4 mg/m of piping length.

Measurements of range to the first target near the inside surface of the pipe, made at the same time and with the same signal, would be used to detect and map larger and irregular pieces of debris. Longitudinal resolution for this measurement would be on the order of 0.25 mm or less.

Equations (4) and (5), together with the experimental result that the acoustic impedance of the mixture is proportional to the density of the powder, imply that echoes from UO_2 powders would be greater than those from the SiO_2 used in these experiments. This would give a greater signal-noise ratio and better spectral sensitivity than found in the experiment.

Between the two measurements, all debris sizes and configurations likely to be in the pipe would be detected and characterized.

66

4. EQUIPMENT AND METHODS

Two classes of hardware, electronic-computer and mechanical, would be needed to make the measurements at TMI-2. The electronic and computer hardware need not be different from that used to make the measurements reported here.

The system used is shown in block diagram form in Figure A-13. The system is field-transportable. During the experiments, the system was housed in the same van that has housed it for the past two years during requalification/in-service inspection measurements in the field at LOFT.

The present scanners have been in successful field use for four years. They were designed, however, for examining relatively narrow circumferential strips at and near the welds in the piping. Extensive design modification would have to be made to provide sufficient scanning in the axial direction.

The basic computer software for mechanical control, data acquisition, data processing, and display exists. Again, it was used in these experiments, and has been in routine use for some time. The software would require extensive modification, however, to incorporate the additional acquisition, processing, and display protocol as automatic functions.

Based on previous experience with requalification/in-service inspection use of the system, it would be able to produce hard copies of the final processed data, ready for interpretation, within a few minutes of the completion of a scan, while the next scan is in progress.

Information on the characteristics of the present system is given in the appendix to this report.

The equipment needed for debris detection, location, and characterization would not break new ground in either concept or design, nor would the software. All are well within the current state of well-established design practice, without need for additional development work.

67

TRAILER

| PDP 11/34a 256 Kbytes Floating Point | 10-Mbyte Disk System | 80-Mbyte Disk System | 9-Track 800-bpi Tape | System Console |

AC Power Conditioner

Electrostatic Printer/ Plotter → Hard Copy

Intercom

Storage Tube Display

Storage Tube Display

Storage Tube Display

Skate

Ultrasonic Signal

Control and Readout

Ultrasonic System

Motor Control System

Raster Scan Color Display

Ultrasonic Signal

J-Box

Coaxial cable

Control and Readout

DATA ACQUISITION

DATA ANALYSIS

INEL-A-17 379

Figure A-13. AUT system block diagram.

The field examination procedures would represent simple extensions of those that have been tried and tested over four years of field service during requalification/in-service inspection operations at LOFT.

Only the area of interpretation would require additional development, primarily in the gaining of experience in interpretation and a background of quantitative measurements.

It is to be noted that the basic system used for debris location would also be capable of examinations of the piping system to establish pressure boundary integrity for the purpose of requalification.

is ready for sustained field operations. Separate areas in the unit are arranged for operations, analysis, systems and shop use, with space for supplies and parts storage.

Inspection starts with data acquisition in a predetermined scan pattern. The sensitivity, dynamic range, scanning grid, and ultrasonic parameters are adjusted to maximize the probability of detection of any target in the volume scanned. The system is noise-limited, with signal-averaging parameters set so that the noise represents primarily grain-scattering clutter. During data acquisition the scan operator sees a real-time C-scan display, which serves the dual purposes of operator reassurance and advanced warning of significant targets. He also has the option to display an A-scan, which shows what the computer is seeing at any point, and which has been labeled to indicate nominal locations of front and back surfaces.

The complete set of raw data is stored on disk. An analyst at another console has access to any completed data file. Operating in a task-prioritized time-sharing mode, he can produce images in several different forms in each of the standard orthogonal planes from any portion of the volume scanned. The processing and display are interactive; in addition to controlling the view direction of volume displayed, the operator also controls the effective sensitivity of the image, confining it to any portion of the amplitude spectrum desired.

Detection of flaws is by image interpretation in a manner analogous to that used in radiography. "Benign" geometric targets can be easily and rapidly recognized and classified as such, and sorted from potential flaws. To aid in interpretation, the analyst has access to any previous ultrasonic data on the part under test (to look for any in-service changes), to the complete fabrication and maintenance history, and to the original fabrication radiographs (and viewer) to clear up any unusual geometric problems.

The operating mode is near-real-time analysis and interpretation. Analysis and interpretation of one scan proceed simultaneously with acquisition of data from the next. This is a two-stage process, with flaw

71

detection and preliminary evaluation, as outlined above, followed by inter-active data acquisition and analysis as needed to fully characterize any flaw so detected.

A number of characterization tools are available. The analyst may call for scans at any desired incident angle or direction needed to determine orientation and define flaw geometry. He may also acquire normalized reflection spectra on-line and subject this information to a variety of numerical processing techniques to extract flaw-surface and dimensional parameters.

Near-real-time interactive data acquisition, analysis, and interpreta-tion, with correlation to all available nondestructive evaluation (NDE) information and historical data, ensures that all necessary data have been acquired for a fully definitive accept-reject decision on the spot. Cor-rective action, if necessary, can proceed with a minimum of delay.

Hard-copy output of all images and data is made from a retrievable and independently auditable inspection record. Raw data files are stored on magnetic tape for future reference; these data can be retrieved and pro-cessed in real time in parallel with new data at future in-service inspections.

6. RECOMMENDATIONS

While the work described above has established the feasibility and estimated the performance of an acoustic-ultrasonic method for detecting, locating, and characterizing debris within the piping system, the engineering design of a final system requires some additional quantitative information to afford an optimum design. The needed information relates primarily to the specifics of the TMI-2 plant.

It is recommended that measurements be made of the variations in effective speed of sound and transmission as a function of frequency of the actual pipe wall, including as-deposited cladding. While the actual piping itself will almost certainly not be available for these measurements, a sample or samples probably already exist in the form of ASME Code-specified ultrasonic calibration blocks. If these cannot be made available for the short period of time needed for the measurements, similar blocks or sections from other plants probably can be.

The second set of measurements would include performance of the spectral experiments described above, substituting UO_2 powder for the previously-used SiO_2. If available, several grit sizes representing a wide range should be measured; if only one grit is available, some useful additional measurements can be made with SiO_2 with normalization to the available UO_2 grit size.

These measurements should take no more than a month, once the required materials are in hand.

Information on cladding process(es) and methods of fabrication of fittings is needed, as has been noted.

Before scanner design could proceed, information on access and restrictions and clearances about the piping system is also needed.

73

The ultrasonic technique is applicable to other geometrics besides the simple pipe configuration discussed in this appendix. Application to other geometrics would be a little more complex, and each geometry would have to be examined on a case-by-case basis.

7. REFERENCES

1. C. P. Griffice, "Numerical Evaluation of the Ultrasonic Pressure in the Fields of Continuous-wave and Pulsed Transducers," Unpublished PhD Thesis, University of Missouri, December 1980.

2. G. P. Singh and J. L. Rose, Ultrasonic Field Analysis Program for Transducer Design in the Nuclear Industry, EPRI report NP-1335, February 1980.

3. A. Weyans, "Radiation Field Calculations of Pulsed Transducers," Ultrasonics, 183, July 1980.

4. J. Krautkramer and H. Krautkramer, Ultrasonic Testing of Materials, New York: Springer-Verlag, 1969, p. 18 ff.

5. R. J. Sciamanda, private communication, EG G Idaho, Inc., August 1980.

6. D. J. Vezzetti and S. O. Aks, "Ultrasonic Scattering Theory II: Scattering from Composites (Review)," Ultrasonic Imaging, 2, 195, 1980.

7. "CW3 Program," a description of which is contained in Reference 2.

8. Nobuo Hamano, "Deconvolution of Ultrasonic Nondestructive Testing Data," unpublished PhD thesis, University of Missouri, December 1980.

9. L. S. Beller, "A Review of Current Research, Development and Application Efforts in Advanced Ultrasonic Testing," Second ASQC Western Regional Energy Conference, Idaho Falls, June, 1980.

10. "Condensed Reference Series for Ultrasonic Nondestructive Testing, Vol. 1, Tables of Refracted Angles," Research Division, Automation Industries, Inc., Boulder, CO, 1969.

APPENDIX B
PRELIMINARY INVESTIGATION OF THE FEASIBILITY OF USING
GAMMA-RAY AND NEUTRON COUNTING TECHNIQUES TO LOCATE
AND CHARACTERIZE FUEL DEBRIS

C. V. McIsaac

APPENDIX B

PRELIMINARY INVESTIGATION OF THE FEASIBILITY OF USING GAMMA-RAY

AND NEUTRON COUNTING TECHNIQUES TO LOCATE AND CHARACTERIZE

FUEL DEBRIS WITHIN THE TMI-2 PRIMARY SYSTEM

C. V. McIsaac

1. INTRODUCTION

The small-break loss-of-coolant accident at Three Mile Island resulted in the escape of large quantities of fission products and an unknown quantity of fuel from the damaged Unit 2 core into its primary system. The hypothesis that a significant amount of fuel left the reactor vessel has been supported by measurements made on a smear disk that was dabbed against an internal surface of one of the letdown filter casings. Four milligrams of fuel were picked up by the smear. Given the fact that the letdown is taken from a cold leg in the primary system, it is highly probable that fuel debris is distributed throughout the primary system.

This appendix presents the findings of a study conducted to determine the feasibility of using gamma-ray and neutron counting techniques to locate and characterize the fuel debris within the TMI-2 primary system.

2. GENERAL CONSIDERATIONS

Any measurement technique designed to locate and characterize fuel debris within the TMI-2 primary system must incorporate in its design features that will allow several formidable obstacles to be overcome. During the August 1980 reentry, ambient fields on elevation 305 ft were measured to be between 300 and 700 mR/hr.[1] For purposes of calculation, the time currently being considered for fuel deposition measurements is mid-1982. The measurements will be performed after the reactor building sump primary system water inventories have been processed through the Submerged Demineralizer System and after most of the external surfaces have been decontaminated. This will obviously decrease the ambient fields but by how much is not now known. Since the assay measurements will be made inside the secondary shield wall in close proximity to the steam generators, reactor coolant pumps, and pressurizer it is prudent to assume that the ambient fields will be high. Therefore, the measurement technique selected must utilize instruments that maintain adequate sensitivity within gamma fields on the order of 100 mR/hr and that are capable of being operated remotely so as to minimize personnel exposure.

The reactor coolant pipe walls and insulation constitute a second non-trivial obstacle to any measurement method. The wall of the hot leg piping is carbon steel and is 3 in. (7.62 cm) thick. The pipe is clad on its inner surface with 0.313-in.-thick (0.795-cm-thick) type 304 stainless steel and is shrouded by a 3.5-in.-thick (8.89-cm-thick) shell of "metallic mirror" insulation. The inner shell wall is 0.037 in. (0.094 cm) thick, and the outer wall is 0.019 in. (0.048 cm) thick.[2] Evenly spaced between the insulation shell walls are 13 concentric cylindral sheaths each 0.004 in. (0.010 cm) thick. The insulation shell walls and liners are all type 304 stainless steel. The wall of the cold-leg piping has a stainless steel liner also 0.313 in. (0.794 cm) thick, but the thickness of carbon steel is only 2.5 in. (6.35 cm). The insulation shell shrouding the cold leg piping is identical to that of the hot-leg piping, except the shell walls of the cold leg insulation are slightly less thick. The separations between the hot and cold-leg pipes and their insulation shells are 0.69 in. (1.753 cm) and 1.19 in., (3.023 cm) respectively.

80

Access to the primary system pipes will be a problem. Figure B-1 illustrates the relation of floor elevations 282, 305, and 347 to the elevations of the primary system piping and components. The cold leg elbows are close enough to elevation 282 to be assayed from it without difficulty. However, the horizontal lengths of the cold leg piping connecting the reactor coolant pumps to the reactor vessel and the horizontal lengths of the hot leg piping have centerlines at elevation 315 ft-6 in. Since any debris in these pipes will have settled to the pipes' lower inner surfaces, it is desirable to place the assay detector on the same radial axis as is the lower pipe surface. It is not clear to me at this time which elevations will be most suitable to operate from to achieve the desired detector-pipe geometry. A floor does not exist inside the secondary shield-wall boundary, at 305 elevation floor so it might be necessary to operate from the top of the primary shield-wall at elevation 322. It is obvious that the detector will either have to be temporarily attached to the pipe or extended by a telescoping rod to assay the bulk of the primary system piping.

An additional access problem is posed by the primary shield wall, which is about 5 ft (1.524 m) thick. Ten ft (3.048 m) of hot leg piping and 20 ft (6.096 m) of cold leg piping are embedded in this wall. Figure B-1 illustrates the physical arrangement of the shield walls in relation to the primary system components. The separation between the pipes' insulation layers and the penetrations' walls is about 4 in. (10.16 cm).

The 440 V welding outlets inside containment are live,[1] and because the 110 V outlets are fed from the same buss, it is likely that instrument power will be available inside containment.

367 ft - 4 in. Top of shielding walls

Floor elevation 355 ft - 6 in.

Floor elevation 347 ft - 6 in.

36 - in. diameter

8 ft

322 ft - 6 in.

79 ft - 8 1/2 in.

319 ft

315 ft - 6 in.

72 ft - 1/8 in.

Floor elevation 305 ft

RC-H-1B

31 ft

24 ft

RC-H-1A

291 ft - 6 in.

9 ft

Floor elevation 282 ft - 6 in.

INEL-A-17 377
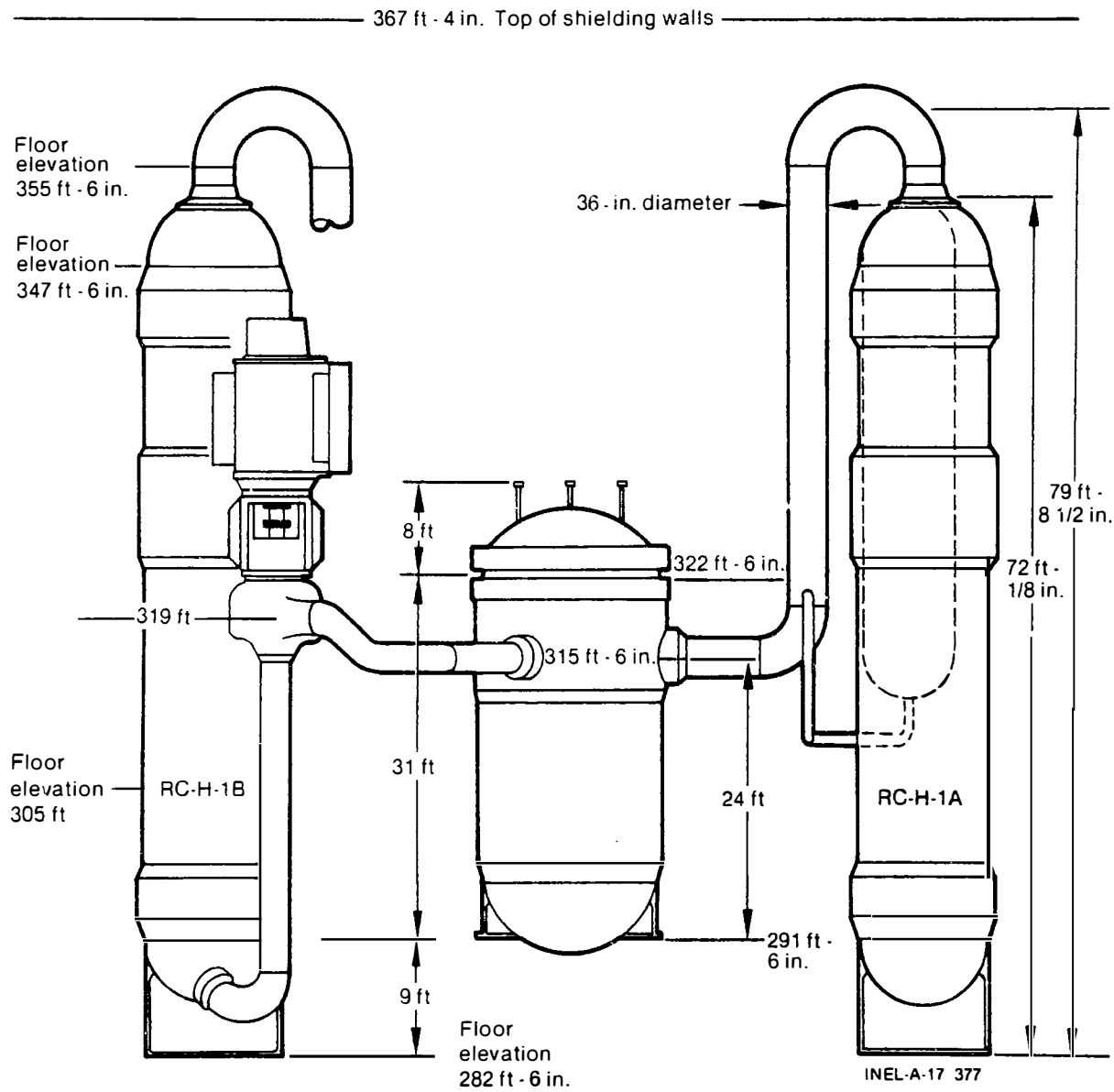
Figure B-1. Reactor coolant system arrangement--elevation.

3. DISCUSSION OF MEASUREMENT TECHNIQUES

In order to minimize personnel exposure during the period that fuel assay measurements are made, and to quickly arrive at an idea of where the fuel debris is located, the measurements ought to commence with a gross gamma survey of the primary system piping and components. Survey instruments such as the Eberline Teletector, Model 6112 (0-1 kR/hr) or the Victoreen Radector 3, Model 236 (0.1 mR/hr-1 kR/hr) could be used to perform this initial survey. The Teletector has a maximum probe length of 13 ft (4.265 m), and the Radector employs an ionization chamber connected by 40 ft (13.123 m) of flexible cable to a readout meter. Neither of these instruments is directionally sensitive, and to make one so by the addition of shielding would require that it be mounted on a boom to support the weight of the shield. For the initial gross gamma survey, directional sensitivity is not necessary.

The non-destructive assay techniques considered for the fuel debris assay either detect neutrons or gamma rays emitted naturally from irradiated LWR fuel or detect neutrons induced by interrogation of the fuel debris with a neutron source. The former are termed passive techniques, the latter active techniques.

3.1 Passive Techniques

3.1.1 Neutron Counting

The spontaneous fission of an even-mass-number transuranic isotope (e.g., ^{238}Pu, ^{240}Pu, ^{242}Cm, or ^{244}Cm) produces two or more neutrons emitted in coincidence. An alternate mode of decay available to the transuranics is the emmission of alpha particles, which can interact with light elements such as oxygen and fluorine, and these reactions produce singly emitted neutrons (e.g., $^{16}O(\alpha,n)^{19}Ne$). Unless the chemical and isotopic composition of the fuel debris matrix is well characterized, measurements of natural neutron radiation may not be used to quantify the amount of fuel.

3.1.2 Gamma-Ray Counting

Many radioactive isotopes emit gamma-rays during decay. The energy and intensity of these gamma-rays uniquely characterize the isotope. All fissionable material is unstable, emitting some form of radiation by alpha, beta, or spontaneous fission decay. In this decay process, some fissionable isotopes emit gamma-radiation that can be quantitatively related to the original isotope. For example, ^{238}U alpha decays to ^{234}Th, which beta decays to ^{234m}Pa, which in turn beta decays to ^{234}U. The beta decay of ^{234m}Pa is characterized by the emission of two low-intensity gamma-rays with energies of 766.4 keV and 1001.1 keV. Similarly, the alpha decay of ^{235}U results in the emission of a gamma-ray with an energy of 185.7 keV.

The low, specific gamma-ray intensities of the ^{238}U daughter gamma rays, 39 γ/s/g and 103 γ/s/g,[3] and the low energy of the principal signature gamma-ray of ^{235}U compromise their usefulness to a passive assay approach. However, a number of long-lived fission products emit high-energy gamma-rays with sufficient intensity to make possible the quantification of the fission product inventory in a length of primary coolant pipe. The amount of fuel in the pipe may be deduced using these measurement data, if the fuel isotopic composition and physical distribution are known.

3.2 Active Methods

To distinguish neutrons that result from the fission of fissionable nuclides in the fuel from the interrogating neutrons, one of the following measurement techniques is commonly used. Both photoneutron and (α,n) sources emit neutrons singly, while a fission event is characterized by the emission of two or more neutrons. Thus, a detector system with coincidence circuitry may be employed to count prompt fission neutrons in the presence of a photoneutron or (α,n) neutron background. A second approach relies on the detection of high-energy fission neutrons. Moderating material is placed between the interrogating neutron source and detectors to degrade the energies of the interrogating neutrons so that they are either absorbed, or

their energies are brought to below the threshold of the detectors. A third approach relies on the detection of delayed-fission neutrons. A number of nuclides produced by fission have been identified as being delayed-neutron precursors. The half-lives of the precursors are sufficiently long to allow transferring an interrogating isotopic neutron source from the assay location to a shielded position before commencing counting. Isotopic neutron sources could be used in a shuffler system to cyclically irradiate a pipe location, and delayed neutrons could be counted cyclically to quantify the fissionable material content of the pipe. Alternatively, a neutron generator could supply the interrogating neutrons.

3.2.1 Isotopic Neutron Sources

The three classes of isotopic neutron sources routinely used for fissionable material assay are photoneutron, (α,n) neutron, and spontaneous fission neutron sources. Photoneutron sources have neutron yields on the order of 10^6 n/s/Ci and produce fairly monoenergetic neutrons in the keV range. The intensities of the (α,n) sources range from 10^4 n/s/Ci to 10^6 n/s/Ci, and the neutron energy spectra of (α,n) sources are all characterized by a large range in emitted neutron energy with mean energies of a few MeV. The spontaneously fissioning nuclide, ^{252}Cf, has a yield of 4.3×10^9 n/s/Ci, and the emitted neutrons have an average of 2.3 MeV.[4]

3.2.2 Cockroft-Walton Neutron Generator

Pulsed neutron generators of the Cockroft-Walton type produce 14.3 MeV neutrons by the deuterium-tritium reaction. These generators have nominal outputs of 1×10^3 n/s and may be operated at pulse rates from 1 to 10 pulses per second.

4. ANALYSIS OF ASSAY MEASUREMENT TECHNIQUES

4.1 Minimum Detectable Level

Minimum detectable levels (MDLs) for the assay techniques studied here have been calculated, using the definition of an MDL given by L. A. Currie.[5] He defines two types of detection limits--an a posteriori limit, L_C, and an a priori limit, L_D. The L_C limit provides a test statistic against which acquired data can be tested in order to determine whether the measured response is statistically nonzero. The higher, L_D, limit defines the detector response required to be certain, to some desired confidence level, that material will be detected. The limits L_C and L_D have been defined by Currie as

$$L_C = k_\alpha \sqrt{2}\, \sigma_B$$

$$L_D = 2L_C + k_\alpha^2$$

where

σ_B =   the standard deviation of the background distribution

k_α =   the percential of the normal distribution at the significance level chosen. $k_\alpha = 1.645$ for a 5% significance level (95% confidence level).

Thus, an a priori minimum detectable level may be determined by dividing the calculated a priori limit L_D by the assay system sensitivity:

$$M_D = \frac{L_D \text{ (counts)}}{S_E \left(\frac{\text{counts}}{\text{gram-s}} \right) \Delta T(s)}$$

where

$$\Delta T \qquad = \qquad \text{count time in seconds}$$

$$S_E \qquad = \qquad \text{counting system sensitivity.}$$

4.2. Passive Methods

4.2.1 Neutron Counting

The neutron source strength due to (α,n) and spontaneous fission events in the TMI-2 fuel inventory has been calculated by Reactor Physics Branch personnel. An initial fuel inventory of 82.06 metric tons of uranium (93.09 metric tons UO_2) with an average enrichment of 2.57 wt% ^{235}U was assumed. Also assumed was a power history representing 96.2 effective full-power days at the rated thermal power of 2772 MW. This represents a fuel burnup of 3250 MWd/MTU. The calculated (α,n) and spontaneous fission neutron source strengths for the TMI-2 full-core inventory are presented graphically in Figure B-2 as a function of time through 1983.

The neutron source strength per gram UO_x was calculated, assuming a homogeneous distribution of transuranics throughout the core fuel inventory. The source strength in June 1982 will be 0.34 n/s-g UO_x. The neutron flux at a detector location external to a pipe containing a source of this strength may be estimated, if the source distribution and detector geometry are defined. Let us consider the fuel to be distributed in a horizontal pipe as a line source that is contiguous with the lowest internal surface of the pipe and that extends longitudinally the length of the pipe. The detector consists of four helium-3-filled proportional counters embedded in polyethylene, and the detector has the shape of a segment of an annulus, so that put in place for counting it surrounds the lower perimeter of the pipe. One inch of polyethylene separates the pipe's external surface from the detectors, which are oriented horizontally along the longitudinal axis of the pipe.
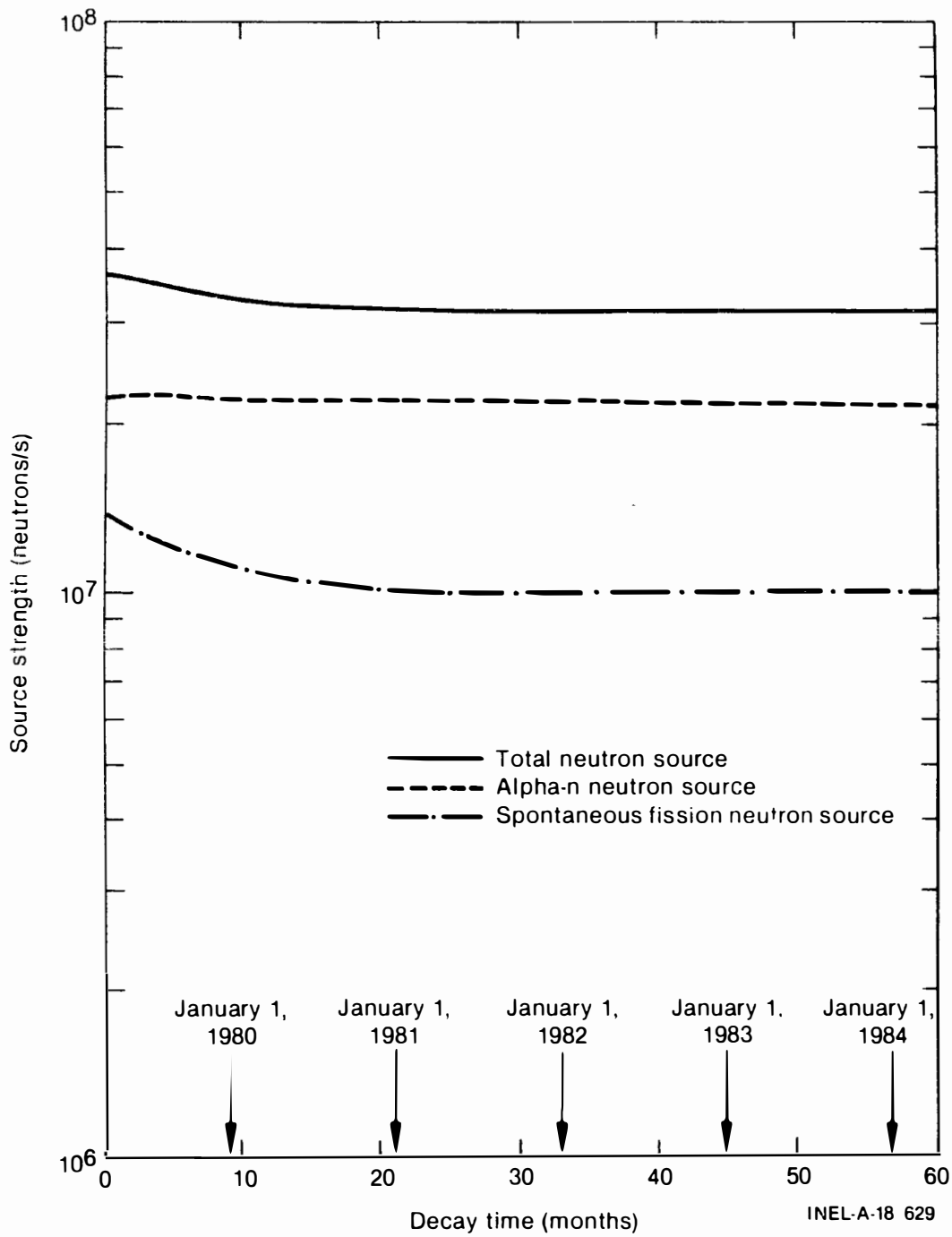
Figure B-2.   Neutron source strengths TMI-2 full core inventory.

The flux at the location of the detectors may be estimated, using the following equation:[7]

$$\phi = \frac{B\ S_L}{4\pi\ a} \left\{ \int_0^{\theta_1} e^{-\Sigma\ x\ \sec\theta}\ d\theta + \int_0^{\theta_2} e^{-\Sigma\ x\ \sec\theta}\ d\theta \right\}$$

where

B = symbolic buildup factor

S_L = source strength of line source (n/s-cm)

a = perpendicular distance from line source to detector (cm)

Σ = macroscopic scattering cross section of pipe wall at 1 MeV ($0.2\ cm^{-1}$)

x = pipe wall thickness (cm)

ϕ = angle subtended by line source at flux point.

Given a longitudinal UO_x deposit of 1 g/cm in a hot leg pipe, the average uncollided flux over the detector assembly when it is placed in contact with the outside lower surface of the pipe insulation is approximately 3×10^{-4} n/s-cm^2. We may estimate the buildup factor in the following way. Calculations have been performed which indicate that about 30% of the source neutrons can be expected to leak out of the pipe.[8] If we consider this leakage to be restricted circumferentially to the lower pipe surface subtending an angle of 90° at the pipe center, then the average flux over that surface is 1×10^{-3} n/s-cm^2. This implies a buildup factor equal to 3.3. This value is not unreasonable, so we shall use the latter value of the average flux to calculate a minimum detection limit.

89

The surface area of the detector considered here is about 1.1×10^3 cm^2. Neutron detectors consisting of arrays of ^{3}He proportional counters embedded in polyethylene moderators have intrinsic efficiencies of about 10%.[9] The detector considered here would have an intrinsic efficiency less than 10%, and we shall assume it to be 5%. Using the average flux determined above, the passive neutron assay system count rate would be 5.5×10^{-2} cps per gram UO$_x$ per cm of pipe length.

The typical background count rate of a detector of the type considered here is between 1 and 5 cps.[10] Using a background count rate of 3 cps and the value of the detector sensitivity noted above, the minimum detectable linear fuel density for a 1 000 second count is 4.7 g/cm. This limit is decreased to 2.8 g/cm if the pipe insulation is removed and the detector is placed against the lower hot leg pipe surface. If the background count rate is 2 cps, the minimum detectable linear fuel density for the latter geometry is 2.4 g/cm of pipe length.

4.2.2 Gamma-Ray Counting

Gamma-rays associated with the decay of uranics or fission products can be counted with a detector collimated to interrogate a section of primary system pipe. The amount of fuel in the pipe can be determined using these measurement data if the fuel isotopic composition and physical distribution are known. As an aid to determining the feasibility of this method, the ORIGEN--ORNL Isotopic Generation and Depletion--Code was used to estimate the fission product inventory of a TMI-2 fuel assembly. The inventory was calculated on the three-month time period beginning January 1, 1982 and ending April 1, 1984. The results of those calculations for a number of fission products are presented in Table B-1.[11] The calculations were performed disregarding fuel assembly perturbation, meaning that the concentrations were calculated without taking into account the inventory losses that have occurred as a result of leaching or other processes.

The activity concentrations of ^{134}Cs and ^{137}Cs indicated in Table B-1 are probably about twice the true concentrations. These isotopes are known to migrate toward the cooler regions of a fuel pile and therefore

90

TABLE B-1. JUNE 1982 ISOTOPIC ACTIVITY CONCENTRATIONS PER GRAM URANIUM[11] OF A TMI-2 FUEL ASSEMBLY

Nuclide	dps/g U	Nuclide	dps/g U
^{90}Sr	3.45 E+08	^{134}Cs	4.68 E+07
^{90}Y	3.45 E+08	^{137}Cs	3.72 E+08
^{91}Y	2.72 E+04	^{144}Ce	6.14 E+08
^{93}Z	1.24 E+04	^{144}Pr	6.14 E+08
^{95}Z	1.28 E+05	^{144M}Pr	7.37 E+06
^{95}Nb	2.76 E+05	^{147}Pm	5.95 E+08
^{99}Tc	5.68 E+04	^{151}Sm	7.45 E+06
^{106}Ru	1.49 E+08	^{154}Eu	3.06 E+06
^{106}Rh	1.49 E+08	^{155}Eu	4.10 E+06
^{125}Sb	1.13 E+07	^{235}U	2.41 E+03
^{125M}Te	2.76 E+06	^{238}U	1.20 E+04

tend to concentrate near the radial and axial boundaries of the fuel pellets.[12] Thus, they are highly susceptible to leaching when fuel is exposed following a cladding breach. Ru-106 has also been observed to migrate. It is volatile and tends to concentrate around the centerline of a fuel pellet. Three nuclides listed in Table B-1 that do not migrate are ^{95}Nb, ^{144}Ce, and ^{154}Eu.[12] One would, therefore, expect these nuclides to remain integrated with the fuel.

Several nuclides listed in Table B-1 may be removed from consideration for fuel assay application because they are either pure beta emitters (^{90}Sr and ^{93}Zr) or because the intensities or energies of the gamma rays emitted are too low (^{90}Y, ^{99}Tc, and ^{147}Pm).

For calculation, a relatively simple source geometry was assumed and the analysis which follows is for that geometry only. The extension to more complicated geometries (e.g. steam generator and pressurizer plenums, demineralizers, and tanks) would require additional modeling and calculation.

A section of hot leg pipe shrouded in insulation is shown in Figure B-3. The end-on view of the pipe indicates the five positions at which the uncollided flux was calculated, given a hypothetical uranium volume source of 5 mm depth running the length of a 1-meter-long pipe. The uncollided flux per source photon is given in Table B-2[13] for each detector location for twelve source gamma-ray energies. Detector position 5 is the position of maximum flux. Table B-3 lists the calculated uncollided fluxes at this position, per gram uranium, of the more intense gamma-rays of ^{238}U and ^{235}U. The intensities of these latter gamma-rays are too weak to be used for assay purposes. The most intense fluxes are associated with gamma-rays emitted by ^{137}Cs and ^{134}Cs. The values of these fluxes are, respectively, 10 and 2 γ/cm^2-s/g U. Three gamma-rays emitted by ^{144}Pr exhibit respectable fluxes at a detector distance of 1 meter from the pipe insulation surface. The 2 186 keV gamma-ray has the highest flux of the three, with a value of about 1.3 γ/cm^2-s/g U. These fluxes could be increased by a factor of 10 by moving the detector closer to the pipe.

The uncollided flux values of Table B-3 determine the count rate that can be expected from a detector whose intrinsic photopeak efficiency and surface area are defined. A photopeak count rate measured by a detector that is collimated to interrogate a section of pipe is expressed as a function of these variables in the following equation.

$$c/s_{ij} = S_j \cdot m \cdot y_i \cdot F_i \cdot A_d \cdot \epsilon_{p_i} + R_{B_i}$$

where

$$c/s_{ij} \qquad = \qquad \text{counts per second in photopeak (i) associated with isotope (j)}$$

$$S_j \qquad = \qquad \text{source strength of isotope (j) in disintegrations per second per gram uranium}$$

Figure B-3. Section of hot leg pipe shrouded in insulation.

93

TABLE B-2. CALCULATED FLUX PER SOURCE PHOTON AT FIVE POSITIONS EXTERNAL TO A SECTION OF TMI-2 HOT LEG PIPE SHROUDED IN INSULATION

	Direct-Beam Flux (#/cm^{2}sec/source particle)[a]				
	Point Detector Position				
Energy (MeV)	1	2	3	4	5
3.0	3.976-9[b]	3.892-9	5.413-9	7.490-8	4.214-7
2.0	1.168-9	1.024-9	1.553-9	3.694-8	2.682-7
1.5	3.742-10	3.162-10	5.113-10	1.890-8	1.745-7
1.0	5.070-11	4.469-11	7.878-11	5.695-9	8.062-8
0.8	1.459-11	1.338-11	2.479-11	2.694-9	4.968-8
0.6	2.521-12	2.496-12	4.938-12	9.352-10	2.500-8
0.5	7.777-13	8.227-13	1.693-12	4.595-10	1.574-8
0.4	1.574-13	1.898-13	4.080-13	1.735-10	8.324-9
0.3	1.385-14	2.198-14	4.947-14	3.880-11	3.114-9
0.2	8.088-17	4.882-16	9.962-16	1.356-12	3.378-10
0.15	8.563.20	7.202-18	1.027-17	1.243-14	1.459-11
0.1	1,196-29	2.482-23	6.956-24	1.239-21	1.376-16

a. One isotropic source particle is emitted in the source volume.

b. Read as 3.976 x 10^{-9}.

TABLE B-3.   CALCULATED UNCOLLIDED FLUX PER GRAM URANIUM AT DETECTOR
POSITION 5 (as of June, 1982)

Nuclide	Half-Life[a,b]	Energy[a,b] (keV)	Branching[a,b] Intensity (%)	Uncollided Flux γ/cm^2-s/g U
137 Cs	30.174 Y	661.645	8.50 E+01	1.03 E+01
134 Cs	2.062 Y	795.845	8.54 E+01	1.97 E+00
144 CeD	284.4 D	2185.700	6.94 E-01	1.26 E+00
134 Cs	2.062 Y	604.699	9.76 E+01	1.17 E+00
106 RuD	368.2 D	621.800	9.81 E+00	4.05 E-01
144 CeD	284.4 D	696.480	1.34 E+00	3.04 E-01
144 CeD	284.4 D	1489.150	2.78 E-01	2.94 E-01
134 Cs	2.062 Y	1365.150	3.04 E-00	2.12 E-01
134 Cs	2.062 Y	801.932	8.73 E+00	2.04 E-01
106 RuD	368.2 D	1050.100	1.46 E+00	1.96 E-01
134 Cs	2.062 Y	569.315	1.54 E+01	1.60 E-01
154 Eu	8.5 Y	1274.450	3.55 E+01	1.44 E-01
134 Cs	2.062 Y	1167.940	1.80 E+00	9.45 E-02
134 Cs	2.062 Y	563.227	8.38 E+00	8.47 E-02
125 Sb	2.71 Y	600.770	1.79 E+01	5.08 E-02
154 Eu	8.5 Y	1004.760	1.74 E+01	4.34 E-02
134 Cs	2.062 Y	1038.570	1.00 E+00	4.11 E-02
125 Sb	2.71 Y	636.150	1.15 E+01	3.83 E-02
125 Sb	2.71 Y	427.950	3.00 E+01	3.52 E-02
154 Eu	8.5 Y	996.320	1.03 E+01	2.52 E-02
154 Eu	8.5 Y	723.300	1.97 E+01	2.42 E-02
125 Sb	2.71 Y	463.510	1.05 E+01	1.55 E-02

TABLE B-3. (Continued)

Nuclide	Half-Life[a,b]	Energy[a,b] (keV)	Branching[a,b] Intensity (%)	Uncollided Flux λ/cm^2-s/g U
125 Sb	2.71 Y	606.820	4.92 E+00	1.44 E-02
95 Nb	35.1 Y	765.781	9.98 E+01	1.25 E-02
154 Eu	8.5 Y	1596.480	1.67 E+00	9.84 E-03
238 U	4.47 E+09 Y	1001.100	8.28 E-01	8.08 E-06
238 U	4.47 E+09 Y	766.390	3.13 E-01	1.73 E-06
235 U	7.04 E+08 Y	185.720	5.400 E+01	3.19 E-07

a. N. C. Dyer et al., "Procedures Source Term Measurement Program," TREE-1178 (1977).

b. R. H. Augustson and T. D. Reilly, "Fund. of Passive Nondestructive Assay of Fissionable Material, LA-5651-M (1974).

m	=	mass of uranium in grams in section of pipe being interrogated
y_i	=	branching intensity of gamma-ray associated with photopeak (i)--gammas per disintegration
$F_i \cdot A_d$	=	geometric detection efficiency = ratio of the number of uncollided photons of energy (i) striking the detector per second to the number of photons of energy (i) emitted per second within the fuel volume
A_d	=	detector face area - cm^2
ε_{p_i}	=	intrinsic photopeak efficiency at energy (i)--ratio of counts per second recorded in photopeak (i) to number of photons of energy (i) striking the detector

$$R_{B_i} \quad = \quad \text{background count rate in photopeak (i).}$$

The background count rates in the photopeaks of the cesiums will be due primarily to cesiums that are plated out on internal pipe surfaces or are in solution in the reactor coolant within the section of pipe being assayed. If plateout is uniform, this background contribution can be estimated by taking two measurements, one on the same radial axis that bisects the lower surface of the pipe and another on the axis that bisects the upper surface. The background count rate would then be given by

$$R_B = \frac{C_2 - C_5 \, x}{1 - x}$$

where

$$C_{2,5} \quad = \quad \text{count rate at detector location 2,5}$$

$$x \quad = \quad \text{fractional decrease in source flux relative to position five.}$$

Values of x may be determined from the data of Table B-2 for the particular source-detector geometries defined previously.

Alternatively, background measurements could be made by assaying vertical sections of pipe that are likely not to contain fuel debris.

Mininum detectable levels are given below as mg UO_x per meter of pipe length for an intrinsic germanium spectrometer with a front face surface area of 15 cm^2 located at detector position 5. Intrinsic photopeak efficiencies were estimated using the measured absolute efficiency of a Ge(Li) spectrometer, PG-1, for a point source at a distance of 30 cm. A live time of 1 000 seconds and background count rates equal to 10% of the source count rates were assumed.

97

Nuclide	Energy (keV)	M_D (mg/m)	Nuclide	Energy (keV)	M_D (mg/m)
^{137}Cs	661.6	9.1	^{106}RuD	621.8	44.0
^{134}Cs	795.8	22.1	^{144}CeD	696.5	53.7
^{144}CeD	2185.7	46.6	^{144}CeD	1489.1	84.3
^{134}Cs	604.7	25.0	^{154}Eu	1274.4	110.0

Detection limits of a NaI(Tl) crystal would be poorer than these, because of the significantly higher background count rates. The sensitivity enhancement possible using hyperpure germanium is entirely attributable to the enhanced resolution of germanium. A high resolution spectrometer is considered essential to determining fission product inventories of the fuel. Portable hyperpure germanium spectrometers are available with relative efficiencies of 5% and greater, and may be purchased with liquid nitrogen dewars sized to last as long as 24 hours.

The conceptual design of a gamma-ray acquisition and analysis system that utilizes a hyperpure germanium spectrometer is shown in Figure B-4. The detector, which is housed in a collimator shield, is fixed on the end of a telescopic boom having three degrees of freedom. The front-end electronics acquisition system includes a vendor-supplied preamplifier and analog-to-digital converter, as well as analog pulse shaping modules and pulser developed by EG&G Idaho. A multi-channel pulse height analysis system (MCA) is mounted in a mobile rack that also houses the front-end electronics and high-voltage power supply. These components compose the integral data acquisition part of the system and would be located inside the containment building.

To allow remote data acquisition and to provide for accurate and timely data analysis, the MCA is interfaced to a central processing unit (CPU) conveniently located location outside the reactor building. Peripherals of the CPU include data storage and retrieval devices, an operator console, and an analysis output printer.

Collimated
germanium detector
on telescopic boom

Gamma
radiation

Reactor
building

Preamp power
Pulser
HV power supply
Shaping amp
Fast amp

Serial interface

CRT

Mag
tape

MCA

CPU

Disk
storage

Front-end electronics
HV power supply
pulser

Operator
console

Line
printer

INEL-A-18 632
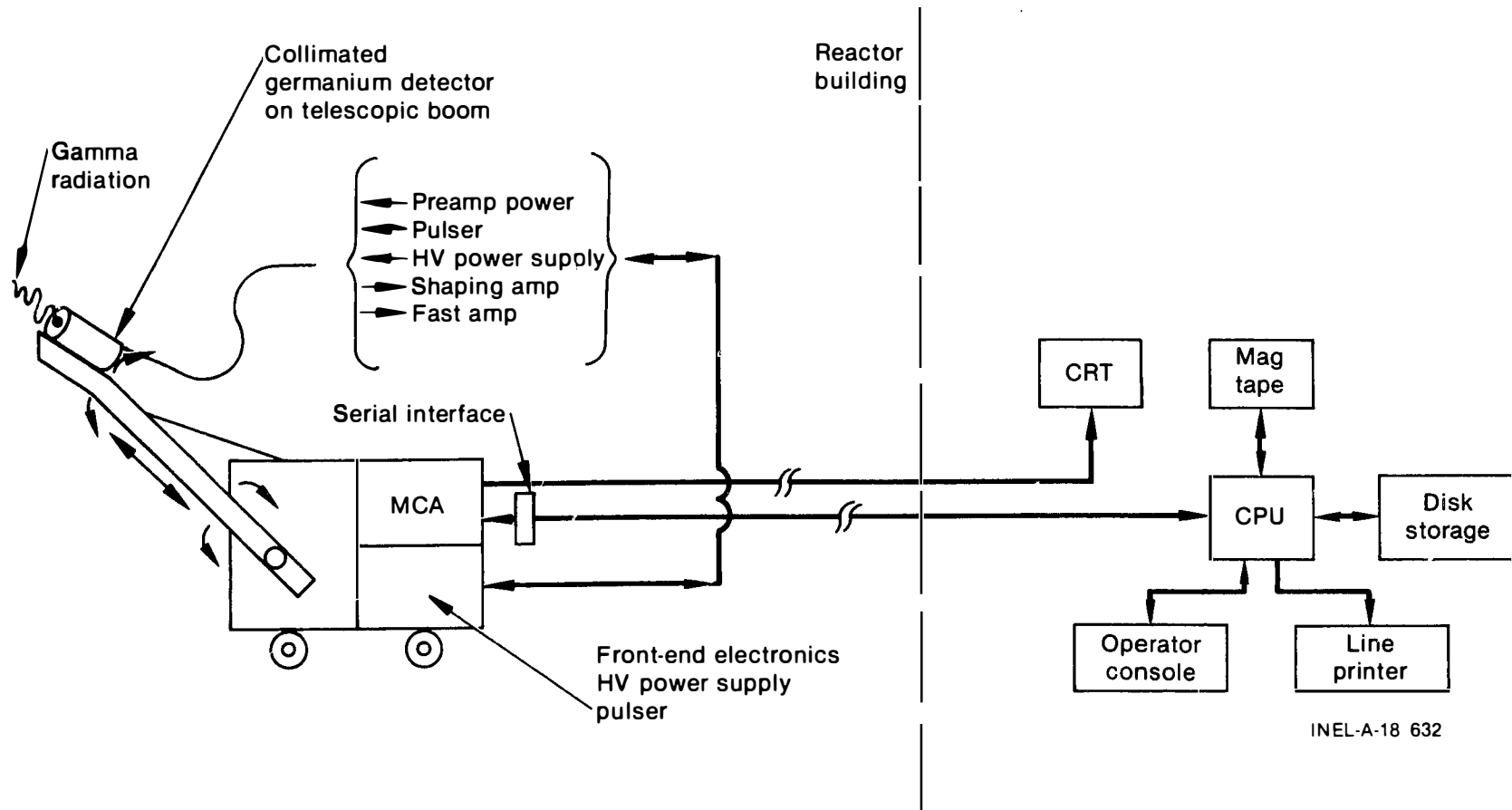
Figure B-4. Gamma-ray acquisition and analysis system.

An itemized cost estimate for this acquisition and analysis system is given in Table B-4. The Nuclear Data model ND66R MCA, with the communications options listed, is the preferred MCA because it could be integrated into the overall system without difficulty and is compatible with the RT-11 operating system.

4.3 Active Neutron Interrogation Methods

About seven photons and either two or three neutrons are promptly radiated in a fission event. In addition to these prompt neutrons and photons, dalayed neutrons and photons are emitted by short-lived fission products.

The presence of large inventories of fission products in the fuel and reactor coolant renders the counting of either prompt or delayed gamma-rays very difficult. For the application being considered here, the counting of neutrons must be the preferred fission signature.

The counting of prompt neutrons when using a neutron interrogating source is complicated by the presence of neutrons from the interrogator. This is because the die-away time of the neutron detector is on the order of the die-away time of the prompt neutrons originating from the source. In order to avoid this difficulty, it is necessary to count the delayed neutrons following fission.

The principle involved in the delayed fission neutron technique is that a fissionable nuclide, upon neutron capture, can fission and emit neutron-rich fission products. Although these fission products often decay by beta emission, a small fraction of them decay by direct neutron emission with a half-life characteristic of the particular fission product nuclide. These delayed fission neutrons can be counted, and provide a quantitative measure of the fissionable content of a section of pipe bombarded with interrogating neutrons.

For this particular assay, the neutron activation analysis/delayed fission neutron (NAA/DFN) technique requires that a pipe location be irradiated with a neutron flux over a predetermined time interval and that

100

TABLE B-4.   GAMMA-RAY ACQUISITION AND ANALYSIS SYSTEM

EQUIPMENT:

Nuclear Data Model ND66R MCA with 8192 channel solid state memory, remote keyboard, and 12-inch CRT monitor	$11,450
Nuclear Data 70-2437 ND66 Serial Interface (1-Port)	625
Nuclear Data 47-0233 ND66 Communications Firmware	1,000
Nuclear Data 47-0207 Extended Communications Firmware Package (1P)	400
Nuclear Data 48-8084 Communications Software	3,000
Nuclear Data Model ND575 ADC	1,250
Nim Bin	700
High-voltage power supply	1,000
Fast front-end electronics	2,000
Pulser	500
PDP 11/23, RL01 Hard Disk, DEC LA120 Console	23,000
Talley Line Printer	6,000
Magnetic tape data storage device	6,000
Hand-held intrinsic germanium detector	9,000
Miscellaneous equipment, parts, etc.	5,000
	$70,925

MANPOWER:

Electronics technician	3.0 months
Electronics engineer	2.5 months
Programmer	3.0 months
Machinist	1.0 month
Scientist	6.0 months

at $50K per man-year	**$64,600**

101

delayed neutrons resulting from the fission of fissionable materials be counted, commencing at the end of a predetermined decay period following termination of the interrogating flux. A number of such cycles could be used to optimize the sensitivity of the method. If an isotopic neutron source provides the interrogation flux, a pneumatic transfer system is necessary to quickly transfer the source between the assay location and a shielded storage location. An interrogation flux could alternatively be obtained, using a Cockroft-Walton type neutron generator. A generator of this type could be integrated with the detector assembly and be fired at a preselected frequency.

The net counts, C_N, expected over n irradiation cycles is given by[14]

$$C_N = \left[\frac{\varepsilon \nu m N_A}{A} \sum_j \bar{\phi}_j(E_j) \sigma_j(E_j) \right] / \sum_{i=1}^{6} \left(\frac{\beta_i}{\gamma_i} \right) \left(1 - e^{-\lambda_i t_0} \right) e^{-\lambda_i t_1} \left(1 - e^{-\lambda_i t_2} U_i \right)$$

where

$$U_i = \left[n - (n+1) e^{-\lambda_i T} + e^{-(n+1)g_i T} \right] / (1 - e^{-\lambda_i T})^2$$

where

ε	=	the efficiency of the neutron counter in counts per delayed neutron
ν	=	the average number of neutrons emitted per fission
m	=	mass of the fissile or fertile material in grams
N_A	=	Avogadro's number (atoms per gram atomic weight)
$\sigma_j(E_j)$	=	fission cross section of the fissionable nuclide energy (E_j) in cm^2

$\bar{\phi}_j(E_j)$ = average neutron flux in the energy band (E_j) that irradiates the fissionable material in n/cm^2-s

A = atomic mass number of the fissionable nuclide

β_i = fraction of fission neutrons emitted as delayed neutrons in group i

λ_i = decay constant of the ith delayed neutron group (s^{-1})

t_0 = irradiation duration(s)

t_1 = decay interval following irradiation (s)

t_2 = counting time (s)

T = the total analysis time/cycle ($t_0 + t_1 + t_2$ + decay time following count) (s).

For post-irradiation decay times of less than about 20 s, undesirable background from delayed neutrons produced from ^{17}O by the fast-neutron reaction

$$^{17}O(n,p)^{17}N \xrightarrow{\beta^-} {}^{17}O^* \rightarrow {}^{16}O + n(\text{delayed})$$
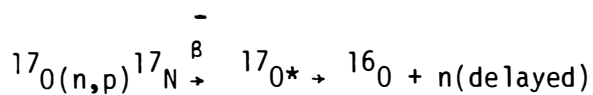
must be considered. The threshold energy for this reaction is 8.2 MeV and the half-life of ^{17}N is 4.16 S.[15]

One-dimensional transport calculations have been performed to estimate the fission rate and delayed neutron leakage rate resulting from the neutron irradiation of a hot leg pipe containing UO_x. The model used for these calculations assume the fuel to be uniformly dispersed in an annulus that is contiguous with the pipe internal surface and 1 cm thick. A reactor

coolant boron concentration of 3500 ppm is also assumed. Fission rates were calculated for three interrogating neutron energies for the case where the interrogating source is located on the outside surface of the hot leg pipe. The calculated values are given below.

$$\text{Fissions/Source Neutron/g UO}_x$$

Source	Mean Energy	With Insulation	Without Insulation
^{88}Y Be	150 keV	7.4 (-6)	---
^{252}Cf	2.3 MeV	6.1 (-6)	9.0 (-6)
Accelerator	14.3 MeV	8.1 (-6)	1.2 (-5)

Inserting 5 cm of stainless steel between the 14.3 MeV interrogation source and the pipe results in no change in the fission rate. Five cm of polyethylene causes a decrease in the fission rate for all three sources. Additional calculations indicate that about 30% of the delayed fission neutrons can be expected to leak out of the pipe. The $^{17}O(n,p)^{17}N$ reaction rate was calculated to be 3.4 x 10^{-7} per 14.3 MeV interrogating neutron and the fraction of the neutrons associated with the decay of ^{17}N that can be expected to leak out of the pipe was determined to be 0.095.

Tables B-5 and B-6 present the calculated net detector response (c/g) and net background counts of active assay systems that employ, respectively, a 10^9 n/s ^{252}Cf source and a 1 x 10^8 n/s neutron generator. The data of Table B-5 were calculated for the case where the source is adjacent to the lower surface of hot leg pipe insulation, and the data of Table B-6 were calculated for the case where the insulation is removed and the accelerator head is adjacent to the lower surface of the hot leg pipe wall. A net background count rate of 2 cps was assumed.

Below are the estimated minimum detection limits as a function of the number of irradiation cycles of a 1 mg ^{252}Cf shuffler assay system and a 1 x 10^8 n/s neutron generator assay system. For each system two cases were considered; in one case the insulation was in place, and in the other the insulation was removed.

104

TABLE B-5. CALCULATED RESPONSE OF ACTIVE ASSAY SYSTEM EMPLOYING A 1 MG ^{252}Cf SOURCE

Irradiation Duration: 20 s   Count Time: 20 s

Decay Time: 0.5 s   Cycle Time: 41 s (0.5 s travel time each way)

Number Cycles	$\Sigma V_i U_i$	C_T/g	$V_N U_N$	B_T	Percent Contribution to Net Counts By Group					
					55.7$\angle$	22.72	6.22	2.30	0.610	0.230
1	2.675(-2)	1.7	4.873(0)	4.0(1)	--	--	--	--	--	--
2	5.683(-2)	3.6	9.762(0)	8.0(1)	3.81	38.58	30.52	25.70	1.31	0.07
3	8.80(-2)	5.6	1.465(1)	1.2(2)	4.31	39.82	29.62	24.90	1.27	0.07
4	1.196(-1)	7.7	1.953(1)	1.6(2)	4.70	40.47	29.09	24.43	1.25	0.07
5	1.513(-1)	9.7	2.441(1)	2.0(2)	4.98	40.84	28.75	24.13	1.23	0.07
6	1.832(-1)	11.7	2.930(1)	2.4(2)	5.20	41.07	28.51	23.93	1.22	0.07
7	2.150(-1)	13.8	3.418(1)	2.8(2)	5.37	41.23	28.34	23.78	1.21	0.07
8	2.469(-1)	15.8	3.906(1)	3.2(2)	5.51	41.35	28.21	23.66	1.21	0.07
9	2.789(-1)	17.8	4.395(1)	3.6(2)	5.62	41.43	28.11	23.57	1.20	0.06
10	3.108(-1)	19.9	4.883(1)	4.0(2)	5.71	41.50	28.03	23.50	1.20	0.06
12	3.746(-1)	24.0	5.860(1)	4.8(2)	5.85	41.60	27.90	23.39	1.20	0.06
14	4.385(-1)	28.1	6.837(1)	5.6(2)	5.94	41.67	27.82	23.32	1.19	0.06
18	5.663(-1)	36.2	8.790(1)	7.2(2)	6.08	41.76	27.70	23.22	1.19	0.06
20	6.301(-1)	40.3	9.767(1)	8.0(2)	6.12	41.79	27.66	23.18	1.18	0.06
30	9.495(-1)	60.8	1.465(2)	1.2(3)	6.26	41.88	27.54	23.08	1.18	0.06
40	1.269(0)	81.2	1.953(2)	1.6(3)	6.33	41.93	27.48	23.02	1.18	0.06

TABLE B-6.   CALCULATED RESPONSE OF ACTIVE ASSAY SYSTEM EMPLOYING A 1×10^8 n/s NEUTRON GENERATOR

Pulse Duration (t_0) = 3 s $\qquad$ Count Time (Δt) = 490 ms

Decay Time (t_1) = 8 ms $\qquad$ Cycle Time (T) = 500 ms

Number Cycles	$\sum_{i=1}^{6} V_i U_i$	C_T/g	$V_N U_N$	B_T	Percent Contribution to Net Counts By Group					
					55.72	22.72	6.22	2.30	0.610	0.230
1	9.632(-4)	1.66(-2)	7.437(-2)	9.8(-1)	--	--	--	--	--	--
2	2.539(-3)	4.39(-2)	2.172(-1)	1.96(0)	0.15	2.48	7.82	39.57	31.98	17.99
3	4.569(-3)	6.89(-2)	4.229(-1)	2.94(0)	0.17	2.75	8.53	41.98	30.85	15.72
4	6.961(-3)	1.20(-1)	6.866(-1)	3.92(0)	0.19	2.99	9.17	43.89	29.66	14.10
5	9.653(-3)	1.67(-1)	1.004(0)	4.90(0)	0.20	3.22	9.75	45.42	28.51	12.90
6	1.260(-2)	2.18(-1)	1.370(0)	5.88(0)	0.22	3.43	10.27	46.66	27.44	11.98
7	1.577(-2)	2.72(-1)	1.781(0)	6.86(0)	0.23	3.64	10.75	47.66	26.47	11.25
8	1.914(-2)	3.31(-1)	2.233(0)	7.84(0)	0.24	3.84	11.20	48.48	25.59	10.65
9	2.267(-2)	3.92(-1)	2.724(0)	8.82(0)	0.26	4.03	11.62	49.15	24.80	10.15
10	2.636(-2)	4.55(-1)	3.250(0)	9.80(0)	0.27	4.21	12.01	49.69	24.09	9.74
15	4.662(-2)	8.05(-1)	6.316(0)	1.47(1)	0.33	5.07	13.65	51.17	21.45	8.34
20	6.903(-2)	1.19(0)	9.923(0)	1.96(1)	0.38	5.85	14.92	51.53	19.77	7.55
30	1.177(-1)	2.03(0)	18.084(0)	2.94(1)	0.49	7.24	16.74	51.07	17.80	6.67
40	1.696(-1)	2.93(0)	26.892(0)	3.92(1)	0.58	8.46	17.94	50.18	16.65	6.18
50	2.237(-1)	3.86(0)	35.981(0)	4.90(1)	0.67	9.54	18.73	49.29	15.90	5.87
60	2.792(-1)	4.82(0)	45.192(0)	5.88(1)	0.76	10.49	19.27	48.48	15.35	5.65

14.3 MeV Neutron Generator

Insulation	Number Cycles	Detection Limit (g UO_x/cm of pipe length)
Yes	30	1.5
Yes	60	0.8
No	30	0.8
No	60	0.5

^{252}Cf Shuffler

Insulation	Number Cycles	Detection Limit
Yes	30	0.07
Yes	40	0.06
No	30	0.04
No	40	0.03

The conceptual designs and costs of these two active assay systems are presented in Figures B-5 and B-6 and Tables B-7 and B-8.
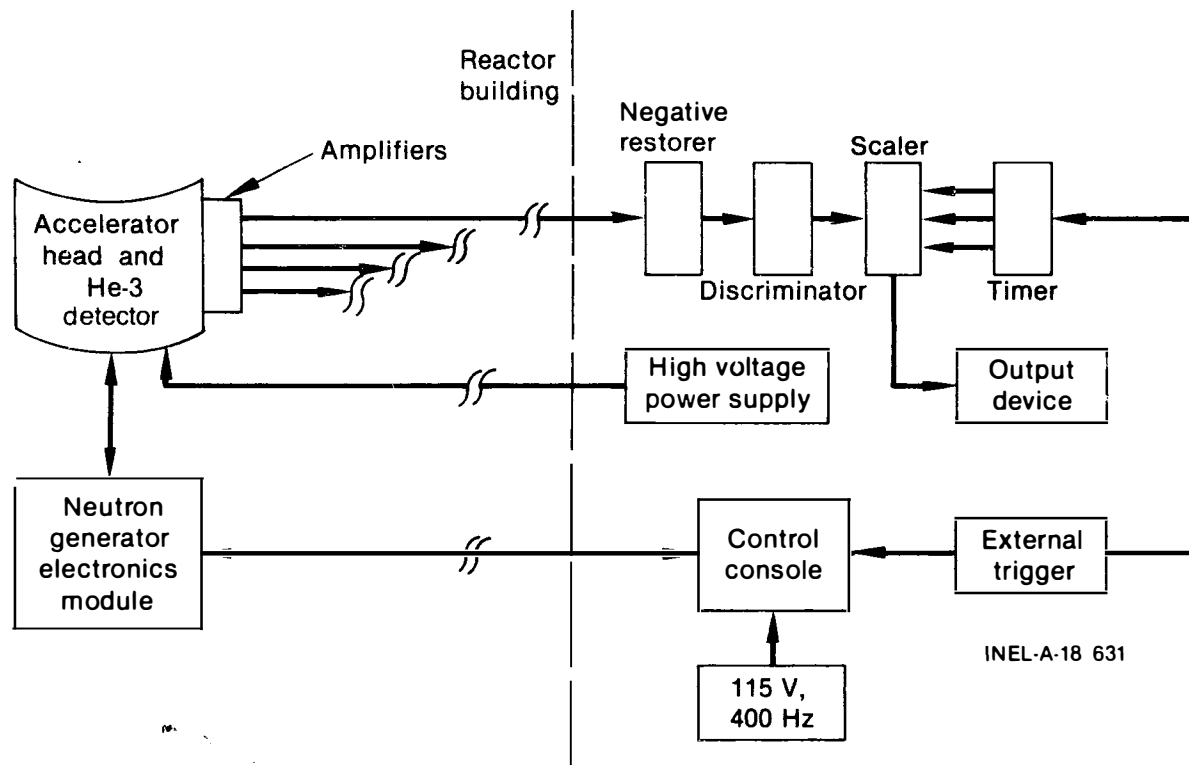
Figure B-5. DFN system with Cockcroft-Walton generator.
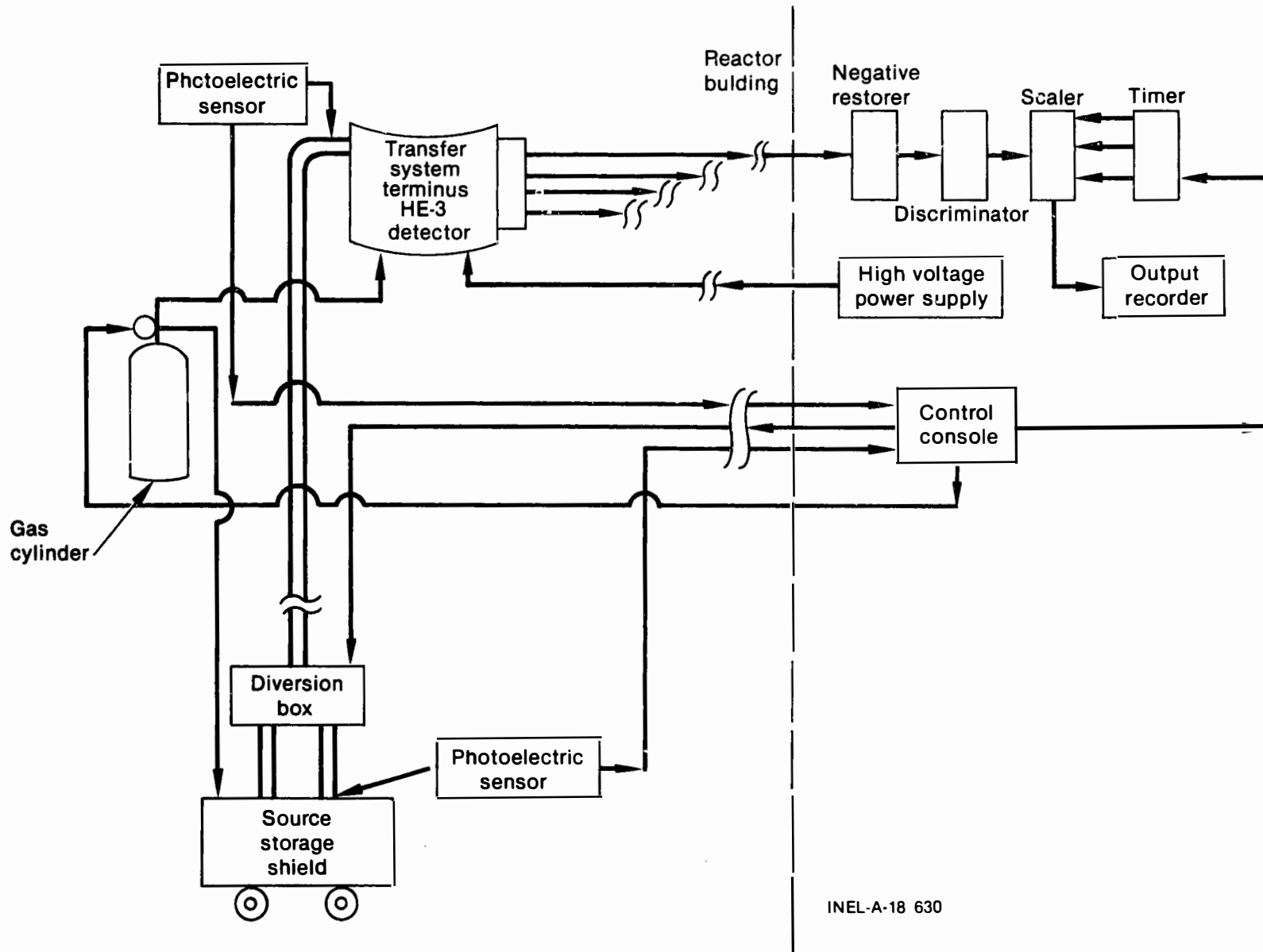
Figure B-6. DFN system with isotopic neutron source shuffler.

TABLE B-7.   DFN SYSTEM WITH COCKCROFT-WALTON GENERATOR

EQUIPMENT:

Kaman Sciences Model A-820A Accelerator Head	$ 5,500
Kaman Sciences Model A-620E Electronics Module	7,000
Kaman Sciences Model A-620R Control Console	3,000
115 V. 400 Hz power supply and cabling	2,000
He-3-filled proportional counters	9,000
High-voltage power supply (2 ea)	2,000
Electronics	25,000
Nim Bin (3 ea)	2,100
Calibration materials and standards	5,000
Miscellaneous equipment, parts, etc.	5,000
	$65,600

MANPOWER:

Electronics engineer	3 months	
Electronics technician	3 months	
Machinist	2 months	
Scientist	12 months	
at $50K per man-year		$83,300

TABLE B-8. DFN SYSTEM WITH CALIFORNIUM-252 SHUFFLER

EQUIPMENT:

Pneumatic transfer system	$13,000
Californium-252	
He-3-filled proportional counters	9,000
High-voltage power supply (2 ea)	2,000
Electronics	25,000
Nim Bin (3 ea)	2,100
Shield materials	4,000
Calibration materials and standards	5,000
Miscellaneous equipment, parts, etc.	5,000
	$65,100

MANPOWER:

Electronics	3 months
Electronics technician	2 months
Mahcinist	3 months
Scientist	12 months

| at $50K per man-year | $83,300 |

111

5. CONCLUSIONS

The assay technique having by far the best sensitivity is the passive gamma-ray counting method. This method relies on the detection of the signature gamma rays of ^{144}Pr, ^{154}Eu, or other isotopes that have been retained by the fuel. Therefore, a preliminary task essential to this technique is the examination of fuel debris samples collected from the letdown filters and casings and other system locations. The isotopic inventories of these samples should be measured to define the ranges of the concentrations of the isotopes that have remained integrated with the fuel. If these ranges are determined to be small, the passive gamma-ray assay technique is the preferred approach.

System calibration can be accomplished by assaying mock-up pipes in which irradiated fuel standards have been placed. The fuel distribution can be varied so as to measure the dependence of the system response on fuel thickness, and the detector-source geometry can be varied to evaluate the dependence on geometry.

The gamma-ray assay technique will provide quantitative measurements of the fission product inventories of fuel debris and could easily be adapted for use in determining fission product transport and deposition in auxiliary systems.

The system sensitivities calculated for the active neutron techniques indicate that a neutron generator and an isotopic source of equal output (n/s) can be expected to yield comparable system sensitivities. To achieve a detection limit significantly better than that which exists with a passive neutron counting system (a few g/cm), it is necessary to use a 1 mg or larger ^{252}Cf source. Such a source would require substantial shielding and would introduce an additional, potential hazard to personnel involved in assay measurements. A Monte Carlo calculation is a necessary preliminary task if any of the neutron counting techniques is considered further.

6. REFERENCES

1. J. A. Daniel, private communication, General Public Utilities TMI October 13, 1980.

2. K. Patten, private communication, Diamond Power Specialty Co., Lancaster, Ohio, October 20, 1980.

3. R. H. Augustson and T. D. Reilly, "Fundamentals of Passive Nondestructive Assay of Fissionable Material," LA-5651-M, 1974.

4. J. R. Beyster and L. A. Kull "Safeguards Applications for Isotopic Neutron Sources," BNL-50267, June 1970.

5. L. A. Currie, Analytical Chemistry, 25, 1968, p. 586.

6. Results of calculations performed by B. G. Schnitzler reported to author via letter, September 11, 1980.

7. Theodore Rockwell III, ed., Reactor Shielding Design Manual, 1956 p. 348.

8. B. G. Schnitzler, private communication, Reactor Physics Branch, EG&G Idaho, October 10, 1980.

9. L. V. East and R. B. Walton, "Polythylene Moderated ^{3}He Neutron Detectors," Nuclear Instruments and Methods, 72, 1969 p. 161.

10. E. B. Nieschmidt, private communication, Applied Physics Branch, EG&G Idaho, August 21, 1980.

11. Results of ORIGEN code calculations performed by B. G. Schnitzler, October 1980.

12. J. R. Phillips et al., "Application of Nondestructive Gamma-Ray and Neutron Techniques for the Safeguarding of Irradiated Fuel Materials," LA-8212, May 1980.

13. Results of QAD code calculations performed by W. Y. Yoon, Reactor Physics Branch, EG&G Idaho, October 1980.

14. S. E. Binney and R. I. Scherpelz, "A Review of the Delayed Fission Neutron Technique," Nuclear Instruments and Methods, 154, 1978, p. 413.

15. K. W. MacMurdo and W. W. Bowman, "Assay of Fissile Materials by a Cyclic Method of Neutron Activation and Delayed-Neutron Counting," Nuclear Instruments and Methods, 141, 1977, p. 299.

APPENDIX C

THE FEASIBILITY OF USING INFRARED TECHNIQUES
FOR LOCATING FUEL DISPERSED IN
THE TMI-2 REACTOR SYSTEM

L. Isaacson

THE FEASIBILITY OF USING INFRARED TECHNIQUES

FOR LOCATING FUEL DISPERSED IN

THE TMI-2 REACTOR SYSTEM

INTRODUCTION

The accident at Three Mile Island (TMI) affords a unique opportunity
to examine the effects of an accident involving nuclear fuel rods. Prior
to opening the primary system and removing fuel rods for examination, it is
desired to remotely examine the TMI-2 reactor for evidence of fuel dispersal
within the primary system. One technique suggested for accomplishing the
remote examination of the primary system is infrared IR thermography. This
appendix examines the feasibility of using infrared thermography to remotely
examine of the primary system of the TMI-2 reactor and locate and quantify
the nuclear fuel dispersed therein.

TECHNICAL DISCUSSION

The infrared radiation emitted from an object can be used as a signa-
ture to differentiate that object from its surroundings. It has been esti-
mated (Appendix D) that about a 9-mm layer of fuel in the insulated pipe in
the primary system of the TMI-2 reactor should produce a 0.36°F (0.2 K)
increase in temperature at the outside surface of the pipe. Thus, it is
reasoned that measurements of the local temperature increases (radiance
changes) along the surface of the pipe should indicate the location and
quantity of fuel dispersed within the primary system. If we are correct,
the infrared region of the electromagnetic spectrum can be used for inter-
preting the temperature rises that occur along the surface of the pipe.

The spectral radiance, N_λ, for a black body is given by the Planck
radiation law as[1,2]

$$N_\lambda = \frac{c_1}{\lambda^5}\left(\exp\frac{c_2}{\lambda t} - 1\right)^{-1} \tag{1}$$

where

λ = wavelength (cm)

T = object temperature (K)

C_1 = 3.7418 x 10^{-12} W cm^2

C_2 = 1.430 cm K.

The maximum black-body spectral radiance, $(N_\lambda)_m$, occurs at the wavelength and temperature that satisfy the equation

$$\lambda_m T = 2897 \ (\mu m \ K). \tag{2}$$

This is the Wien displacement law. Table C-1 lists the maximum spectral radiance (watts $cm^{-2} \ \mu m^{-1}$) and the wavelength λ_m of this maximum value for the temperature range 250 to 350 K.

When $\exp (C_2/(\lambda T) \gg 1$, then Equation (1) can be approximated by

$$N_\lambda = \frac{C_1}{\lambda^5} e^{[-C_2/(\lambda T)]} \ \text{watts} \ cm^{-3} \ . \tag{3}$$

This is the Wien radiation law. For wavelengths of 3 to 10 μm, and temperatures of 250 to 350 K, Equation (3) can be used to compute the spectral radiance emitted from a black-body source. Ambient temperatures in the neighborhood of 90°F (305 K) can be expected for primary system pipe surfaces at TMI; thus, a temperature range of 250C to 350K is reasonable to assume in our analysis. An infrared thermographic camera system functioning in the 8 to 12 μm regime would be operating in the region of peak infrared radiance output if object temperatures of 250 to 350 K are attained. Detectors of mercury cadmium telluride (HgCdTe) composition are, in fact, available on systems where infrared measurements are made in the 8 to 12 μm region.

118

TABLE C-1.   MAXIMUM SPECTRAL RADIANCE $(N_\lambda)_m$, AND ASSOCIATED
WAVELENGTH, λ_m, FOR THE TEMPERATURE RANGE 250 to 350 K

Temperature (K)	Wavelength $\lambda m_{(\mu m)}$	Maximum Spectral Radiance $(N\lambda)_m$ (W cm^{-2} μm^{-1})
350	8.28	7×10^{-3}
340	8.52	6×10^{-3}
330	8.78	5.2×10^{-3}
320	9.05	4.5×10^{-3}
310	9.34	3.8×10^{-3}
300	9.66	3.2×10^{-3}
290	9.99	2.7×10^{-3}
280	10.35	2.3×10^{-3}
270	10.73	1.9×10^{-3}
260	11.14	1.6×10^{-3}
250	11.59	1.3×10^{-3}

For non-black-body sources (emissivity $\epsilon < 1$), Equations (1) and (3) are modified as

$$N_\lambda' = \epsilon N_\lambda \ . \tag{4}$$

The emissivity, ϵ, can be a function of both wavelength and temperature. The effect of emissivity on the measured temperature, assuming a black-body radiator, is to yield an apparent temperature that is lower than the true temperature. This is illustrated by use of Equation (4). The measured radiance, N_λ, is reduced from the true radiance by the value of the emissivity. Table C-2 lists the black-body temperatures inferred for a 310-K object radiating with emissivities of 1.0, 0.9, 0.5, and 0.1 at 3.5 μm and 10 μm. For materials with low emissivities, significant errors can be made in inferring true surface temperatures if the emissivity is not taken into account. Note from Table C-2 that less error in the inferred black-body temperature is made at 3.5 μm versus 10 μm. However, overall radiance values are an order of magnitude greater at 10 μm than at 3.5 μm.

TABLE C-2. EFFECT OF EMISSIVITY ON THE INFERRED BLACK BODY TEMPERATURE

	Wavelength 10μm		Wavelength 3.5 μm	
Emissivity	Radiance $(Wcm^{-2} \mu m^{-1})$	Inferred Black Body Temperature (K)	Radiance $(Wcm^{-2} \mu m^{-1})$	Inferred Black Body Temperature (K)
1.0	3.75×10^{-3}	310	1.46×10^{-4}	310
0.9	3.38×10^{-3}	$\sim$304	1.32×10^{-4}	$\sim$308
0.5	1.88×10^{-3}	$\sim$270	7.315×10^{-5}	$\sim$295
0.1	3.75×10^{-4}	$\sim$206	1.463×10^{-5}	$\sim$264

When the emissivity is not known, there are several measurement techniques that can be used to compensate for the unknown emissivity of the object. In the first technique, if the object temperature and the background temperature are not too different and the material composition of the

object and the background are the same, then it can be assumed that ε is a constant. Measurements of the object and background infrared radiances at the same wavelength yield the temperature difference. The meaurements yield non-black-body object and background radiances, $(N_\lambda)_0$ and $(N)_b$ respectively, as

$$(N_\lambda')_0 = \varepsilon_0 C_1 \lambda^{-5} \exp - \frac{C_2}{\lambda T_0} \tag{5a}$$

$$(N_\lambda')_b = \varepsilon_b C_1 \lambda^{-5} \exp - \frac{C_2}{\lambda T_b} \tag{5b}$$

where

$$\varepsilon_0 = \varepsilon_b$$

$$\varepsilon_0 = \text{emissivity of object}$$

$$\varepsilon_b = \text{emissivity of background}$$

$$T_0 = T_b + \Delta T.$$

If T_b is known, then the temperature difference, ΔT, can be calculated using Equations (5a) and (5b),

$$\Delta T = \frac{\lambda T_b^2}{C_2} \ln \frac{(N_\lambda')_0}{(N_\lambda')_b} \quad . \tag{6}$$

In the second technique, two wavelengths are used for the measurements. If the object is a gray body (ε = constant < 1), and the emissivity does not change rapidly as a function of wavelength, then infrared radiance measurements made at two wavelengths yield both the emissivity and the true temperature of the object. The measurements yield

$$\left(N'_{\lambda_1}\right)_0 = \left(\epsilon_0\right)_{\lambda_1} C_1 \lambda_1^{-5} \exp\left(\frac{C_2}{\lambda_1 T_0}\right) \tag{7a}$$

$$\left(N'_{\lambda_2}\right)_0 = \left(\epsilon_0\right)_{\lambda_2} C_1 \lambda_2^{-5} \exp\left(\frac{C_2}{\lambda_2 T_0}\right)$$

$$\left(\epsilon_0\right)_{\lambda_1} = \left(\epsilon_0\right)_{\lambda_2} \quad . \tag{7b}$$

The temperature is calculated from

$$T_0 = -C_2 \left[\frac{1}{\lambda_1} - \frac{1}{\lambda_2}\right] \ln \frac{\lambda_1^{-5} \left(N'_{\lambda_2}\right)_0}{\lambda_2^{-5} \left(N'_{\lambda_1}\right)_0} \tag{8}$$

and the emissivity is calculated from Equation (7a) or Equation (7b). Two-wavelength thermography or radiometry allows both the emissivity and the true surface temperature to be determined.

Infrared imaging thermographic camera systems (discussed in next paragraph) usually function in two-wavelength regimes. These are 2 to 5 μm and 8 to 12 μm. Solid-state detectors operating in the former wavelength regime use indium antimonide (InSb) or mercury cadmium telluride (HgCdTe) with a special filter, whereas solid-state detectors operating in the latter regime use HgCdTe. For comparison, we have prepared single-wavelength-spectral-radiance versus temperature plots for the temperature range 200 to 340 K for wavelengths of 3.5 μm and 10 μm. These are given in Figure C-1. The spectral radiance at 10 μm is one to three orders of magnitude greater than the spectral radiance at 3.5 μm for black-body sources over the temperature range 200-340 K. For detectors with bandwidth $\Delta\lambda$, Equations (1), (3) and (4) can be integrated between finite limits via an integral of the type
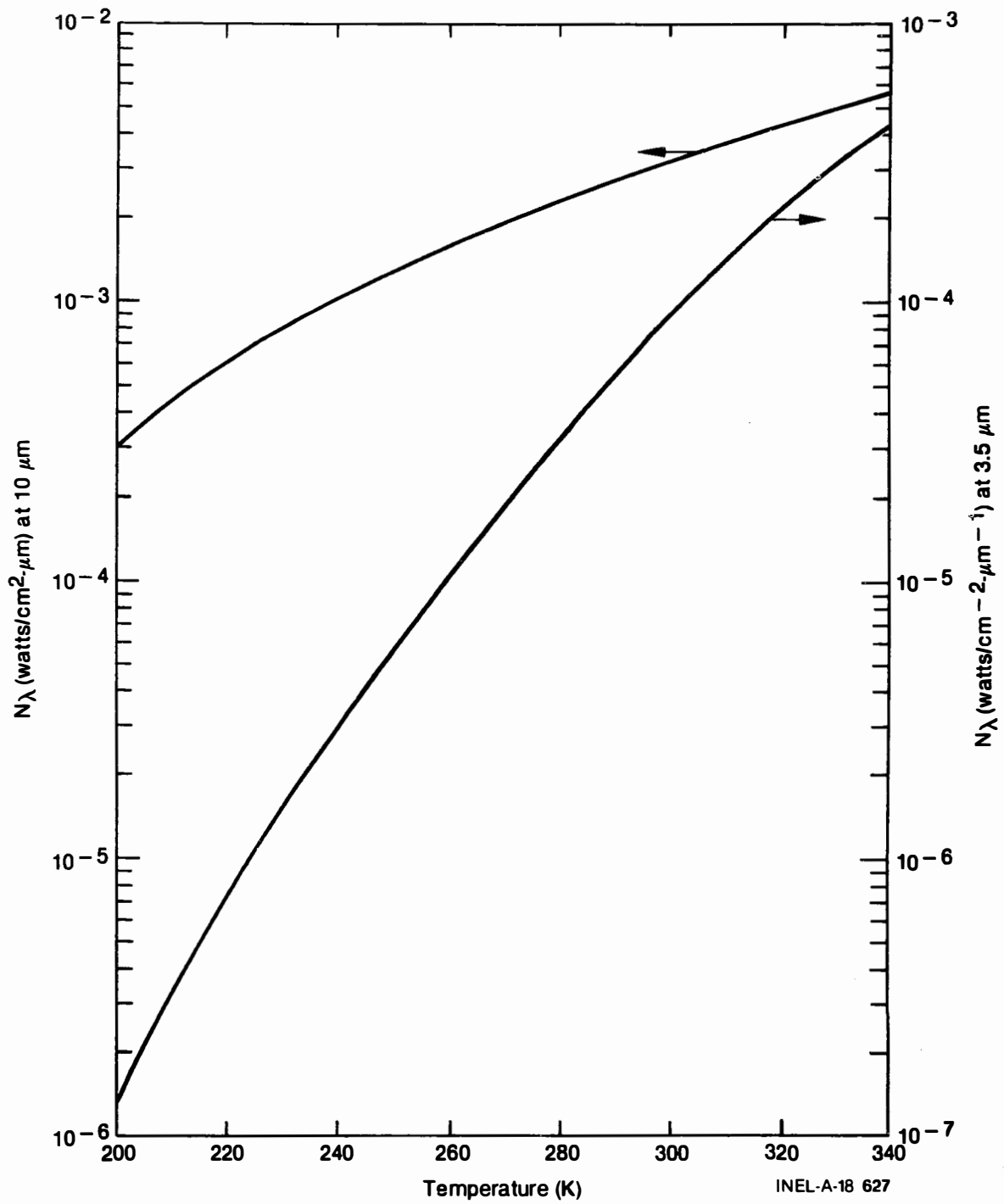
122

Figure C-1.   Spectral radiance/temperature plots for the temperature **range** 200 to 340 K for wavelengths of 3.5 and 10 μm.

$$N = N_\lambda \, d\lambda = \int_{\lambda_1}^{\lambda_2} C_1 \lambda^{-5} [\exp(\frac{C_2}{\lambda T}) - 1]^{-1} d\lambda \ \text{watts cm}^{-2} \ . \tag{9}$$

A hand-calculator program to compute Equation (9) is given in Reference 3. With ambient black-body temperatures of 300 K, thermographic imaging systems operating in the 8 to 12 μm region could be a distinct advantage.

A number of ground-based, infrared imaging, thermographic systems are available. Table C-3 summarizes the characteristics of the available imaging systems. Many of the systems are portable, and allow for remote interrogation. As noted in the table, indium antimonide (InSb) and mercury cadmium telluride (HgCdTe) are the two detectors used in present infrared camera systems. The use of HgCdTe has substantially increased over the past several years as advancements in detector technology have taken place. The temperature regime expected at TMI indicates that HgCdTe systems should be carefully scrutinized for use on this program. If possible, calibration and side-by-side comparison tests should be performed to choose the system best able to perform the infrared measurements. The calibration measurements can be used in conjunction with measurements in the TMI-2 primary system to determine the location and quantity of fuel dispersed in the primary system at TMI.

CONCLUSIONS AND RECOMMENDATIONS

Infrared techniques can be used to measure the temperature differences that are produced by fuel dispersed in the primary system of the TMI-2 reactor. These measurements should discern changes of at least 0.2 K from the ambient pipe temperature. Infrared camera systems are available that allow remote interrogation of the primary coolant system. Both hand-held and man-portable systems are available. In order that a proper baseline or data base be established, we recommend that a series of calibration and validation measurements be performed prior to any equipment use at TMI.

TABLE C-3.   GROUND-BASED INFRARED IMAGING THERMOGRAPHIC SYSTEMS

Manufacturer and Model	Detector and Spectral Range (µm)	Field of View (degree)	Spatial Resolution (mr)	Minimum Detectable Temperature Difference (K)	Temperature Range (K)	Display Type[d]	Portable
AGA Secaucus, NJ							
Model 110	InSb 2 to 5.6	6 x 12	2.0	0.1	-30 to 800	CRT	Yes
720	InSb 2 to 5.6	12 x 12	1.9	0.1	-20 to 200	CRT	Yes
782	HgCdTe 8 to 12	7 x 7[c]	1.1[c]	0.1	-20 to 900 to 1600, with filters	VTR or CRT	Yes
780 (dual range)	InSb 2 to 5.6 and HgCdTe 8 to 12	7 x 7	1.1	0.1	-20 to 900 to 1600, with filters	TVM or VTR	No
FLIR Systems Lake Orange, OR	HgCdTe 8 to 12	21H x 28V	1.8	0.2	-20 to 1500	TVM or VTR	Yes
Hughes Industrial Products Division Culver City, CA							
Probeye	InSb 2 to 5.6	18H x 7.5 V[b]		0.1 at 25°C	-25 to 850	LED	Yes
Inframetrics Bedford, MA							
Model 525	HgCdTe 8 to 12	14 x 18[d] (4:1 zoom) (3.5 x 4.5)	2	0.2	-20 to 1500	TVM VTR (polaroid adapter)	Yes
210 (dual range)	HgCdTe 3 to 5 8 to 12	14 x 18 (4:1 zoom)	2	0.2	-20 to 200 1500	TVM	Yes (if 110v available)
UTI Sunnyvale, CA							
Model 900	HgCdTe 2 to 13	30 x 30	1.3	0.2 to 20 depending on scale	-9 to 99 also 3X and 10X gives range from -27 to 1000	CRT	No

a. CRT = Cathode Ray Tube; VTR = Videotape Recorder; TVM = Television Monitor; LED =

b. H = horizontal, V = vertical.

c. Alternate lenses available: 3.5° x 3.5°, 0.5 mr; 12° x 12°, 1.9mr; 20° x 20°, 3.4mr, 40° x 40°, 5.8mr.

d. Alternate lenses available (3x-4.2 x 5.4 .7mr 3 in., 6 in. 12 in. close up lenses; microscope -0.0002 inch square field, 0.001 inch spatial resolution). (10 x -1.4° x 1.8°; .2mr)

The calibration and validation measurements that are undertaken should use a mock-up of, or simulate, the TMI-2 primary system. Specific quantities of spent fuel, or a heater unit, to simulate the expected heat flux should be considered for use as the thermal source. A set-up with spent fuel allows

- procedures of remote interrogation of the primary system to be established

- validation of the model used to calculate the temperature increases expected in the primary system at TMI-2

- determination of the gradients and spatial extent of the infrared radiation along the surface of the pipe

- determination of the correlation of the quantity of spent fuel present within the pipe with the infrared radiance measured along the pipe surface

- comparison of several broad-band, infrared scanning systems and the selection of the best system of actual TMI measurements

- the use of narrow-band infrared meaurements to complement and extend the broad band measurements.

This series of validation and calibration measurements increases the likelihood of success when measurements are actually made at TMI-2.

REFERENCES

1. F. E. Nicodemus, "Radiometry," in "Radiometry," selected reprints published for the American Association of Physics Teachers by American Institute of Physics, New York, p. 13.

2. W. L. Wolfe, G. J. Zissis, "The Infrared Handbook," Office of Naval Research, Department of the Navy, Washington, D.C., 1978, p. 1-1.

APPENDIX D
CALCULATION OF THE SURFACE TEMPERATURE OF AN
INSULATED PIPE CONTAINING DEPOSITED FUEL

by
K. Vinjamuri
M. S. El-Genk

APPENDIX D
CALCULATION OF THE SURFACE TEMPERATURE OF AN
INSULATED PIPE CONTAINING DEPOSITED FUEL

Infrared techniques can be used to detect fuel deposition in the primary coolant system of the TMI-2 reactor, provided $\Delta T > 0.36$ °F (0.2 °C) where

$$\Delta T = T_{sw} - T'_{sw}$$

T_{sw} = surface temperature of the insulated primary coolant pipe with fuel deposited inside the pipe.

T'_{sw} = surface temperature of the insulated primary coolant pipe without fuel deposited inside the pipe.

An increase in wall temperature due to a fuel layer of finite thickness is expected due to the decay heat of fuel. The volumetric decay heat rate (Q) is calculated below.

VOLUMETRIC DECAY HEAT RATE

Relevant parameters needed to calculate the volumetric decay heat rate, Q (Btu/hr ft^3) are presented in Table D-1 for TMI-2 fuel. The rate of emission of beta and gamma energy is often called the decay heat power, since the decay heat energy appears in the form of heat.

The decay heat is given by[1]

$$P = 6.1 \times 10^{-3} P_o \left[(t - t_o)^{-0.2} - (t)^{-0.2} \right]$$

where

P_o = steady state reactor thermal power

TABLE D-1. PARAMETERS NEEDED TO CALCULATE THE VOLUMETRIC DECAY HEAT OF TMI-2 FUEL

Total amount of UO_2 fuel (lb)	2.05×10^5
Irradiation time, t_0 (Effective full power days)	96.2
Decay time $(t - t_0)$ (days)	1095.0
Thermal power (Btu/hr)	9.463×10^9
Fuel density (lbs/ft^3)	650.5
Primary coolant pipe diameter, OD (ft)	3.48
Primary coolant pipe diameter, ID (ft)	3.0
Wall thickness (ft)	0.24
Stainless steel insulation (ft)	0.04
Water flow rate in the pipe (ft/hr)	3.50
Inside water ambient temperature ($^\circ F$)	130.0
Pipe wall thermal conductivity (Btu/hr ft $^\circ F$)	33.4
Fuel thermal conductivity (Btu/hr ft $^\circ F$)	5.3
Outside pipe wall ambient temperature ($^\circ F$)	80.0

$(t - t_0)$ = decay time (days)

t = irradiation time (days).

Using the parameters in Table D-1,

$P = 6.96 \times 10^4$ watts $= 2.38 \times 10^5$ (Btu/hr).

The volumetric decay heat rate is given by

$$Q = \frac{P}{M} \times \rho = 755.2 \ (Btu/hr \cdot ft^3)$$

where

ρ = fuel density

M = total amount of UO_2 fuel.

CALCULATION OF ΔT

The outside wall temperature, T_{sw}, due to a finite thickness, a (ft), of
fuel deposited in the pipe can be calculated from steady state heat con-
duction in a plane wall with convective cooling of the walls and with a heat
source. Since the radius and length of the pipe are sufficiently large com-
pared to wall thickness, only one-dimensional slab geometry was assumed.
We have also assumed no heat loss circumferentially in the pipe. The tem-
perature (T_{sw}) calculated at the surface of the insulated pipe wall would
be somewhat less without this assumption.

The characteristics of the physical system are shown in Figure D-1.

If Q represents the volumetric thermal source strength, expressed as heat
generated per unit volume and unit time, then the steady state heat
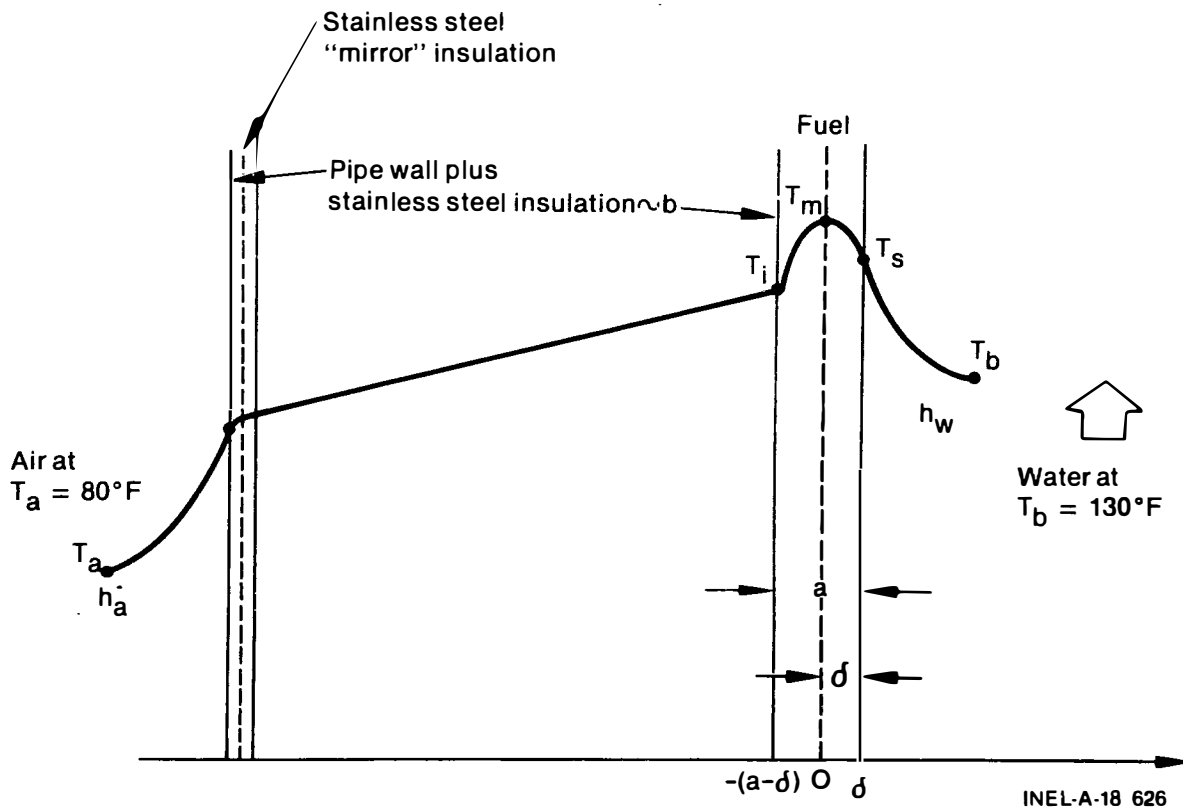conducton equation is given by

Figure D-1. Sketch illustrating one-dimensional steady state conduction
with corrective cooling of the walls with a heat source.

133

$$- K_f \frac{d^2 T}{dx^2} = Q \tag{1}$$

where K_f is the thermal conductivity of the fuel. Integrating equation (1), we have

$$- K_f \frac{dT}{dx} = Qx + C_1 \tag{2}$$

where C_1 is a constant that is equal to 0 from the boundary conuition

at $x = 0$, $\frac{dT}{dx} = 0$. Integrating equation (2) we have

$$T = - \frac{Qx^2}{2K_f} + C_2 \tag{3}$$

where $C_2 = T_m$ from the boundary condition that at $x = 0$, $T = T_m$.

Therefore $T_m - T = \frac{Qx^2}{2K_f}$. $\tag{4}$

At $x = \delta$, $T = T_s$.

Therefore $T_m - T_s = \frac{Q\delta^2}{2K_f}$ $\tag{5}$

From heat convection, the temperature at the interface between the debris and the coolant is given by

$$T_s - T_b = \frac{Q\delta}{h_w} \tag{6}$$

134

where h_w is the convective heat transfer coefficient of water at bulk temperature; T_b = 130°F and the coolant flow rate is 3.5 ft/hr. Adding Equations (5) and (6), we have

$$T_m - T_b = \frac{Q\delta^2}{2K_f} + \frac{Q\delta}{h_w} \tag{7}$$

Heat balance at T_I leads to

$$T_I - T_a = QR \ (a-\delta) \tag{8}$$

where

$a \quad = \quad$ fuel layer thickness

$R \quad = \frac{1}{h_a} + \frac{b}{K_w} =$ thermal resistance $\tag{8.1}$

$h_a \quad = \quad$ convective heat transfer coefficient of air

$b \quad = \quad$ wall thickness plus stainless steel mirror insulation

$\delta \quad = \quad$ thickness where the temperature is maximum.

From Equation (4) at $T = T_I$, we have

$$T_m - T_I = \frac{Q(\delta - a)^2}{2 K_f} \tag{9}$$

From Equations (8) and (9), we have

$$T_m = T_a + Q \ (a-\delta) \ R + \frac{Q \ (a-\delta)^2}{2 K_f} \ . \tag{10}$$

Solving for δ from Equations (7) and (10), we have

$$\delta = \left(\frac{T_a - T_b + QaR - \frac{Qa^2}{2 K_f}}{\frac{Q}{h_w} + QR + \frac{Qa}{K_f}} \right) \tag{11}$$

Also, from heat balance at T_{sw} we have

$$T_I - T_{sw} = \frac{h_a b}{K_w} (T_{sw} - T_a) \quad . \tag{12}$$

Solving for T_{sw} from Equations (12) and (8), we have

$$T_{sw} = \left(\frac{T_a + \frac{h_a b T_a}{K_w} + QaR - Q\delta R}{(1 + \frac{h_a b}{K_w})} \right) \quad . \tag{13}$$

Convective heat transfer coefficients of air and water are given by[2-4]

$$h_a = 0.27 \left(\frac{T_{sw} - T_a}{D_o} \right)^{0.25} \qquad \text{(Reference 4)} \tag{14}$$

and

$$h_w = 1.86 \frac{K_w}{D_e} \left(\frac{Re\ Pr\ D_e}{L} \right)^{0.33} \frac{\mu}{\mu_o}^{0.14} \qquad \text{(Reference 3)} \tag{15}$$

where

$\quad D_o \quad = \quad$ pipe outside diameter

$\quad Re \quad = \left(\frac{D_e V \rho_w}{\mu} \right) =$ Reynolds number

136

$$Pr = \left(\frac{C_p \mu}{K_w}\right) = Prandtl \ number$$

D_e = Hydraulic diameter given by

$$D_e = \frac{\frac{\pi r^2}{90}\left[360 - Sin^{-1}\left(\frac{r-a}{r}\right) + \left(\frac{r-a}{r}\right)\right]}{2\pi r + 2\sqrt{2ra - a^2} - \frac{\pi}{180} r \ Sin^{-1}\left(\frac{r-a}{r}\right)} \qquad (15.1)$$

$2r$ = pipe inner diameter

a = fuel thickness

L = pipe length.

There are four unknowns and four equations. The four unknowns are T_{sw}, δ, R, and h_a, and the four equations are 13, 11, 8.1, and 14. The four equations are solved by using a computer subroutine. The outside pipe wall temperature T_{sw} was calculated for various fuel thickness layers ranging from 10^{-4} ft to 1.5 ft.

The differential temperature is $\Delta T = T_{sw} - T_{sw}$ where T_{sw} is the out-side pipe wall temperature without source. For a first approximation, the wall temperature for a fuel thickness of 10^{-4} ft corresponds to T_{sw}. A plot of the differential temperature ΔT versus fuel thickness layer a, is presented in Figure D-2. Since the tolerance of the infrared probe is = 0.36 °F, from Figure D-2 it can be noticed that the minimum fuel layer thickness that can be detected with an infrared probe is about 9 mm. It is possible to scan the bottom of the horizontal pipe and map ΔT and hence fuel layer thickness. From the shape and thickness of the fuel layer, one can quantitatively determine the amount of fuel deposited in the pipe. However, care should be taken to measure accurately the ambient air temperature T_a, the ambient water temperature T_b, and the water flow rate, and to calculate T_{sw} using the computer subroutine. The calculations presented in Figure D-2 are based on T_a = 80°F, T_b = 130°F, and V = 3.5 ft/hr (flow rate).
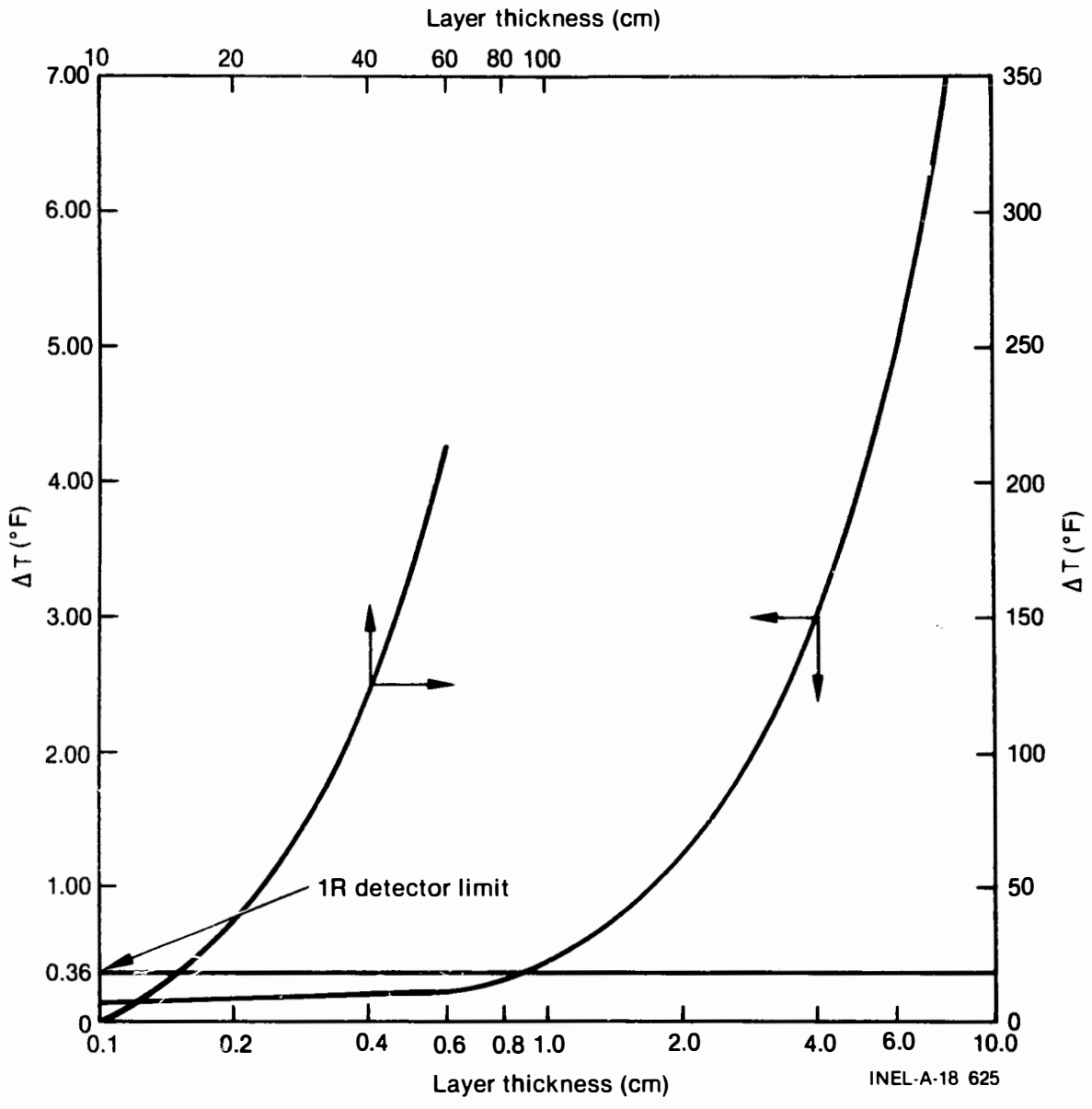
137

Figure D-2. Plot of ΔT versus debris layer thickness.

REFERENCES

1. S. Glasstone and A. Sesonske, Nuclear Reactor Engineering, Princeton, New Jersey: Van Nostrand Company, Inc., 1963.

2. J. P. Holman, Heat transfer, New York: McGraw-Hill Book Company, Inc. 1972 p. 219.

3. R. B. Bird, W. E. Stewart, and E. N. Lightfoot, Transport Phenomena, John Wiley and Sons, Inc., p. 399, 1960.

4. W. H. McAdams, Heat Transmission, New York: McGraw-Hill Company, Inc., 1954 p. 177.

APPENDIX E
THE FEASIBILITY OF
USING OPTICAL TECHNIQUES TO LOCATE
FUEL AND NON-FUEL DEBRIS

K. Vinjamuri
M. R. Martin

APPENDIX E
THE FEASIBILITY OF
USING OPTICAL TECHNIQUES TO LOCATE
FUEL AND NON-FUEL DEBRIS

Optical techniques include (a) fiber optics and (b) remote video exami-
nation. The feasibility of assaying fuel debris in the TMI-2 piping is
briefly discussed in this appendix.

1. Fiber Optics

The use of fiber-optic imaging probes has been investigated for poten-
tial post-operation inspection applications inside the reactor vessels of
the Loss of Fluid Test (LOFT) at the Idaho National Engineering Laboratory
and the Three Mile Island reactors. The results of these investigations
indicate that current state-of-the-art developments in image-grade optical
fibers are insufficient to meet the environmental requirements for these
applicatons. Chief among the several technical problems encountered is the
poor radiation tolerance. For applications involving gamma-radiation
fields, only high-quality glass fibers can be used (as opposed to the
special plastic fibers more commonly employed). The highest radiation
tolerance for glass fibers currently on the market is available from Schott
Optical Co. (W. Germany), and the cumulative dose is 10^3R. For the appli-
cations considered, the allowable in-reactor residence time would range from
1/2 to 5 minutes. This time interval is considered too short to provide the
inspection data required, especially in view of the substantial costs asso-
ciated with custom probe development and fabrication.

Other technical problems encountered by the investigations are more
application-dependent. In several cases, the problems for the custom appli-
cation represent more of a cost-effectiveness question than a formidable
technical difficulty. These technical considerations include following:

1. Overall Length--Current fiber optic inspection probes are gener-
   ally less than 25 ft long, with an upper limit of about 40 ft;
   this length is inadequate for the application requirements

143

2.	Control & Guidance--Manipulating a long flexible probe through a confined opening and a circuitous path requires special development

3.	Bend Radius--Fiber bundles require fairly large bend radii to avoid over-stressing and subsequent failure of individual strands; special handling, coiling, and feeding problems must be dealt with to prevent bundle damage

4.	Water-Tight Construction--The fiber bundle and objective lens must be housed in a flexible sheath that precludes any water leakage, with special attention to the seal around the lens

5.	Custom Objective Optics--The objective lens must be a custom-design meeting angle-of-view, focal range, and refraction requirements, as well as the lens-to-fiber interface

6.	Lighting--Ambient light is nonexistent in the applications considered; auxiliary light, provided either by a second coaxial fiber bundle or by attached electrical systems, severely limits the viewing range of the probe.

Based on this investigation, the fiber optics technique is not suitable for remote examination of fuel debris in TMI-2 piping.

2. REMOTE VIDEO EXAMINATION

Closed circuit television cameras are available for remote video examination of debris in pipes and tubes. The visual examination system consists of a television camera, a control unit, a range of interchangeable view heads that incorporate lighting, camera cable lengths of up to 1300 ft, and a video viewer and recorder. The system is designed for rugged and demanding environments, such as operating temperatures ranging from -250 to 330 K, underwater depth of 900 ft (272 m), and gamma radiation total absorbed dose of 10^8R.

The features allow entrance through any opening larger than 1.6 in. (4.1 cm) diameter. The view heads carry their own integral lighting source, but an auxiliary lighting source can be attached. The camera control unit is modular and portable. The remote video examination system is field-proven, and these systems are monitoring critical areas for a number of nuclear utilities.

Specification data of remote video examination systems from a selected number of suppliers are presented in Table E-1.

A remote video examination system will permit video recording of the topographic view of fuel and non-fuel debris configuration in the Primary Coolant System (PCS). By remote video examination, the PCS piping can be surveyed prior to the use of other nondestructive debris assay techniques. The only drawback with this technique is that the reactor core head must be removed to gain accessibility to the piping. Also, the size of holes in the hot leg guard plate may cause problems for inserting the camera view head.

TABLE E-1. REMOTE VIDEO EXAMINATION SYSTEMS

Manufacturer and Address	Model	Mechanical	Transmission Distance	Environmental	Resolution
1. Diamond Electronics Division of Arvin Systems Inc. Co. P.O. Box 200 Lancaster, Ohio 43130 (614) 756-9222	ST-5 1000 line underwater radiation resistant camera and accessories	Camerahead: 2 7/8 in. diameter 25-5/8 in. overall length Weight: 14 lb.	100 feet, 500 feet is available	Temp: Camerahead: -20 to 60°C control unit: 0 to 50°C water depth = 100 feet. Total absorbed radiation tolerance = 10^8R gamma radiation at dose rate of 10^6R/hr.	Horizontal center: 1000 lines at 525 lines per frame.
2. Telemation P.O. Box 15068 Salt Lake City, Utah 84115 (801) 972-8000	80 series wet or dry applications Camera: R80-TM and R81-TM Viewing heads: R80/01-TM R80/02-TM R80/03-TM	Camera overall diameter = 1.73 in. (44mm) Length: 15.5 in. (393·6mm) Weight: 2.2-3.79 lb.	450 feet submersible. 360° radial scanning	Operating temperature -10 to 55°C. Radiation: 10^8R total absorbed dose of gamma radiation.	Horizontal center 300 TV lines.
3. Fernser Inc. The Video Corporation of Bell & Howell and Robert Bosch P.O. Box 15068 Salt Lake City, Utah 84115	R93-TM Miniature CC TV Camera	Camerahead: Diameter 1-19/32 in. (40.5mm) Length: 11-5/16 in. (287 mm) Weight: < 4 lb. Built-in light source, with head rotation.	900 feet Submersible. Cable length to 1300 feet	Temperature -25 to 60°C Radiation: 1.6 x 10^8R gamma total absorbed dose.	Horizontal center: 600 TV lines using standard 11 mm lens.

146

APPENDIX F
PULSED EDDY-CURRENT TECHNIQUE

In this appendix, a brief discussion of the applicability of the pulsed eddy-current technique for assaying fuel debris in the primary coolant piping of TMI-2 reactor is presented.

The pulsed eddy-current system uses a series of current pulses passing through a field coil to induce eddy currents in the specimen under investigation. The eddy currents are influenced by the specimen's characteristics: permeability, conductivity, wall thickness, and distance between the probe and specimen. The resulting eddy currents produce a pulsed magnetic field that induces a voltage pulse in the pickup coil.

This technique has been successfully applied at the Idaho National Engineering Laboratory to detect cladding surface defects and make cladding wall thickness measurements on fresh and previously irradiated light water reactor fuel rods.

For assaying fuel debris in the TMI-2 piping, the following items should be considered:

1. Eddy-current transducers will not sense ceramic materials such as urania and zirconia.

2. Considering the wall thickness of the piping (3 in.), its cross section (36 in.), and the type of material used (carbon steel), any detection of debris would have to be done with the transducer mounted in the inside wall of the piping.

3. An eddy-current type transducer will operate at high temperatures up to 811 K (1 000°F), in a water environment, and under radiation.

4. Transducers that are generally available have diameters of less than one inch. The range of detection of a transducer is approximately equal to its diameter.

149

5. Because of the transducer's range and size, many transducers would be required.

6. It would be best if transducers were rigidly mounted to the inside wall of piping. This task would be highly impractical.

Considering the task of detecting fuel and nonfuel debris, a pulsed eddy-current transducer would not be recommended for the following reasons:

1. It cannot detect fuel debris.

2. Considering pipe diameter (36 in. OD), the transducer would have a very limited useful range.

3. Accessibility to the inside piping wall and remote control and operation are impractical.